Spring 2002

Comparative performance of rubberized hot mix asphalt under ALF loading

Hanlin Qin
Louisiana Tech University

Recommended Citation

Qin, Hanlin, "" (2002). *Dissertation*. 727.
https://digitalcommons.latech.edu/dissertations/727

INFORMATION TO USERS

This manuscript has been reproduced from the microfilm master. UMI films the text directly from the original or copy submitted. Thus, some thesis and dissertation copies are in typewriter face, while others may be from any type of computer printer.

The quality of this reproduction is dependent upon the quality of the copy submitted. Broken or indistinct print, colored or poor quality illustrations and photographs, print bleedthrough, substandard margins, and improper alignment can adversely affect reproduction.

In the unlikely event that the author did not send UMI a complete manuscript and there are missing pages, these will be noted. Also, if unauthorized copyright material had to be removed, a note will indicate the deletion.

Oversize materials (e.g., maps, drawings, charts) are reproduced by sectioning the original, beginning at the upper left-hand corner and continuing from left to right in equal sections with small overlaps.

Photographs included in the original manuscript have been reproduced xerographically in this copy. Higher quality 6" x 9" black and white photographic prints are available for any photographs or illustrations appearing in this copy for an additional charge. Contact UMI directly to order.

UMI®

COMPARATIVE PERFORMANCE OF RUBBERIZED HOT MIX

ASPHALT UNDER ALF LOADING

by

Hanlin Qin, M.S.

A Dissertation Presented in Partial Fulfillment
of the Requirements for the Degree
Doctor of Engineering

COLLEGE OF ENGINEERING AND SCIENCE
LOUISIANA TECH UNIVERSITY

March 2002

UMI®

LOUISIANA TECH UNIVERSITY

THE GRADUATE SCHOOL

12/18/2001
Date

We hereby recommend that the thesis prepared under our supervision

by ___ Hanlin Qin

entitled ___ Comparative Performance of Rubberized Hot Mix Asphalt under ALF Loading

be accepted in partial fulfillment of the requirements for the Degree of

___ Doctor of Engineering

Supervisor of Thesis Research

Head of Department

Civil Engineering
Department

Recommendation concurred in:

Advisory Committee

Approved:

Director of Graduate Studies

Dean of the College

Approved:

Dean of the Graduate School

GS Form 13
(1/00)

ABSTRACT

In response to the Intermodal Surface Transportation Efficiency Act (ISTEA) of

1991, Louisiana constructed five projects to evaluate several methods of using discarded

tire rubber in highway pavements. The field performance was quite variable. To achieve

the agreement among state agencies on the engineering benefits of using crumb rubber

modifier (CRM) in HMA pavement and to define the circumstances where the LaDOTD

can use asphalt rubber materials in the most cost-effective way, a full-scale research

program has been conducted at the Louisiana Transportation Research Center (LTRC) to

evaluate the performance of CRM-HMA asphalt pavement under Accelerated Loading

Facilities (ALF). Three ALF test lanes were constructed at the Louisiana Pavement

Research Facility (LPRF), one with conventional mixtures, one with a CRM-HMA

wearing course and one with a CRM-HMA base course. The observed field data were

used as the basis for the performance comparisons among the test lanes.

In this study, the 2-D finite element analytic model called FLEXPASS was used

to predict the performance of the ALF test lanes. Laboratory test data was collected to

develop appropriate material modeling parameters that are used to predict the

performance of the ALF test lanes. The predicted results of performance derived from

these numerical simulations of the test lanes have been evaluated and compared with the

field data to determine how well the numerical model predicted performance.

The purposes of this study includes evaluating the overall performance of hot mix asphalt mixtures containing CRM as compared with similar mixes with conventional HMA under ALF loading, and identifying the optimal location in the pavement structure that the LaDOTD can use asphalt rubber materials in a cost-efficient manner.

Based on the results from this study, it is observed that there is good agreement between FLEXPASS predictions and measured field performance and that FLEXPASS can be used to successfully model Louisiana flexible pavements.

Based on the results of this study, it is found that even though CRM asphalt mixtures and conventional asphalt mixtures behaved very similarly in the laboratory characterization, ALF test lane contained CRM-HMA base course exhibited significantly smaller rut depth than the other two test lanes. Test lane contained CRM-HMA wearing course exhibited similar rut depth as the lane with conventional mixes.

Predictions of serviceability for the lane with CRM-HMA Type 5A base course were higher than the lanes with all conventional materials or with the CRM-HMA Type 8 wearing course. The overall performance of CRM-HMA base course was better than the performance of CRM-HMA in the surface course.

From the results of this study, the author concluded that: (a) the DOTD should consider extending the use of modified binders in all flexible pavement layers in the light of the superior performance of the AR Type 5A base section; and (b) the DOTD should consider adding asphalt rubber hot mix to its list of available base course materials.

TABLE OF CONTENTS

LIST OF TABLES

xi

LIST OF FIGURES

xiv

ACKNOWLEDGEMENTS

I would like express my deepest gratefulness and appreciation to Dr. Freddy L. Roberts, my research advisor and the chairman of my graduate committee, for his kindness, patience, invaluable advice and guidance, and financial support throughout my graduate study in Louisiana Tech University.

I would also like to express my special thanks to other members of my graduate committee, Dr. Raja Nassar, Dr. Norman Pumphrey, and Dr. William M. Jordan, for their time, effort, and helpful advice for my research work.

I also wish to thank the Louisiana Transportation Research Center (LTRC) for providing facilities and data for this study. Special thank goes to Mr. Masood Rasoulian, ALF Project Director; Dr. Louay N. Mohammad; and Dr. Baoshan Huang for providing helpful suggestions and support during the process of completing this study.

Finally, I would like to use this opportunity to express my special gratitude for my parents, Shaowen Zhang and Youbo Qin, for their love, encouragement; and my husband, Gang D. Lee, for his understanding and support throughout my graduate study in Louisiana Tech University.

CHAPTER 1

INTRODUCTION

This document describes the research work and findings of the comparative performance of conventional and rubberized hot mix asphalt under accelerated loading facilities (ALF). Chapter 1 is an introduction that includes the problem statement and the background information of the research project. Chapter 2 presents the objectives and scope of the research. Chapter 3 presents literature review of research on asphalt rubber hot mix. Chapter 4 describes ALF testing, materials used in the study, and test lanes construction. Chapter 5 shows the numerical simulation of ALF testing lanes. Chapter 6 describes the two failure criteria models used for pavement performance prediction in this study. Chapter 7 describes the material testing to characterize the pavement materials. Chapter 8 describes FLEXPASS, the 2-D finite element model, used to predict the performance of the test lanes. Chapter 9 is the discussion of results and conclusion.

Problem Statement

Waste or scrap tires pose a substantial waste management challenge due to the large number of scrap tires generated annually around the whole nation. To reduce these scrap tire inventories, applications and markets for scrap tire rubber have to be developed and enhanced. In 1991, the Intermodal Surface Transportation Efficiency Act (ISTEA) specified that any asphalt pavement project funded by federal agencies must use certain percentages of scrap tires [1]. A number of activities were underway as a result of this

1

act. Although this mandate was dropped from the ISTEA legislation, it did encourage the research and application of HMA materials that include crumb rubber modifier (CRM) in pavement construction.

CRM has been used in asphalt pavement construction for over 40 years principally as local repair material, as interlayers, or in seal coat construction. Since 1960, shredded waste tires have been used in HMA mixtures. It was not until late 1980s that the extensive use of recycled tire crumb rubber in asphalt mixtures occurred.

There are two aspects of the use of CRM in HMA materials: environmental and engineering benefits. The environmental benefits are widely accepted because recycled tire crumb rubber reduces landfills and eliminates potential pollution. On the engineering benefits, however, there are still some principal unresolved issues regarding the use of recycled rubber in asphalt pavement. One of them is the actual field performance of the material as compared with conventional asphalt materials. The other is the optimal position within the pavement structures to use these materials. While most of the applications of CRM are on the surface course, the application on the base course using CRM might give better performance as laboratory results from previous research indicate that the asphalt rubber materials show reduced thermal and reflective cracking, reduced rutting, and slower aging when compared with conventional mixes [2]. Indeed, by placing the asphalt rubber in a thicker base, a) considerably more rubber would be used; therefore, also achieving the goal of disposing of more discarded tires, and b) difficulties involved in recycling asphalt rubber materials would be eliminated.

Because of the need to evaluate the engineering benefits of using CRM, to determine the optimal position within the pavement structures to use these materials, to

dispose of tires in an economical fashion, and to determine the appropriate structural coefficient for use in pavement thickness design, a field study is needed to evaluate the performance of HMA materials that include CRM. Full-scale testing using Accelerated Loading Facility (ALF) provides the best alternative for a relative quick assessment of the cost-effectiveness of CRM-HMA. Additionally, numerical simulation and performance prediction of the pavement structure will help to extend the field performance evaluation and comparisons.

Background Information of the Research Project

There are currently two methods of applying crumb rubber in asphalt mixtures: a wet process and a dry process. The dry process uses ground rubber particles as an aggregate substitute in the mixture. The wet process involves preblending the ground rubber with the asphalt cement for a period of time at high temperature before mixing with the aggregate. Common wet process methods include the McDonald, Ecoflex, and Wet Rouse continuous blending methods [3].

In response to the Intermodal Surface Transportation Efficiency Act (ISTEA) of 1991, Louisiana constructed five projects to evaluate several methods of using discarded tire rubber in highway pavements. Eight variations of these two processes were constructed on the following projects [4]:

- US 61: Patented wet process—Gap graded mixture (Arizona Process)

- LA 15: Generic wet process—Gap graded, 16 mesh mixture and Dense Graded 80 mesh mixture (Rouse)

- LA 1040: Patented dry process—Gap graded (Plus-Ride)

- US 167: Generic Dry process—Gap graded, 16 mesh mixture and Dense Graded 80 mesh mixture (Rouse)

- US 84: Pre Blended Rubber—Presently allowed by the Specifications (Neste-Wright)

The generic "wet process" method with 80 mesh powdered Rouse rubber stood out among all these pavements due to its adaptability to current construction practice. This type of process is used with conventional dense-graded mixes, and no patents are associated with the process. Construction of the ALF project incorporated the use of the 80 mesh powdered Rouse rubber in a wet process termed as Asphalt Rubber-Hot Mix Asphalt (AR-HMA). The Rouse materials are readily available from Vicksburg, Mississippi.

To evaluate the engineering benefits of using CRM in HMA pavements and to define the circumstances where the LaDOTD can use asphalt rubber materials in the most cost-effective way, a full-scale research project was conducted at the Louisiana Transportation Research Center (LTRC) to evaluate the performance of CRM-HMA asphalt pavement under accelerated loads. Two CRM-HMA mixtures were designed based on the existing Louisiana Type 8 wearing course and Type 5A base course mixtures. Three ALF test lanes were constructed at the Louisiana Pavement Research Facility (LPRF), one with conventional mixtures, one with CRM-HMA wearing course, and one with CRM-HMA base course. The measured performance data will be used as the basis for the performance comparison among the test lanes. Additionally, the predictions of performance derived from numerical simulations of the test lanes will be also prepared and compared with the field observations.

CHAPTER 2

OBJECTIVES AND SCOPE

Objectives

The objectives of this study were as follows:

- Evaluate the overall performance of hot mix asphalt mixtures containing CRM as compared to similar mixes with conventional HMA under ALF loading.

- Identify the optimal location in the pavement structure that the LaDOTD can use asphalt rubber materials in a most cost-efficient manner.

- Evaluate the structural analysis responses of hot mix asphalt mixtures containing CRM as compared with similar mixes with conventional HMA under ALF loading.

To achieve these objectives, three test lanes were constructed at the Louisiana ALF site using conventional and rubberized HMA. ALF loads were applied until failure occurred using the selected failure criteria.

The second part of this study involves conducting numerical simulation of ALF test lanes. A finite element computer software called FLEXPASS is used for performance prediction. The input parameters for FLEXPASS were based on the results from laboratory tests performed on pavement materials from the ALF site and field

5

information. The predicted performance includes rutting, fatigue cracking, slope variance and present serviceability index (PSI).

The third part of this study involves comparing the field performance of three test lanes constructed at the LPRF to predicted performance of the same three lanes. The specific comparison of performance will be made for HMA and asphalt rubber materials in the surface and base position for these three lanes subjected to ALF loading.

The performance will be evaluated using number of applied loads, observed distresses at specified loading intervals, monitoring pavement response to non-destructive testing, and comparisons between predicted and observed performance measures.

Scope

Only the wet Rouse method for processing asphalt rubber materials was investigated in this study. Because asphalt rubber materials were placed only in a 1.5-inch wearing course and a 3.5-inch base course, performance comparisons apply only to these two locations.

CHAPTER 3

REVIEW OF RESEARCH ON ASPHALT RUBBER HOT MIX

History of Asphalt Rubber in Pavement

The history of adding recycled tire rubber to asphalt paving material can be traced back to the 1940s when U.S. Rubber Reclaiming Company began marketing a devulcanized recycled rubber product, called Ramflex™, as a dry particle additive to asphalt paving mixtures. In the mid-1960s, Charles McDonald began developing a modified asphalt binder using crumb rubber. This product was marketed by Sahuaro Petroleum and Asphalt Company as Overflex™. The Arizona Refining Company, Inc., created a second modified binder in the mid-1970s replacing a portion of the crumb rubber with devulcanized recycled rubber and marketing it under the name Arm-R-Shield™. Both Overflex™ and Arm-R-Shield™ were patented and eventually brought under single ownership. The companies marketing these two products founded a trade association known as the Asphalt Rubber Producers Group in the mid-1980s. Ramflex™ disappeared from the market when U.S. Rubber Reclaiming Company was sold by its parent corporation.

The other half of the history originates in Sweden. In the 1960s, two Swedish companies began developing an asphalt paving surface mixture that would resist studded tire and chain wear. The mixture included a small amount of crumb rubber as an

7

aggregate and was called by the trade name Rubit™. In the late 1970s, this product was introduced and patented in the United States as PlusRide™ by All Seasons Surfacing Corporation. The design of PlusRide™ evolved through a series of field projects in Alaska and other States from 1979 through 1985. PlusRide™ has been managed by a number of firms and is presently marketed by EnvirOtire, Inc.

With the environmental interest to find alternative uses for scrap tires and the enactment of ISTEA in 1991, asphalt technologists and rubber-recycling entrepreneurs began investigating ways to modify or improve existing technologies available for adding crumb rubber to asphalt paving materials. Several new technologies have emerged and are being evaluated. The initial field test sections of crumb rubber asphalt mixtures similar to PlusRide™ and McDonald technology were laid in 1989 and 1990, respectively. Additional technologies have been introduced since that time but have not been widely evaluated.

Generally, tire rubber is prepared for recycling by reducing its size by mechanical shearing or grinding to particle sizes less than 6.3mm (¼"). This form of tire rubber is designated as Crumb Rubber Modifier (CRM). When the CRM is added to asphalt cement, the rubber particles will interact with the asphalt and swell. Asphalt Rubber (AR) is the asphalt cement modified with CRM. The methods of producing crumb rubber impart different shape and texture characteristics to each particle which have a significant effect on the properties of the asphalt rubber material.

When CRM is added to asphalt cement, the rubber particles will generally become swollen in the asphalt, increasing the mixtures viscosity. Laboratory results from previous research indicate that the asphalt rubber materials show reduced thermal and

reflective cracking, reduced rutting, and slower aging when compared with conventional mixes. A field evaluation is needed to determine whether these benefits can be realized.

Review of Research on CRM in HMA Mixtures

Many state highway agencies and private sector organizations have conducted their own research on the applications of crumb rubber in HMA mixtures.

Charles H. McDonald, consulting engineer, Phoenix, Arizona, is considered to be the father of the asphalt-rubber systems developed in the United States. His laboratory work, which was initiated in 1963, resulted in the placement of patching materials in the mid 1960s.

Arizona, arguably, has the longest sustained experience with CRM mixes of any State. Though many of their older projects used asphalt rubber in interlayers exclusively to mitigate reflection cracking, these products were expressly excluded from study in this project, which focuses on traditional HMA applications. Much of the CRM-HMA performance information available is from projects initiated in the late 1980s [5].

Currently, the city of Phoenix uses significant quantities of gap-graded CRM mixes in overlays of residential streets. Before 1992, the CRM mixes used a patented asphalt-rubber binder. During the 1995 construction season about 26 km (16 mi) of CRM mix will be placed. Typical overlay thicknesses are 30 mm. Overall, performance is reported to be better than conventional mixes. Recently, some early reflection cracking has been reported [5].

California first began using the asphalt rubber to improve the durability of HMA. It has performance history on CRM materials dating back to 1978. Both wet and dry process mixes have been placed over existing flexible and rigid pavements with and

without interlayers. Evaluation of these projects has led CALTRANS to use only asphalt-rubber (wet process) gap-graded and dense-graded mixes in nonexperimental work. Investigation of other CRM mix types is continuing; however, this work is limited. Although distresses have been reported (rutting, bleeding, and raveling), the majority of projects are performing well. CALTRANS reports improved durability, reflection crack control, and resistance to chain wear when asphalt-rubber hot mixes are used. Side-by-side performance comparison of thinner CRM and conventional overlays led CALTRANS to reduce required overlay thickness when CRM is used. With additional experience, California developed a design guideline in 1992 that allows for reduced overlay thickness for a gap-graded HMA with asphalt rubber on specific types of applications [5].

Although Florida first placed CRM material in the 1970's, the bulk of their performance experience is limited to projects placed since 1989. Florida has several years' experience with CRM as the wearing course. Florida DOT uses crumb rubber in membrane interlayers, and in open-graded and dense-graded friction courses. Open-graded friction courses (OGFC's) are required on all multilane facilities with design speeds equal to or greater than 73 km/h (50 mi/h). No structural value is typically assigned to the OGFC. Dense-graded friction courses (DGFC's) are used where an OGFC is not required. To date, performance has been good. Florida DOT began constructing demonstration projects of asphalt pavement with crumb rubber wet processes in 1989 and has reported satisfactory pavement performance [6]. Beginning in January 1994, all OGFCs and DGFCs must include an asphalt-rubber binder. Florida DOT expects

improved durability and better temperature susceptibility performance from the CRM mixes.

Two crumb rubber processes (McDonald and Rouse) were used in Virginia in 1996 with the result that the inclusion of asphalt rubber in HMA pavements increases construction cost by 50 to 100 percent as compared to the cost of conventional mixes. Troy *et al* [7] conducted research on crumb rubber modified asphalt mixtures in Nevada. In the Nevada study, CRM binder was evaluated using the Superpave binder testing protocols while the mix was designed using the Hveem procedure.

Federal Aviation Administration (FAA) and U.S. Department of Transportation has conducted a research on laboratory testing and mix design of asphalt-rubber concrete in civil airport pavements from 1983-86. In this study, asphalt-rubber concrete and an asphalt concrete control were tested in the laboratory and material properties were determined. The materials properties and airplane gear loads were input into a computer program for analysis of relative lives and prediction of pavement damage. An economic evaluation was performed comparing the costs and service lives of each material. The criteria for asphalt-rubber concrete in civil airport pavements were created [8].

In the present ALF project, asphalt rubber prepared using the Wet Rouse process will be incorporated into both a surface course and a base course. The performance of the LaDODT Type 8F Wet Rouse asphalt rubber wearing course will be compared with that of the conventional LaDODT Type 8F wearing course. Similarly, the performance of Type 5A Wet Rouse asphalt rubber base will be tested and compared to that of a LaDODT Type 5A base.

CHAPTER 4

DESCRIPTION OF ALF TESTING

The project consists of construction and ALF loading of three test lanes at the Louisiana Pavement Research Facility (LPRF) under accelerated loading. The experiments have been designed so that direct pairwise comparisons can be made between the three lanes.

ALF Machine

The Accelerated Loading Facility (ALF) is a relocatable road testing machine which applies controlled full-scale rolling wheel loads to a test pavement. The ALF was designed and manufactured for AUSTROADS by the Road Transport Authority (RTA) in New South Wales (NSW), Australia in 1984. One of the machines was purchased by the LTRC and delivered to the Pavement Research Facility outside Port Allen, Louisiana by LTRC in April 1994.

Figure 4.1 shows the schematic diagram of ALF. It is a 100 ft long, 55-ton structural frame with a moving wheel assembly that travels 0 to 12 mph on rails attached to the frame and is in contact with a 38-ft pavement section. At each end of the frame, the rail curves upward to permit gravity to accelerate, decelerate, and change the direction of the wheel assembly. Loads are applied in one direction, and the loads can be distributed laterally to simulate traffic wander in the wheel path.

12
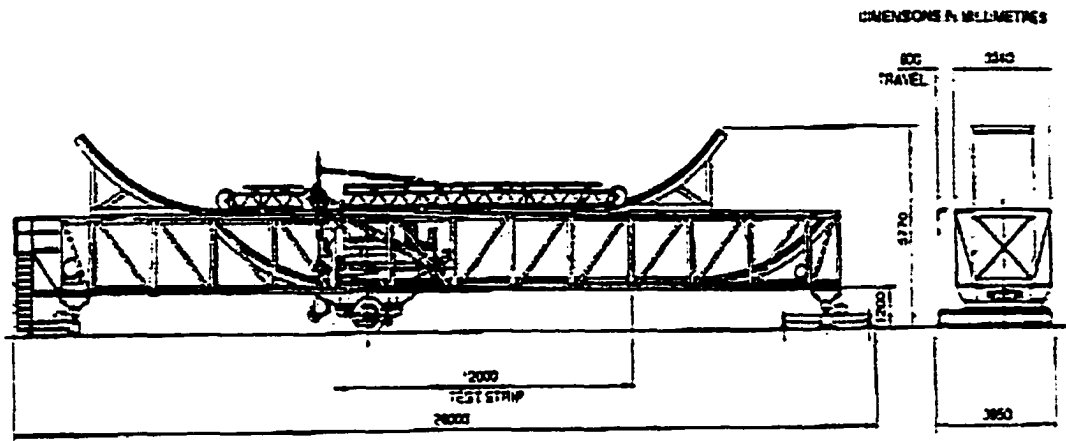
Figure 4.1 Schematic Diagram of ALF

A trolley assembly, Figure 4.2, is used to apply loads to the test pavement. The wheel assembly can be detached from the trolley through a bolted connection at the elevation of the load cells. The ALF has both single and dual tire wheel assemblies that model one-half of a single axle. The loads applied to the pavement can be varied from 9,000 to 22,500 lb by adding or subtracting ballast weights. Thus, dual or single tire, single axles can have loads ranging from 18,000 to 45,000 lb. Approximately 380 load cycles per hour or 8,640 load cycles per day can be applied.

The benefits ALF provides to a highway agency include the following:

- The ability to observe the behavior and the damage patterns that develop under traffic loads in a short period of time, thereby avoiding the need for costly, full-scale pavement tests like AASHO Road Test.

- The ability to compare performance of new materials with currently used materials.

- The generation of high-quality, reliable field data that cannot be obtained from other forms of full-scale testing.

- The ability to established links between results obtained from the field trials and laboratory material tests.
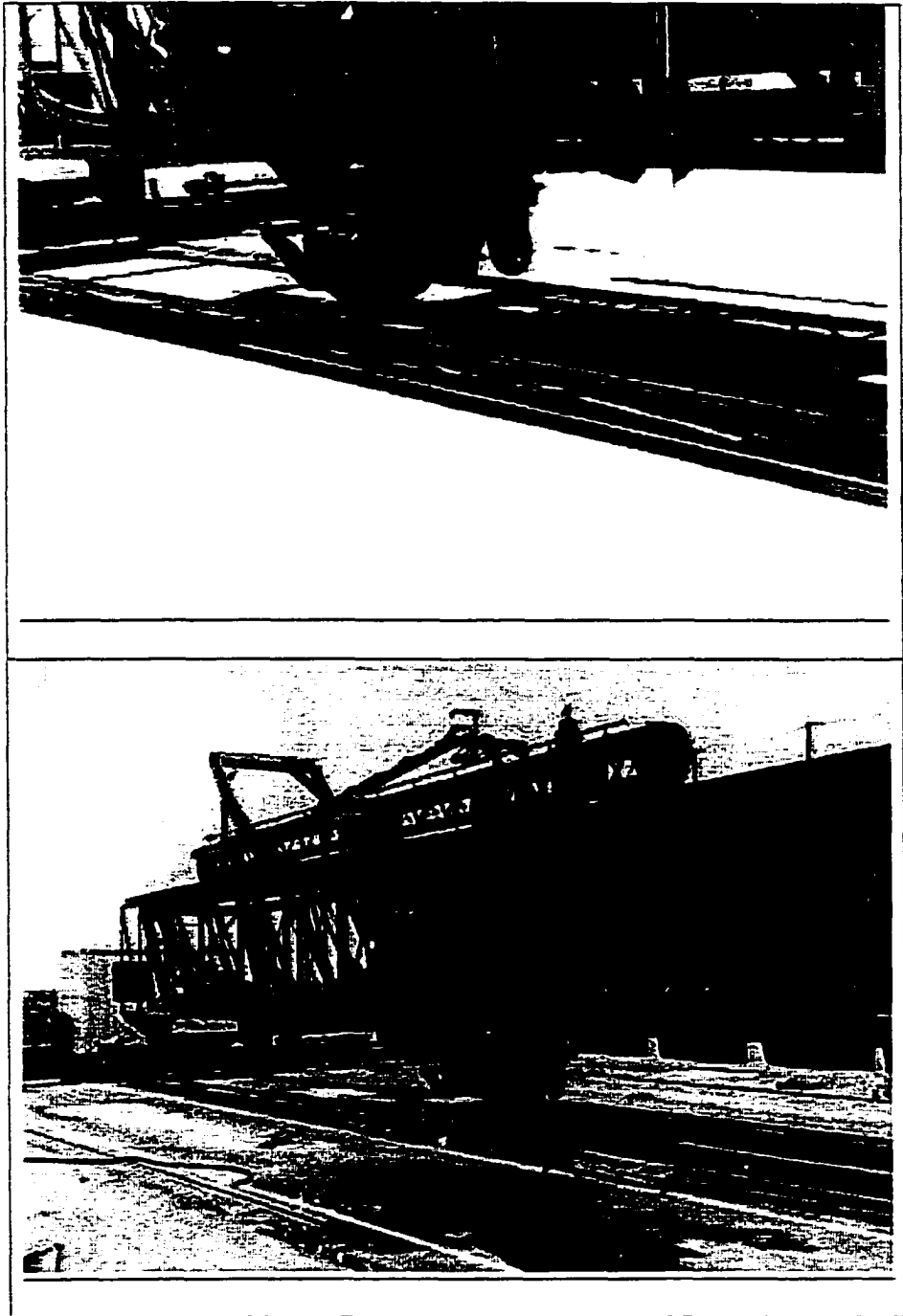
Figure 4.2 ALF Machine at Test Site

Summary of Some ALF Trials Conducted in Australia

In 1983 the Department of Main Roads, NSW produced the Accelerated Loading Facility (ALF) and it was proudly displayed at the PIARC1 World Road Congress in Sydney in front of the Opera House. This device looked industrial, yet it was the equivalent of space age technology for road research. The ALF is now the cornerstone of much of Australia's flexible pavement research and represents about a $1 million annual expenditure to AUSTROADS members and industry. As of June 1996, the Australian ALF has completed 17 trials and applied almost 25 million load cycles to about 90 pavement types [9]. The various trials have been identified by the locations and several are documented below:

1. Somersby trial [10]. This was the first trial with ALF. The focus of this trial was the proof testing of ALF. In this trial the ALF machine was confirmed as a reliable and effective device.

2. Benella trial [10]. The objective of this trial was to evaluate the high-quality dense crushed rock base pavement for heavy traffic. A heavy-duty unbound pavement comprising a double seal over 400 mm of crushed rock base and 170 mm of ripped sandstone subbase was tested. It was confirmed that the pavement would withstand the heavy traffic. Australian states incorporated higher compaction levels for unbound bases designed for heavy-duty pavements based on results from this trial.

3. Beerbuurum trial [10]. The main objectives of the trial were to compare thin (200mm) and standard (300mm) cement treated bases (CTB) and to compare the performance of pavements with or without bitumen heavy cure coat interlayers

between lifts of CTB and those constructed in one lift instead of two or three lifts[46]. This trial led to improved construction practices to establish the bond between lifts of CTB.

4. Beerbuurum II trial [11]. The objectives of the trial were to compare the performance of two thickness of recycled sandstone bases, to determine the effects of bitumen and bitumen/cement stabilization on the performance of a reconstructed high-quality crushed rock pavement, to compare the performance of crushed rock pavements constructed at different moisture/compaction conditions, and to determine the number of axle load that could be carried by a typical crushed rock pavement (300 mm thick) subjected to ALF under single axle dual-wheel loads of 40, 60 and 80 KN.

5. Prospect trial [12]. This trial addressed the performance of blast furnace slag as a base material and as a stabilizing agent. The successful performance of the blast furnace slag as a base was confirmed and specifications for road base materials were adjusted to permit wider use of the slag materials.

6. Callington trial [13]. This ALF trial was the first trial to address the relative performance of variety of asphalt surfacings in the context of pavement rehabilitation. The findings of this trial were compared with conventional binder.

7. Mulgrave trial [14]. In this trial, asphalt fatigue relationships were developed for three different fatigue cracking levels of a hot mix asphalt pavement over a cement treated crushed rock subbase course.

8. Brewarrina ALF trial [15]. This trial was conducted to examine the performance of pavements made with a geo-textile reinforced surface seal. The guidelines were

established for the design and construction, maintenance, and management of the geo-textile reinforced surface seal pavements.

9. Field Trials at Cooma [16]. In 1990 an investigation commenced into the feasibility of deep-lift stabilization of granular pavements to satisfy the structural design requirements of heavily-trafficked rural pavements. The investigation had taken into consideration construction techniques that had been developed from pilot and full-scale trials in NSW in co-operation with industry. Using this stabilization techniques, it was estimated in 1994 that savings of 20-40% over the cost of granular overlays could have been achieved in NSW which translated into a $4M-$6M per annum saving for a $20M rehabilitation program. The Cooma ALF trial was conducted from May to October 1994 adjacent to the Monaro Highway some 20 km north of Cooma in southern NSW. The objectives of the trial were to establish the performance of deep-lift recycled pavements, using stabilization equipment now available, over subgrades of relatively low and relatively high strengths; to gain a better understand of the distress mechanisms and hence possible interventions to extend pavement life, and to determine how pavement performance depends on stabilization depth; and further to compare the observed pavement lives under accelerated loading with fatigue lives predicted by STRAND6, an Australian general purpose finite element analysis package in a Windows format. The project was very successful and gained much interest from overseas pavement engineers. The final report [16] and a subsequent publication from the RTA [17] allowed the deep-lift process to continue in NSW with greater pavement reliability and minimization to construction risks.

10. Flyash Trials at Erraring. Pacific Power is conducting a major three-year research and development project to examine the possible use of flyash (a waste product from conventional coal-fired power generation) as a pavement material. The major aim of the project is to demonstrate the cost-effective use of flyash in road construction and to generate high quality data on the use of flyash, with a view to promoting the results widely to potential road builders. A major component of the project was an accelerated pavement loading trial using the Accelerated Loading Facility. The performance of cement-stabilized flyash base and subbase pavements placed on a coal haul road within the Erraring Power Station is being monitored. Given the performance of the cement-stabilized flyash base pavements under ALF loading, the cement-stabilized flyash base pavement should last well in excess of 20 years [18].

11. Dandenong ALF Trial on Marginal Materials. Austroads and various industry organizations are currently supporting the Accelerated Loading Facility Trial in Dandenong, east of Melbourne [19]. This $0.55 million trial includes a series of different binders in a very marginal soil from Victoria. The two major binders are a 2% portland cement and 2% bitumen, and a 4% slag/lime (85%/15%) cementitious blend. The pavement thickness is 200 mm on 2% lime stabilized (300 mm deep) clay subbase. In addition, testing was carried out on a crushed rock pavement from Boral Montrose quarries. Trafficking of the trial pavements was completed in March 1997 and the results are likely to be available in late July 1997.

ALF Trials in USA

Currently, four facilities in the United States use mechanical testing devices to conduct accelerated pavement tests with three using ALF machines. Table 4.1 gives the simple descriptions of the pavement testing machines used by these facilities.

Table 4.1 Pavement Testing Machine [20]

Organization (Machine)	Pavement Type Tested	Load (KN)	Rate Pass/hour	Date Opened	Funding Source
FHWA (Accelerated Loading Facility)	HMA	40-100	380*	1986	F**
Louisiana (Accelerated Loading Facility)	Composite	40-100	380	1994	S/F
Indiana (Accelerated Loading Facility)	HMA	40-90	1333	1991	S/F/I
California (Heavy Vechicle Simulator)	HMA	20-200	850	1995	S/F

**F=FHWA, S=State, I=Industry/Private
*Applying an 80-KN (18,000-lb) load at 380 passes/hour to a test section is equivalent to applying 2,100,000 ESALs per year

In September 1984, FHWA entered into an agreement with Department of Main Roads, Australia, to provide plans, specifications, and technical assistance for the construction of an ALF in the United States. Construction of the U.S. ALF began in July 1985 and the completed machine was delivered to Turner-Fairbank Highway Research Center (TFHRC) in August 1986 [21]. The ALF has been in nearly continuous operation since its delivery. From August 1986 through March 1989, the first phase of pavement research was conducted to establish operating and data collection procedures, to assess the rationality of pavement performance data obtained with the ALF, and to study the

pavement response and performance for a range of loads and tire pressures with particular emphasis on tire pressure [21].

In 1989 a field-testing program was conducted by Pavement Testing Facility (PTF) in conjunction with Montana and Wyoming to document the benefits, costs, and difficulties associated with using ALF to test in-service pavements and also to evaluate the measures taken in the western states to prevent premature rutting in asphalt pavement. This field trial demonstrated the mobility of ALF and provided experience with site preparation, traffic control, and site restoration [22].

The second phase of the initial ALF trial started in January 1990 and the main objective was to study the effect of wide-based single tires as compared to dual-wheel tires on pavement performance. The performance data of this trial showed that the replacement of conventional dual-wheel tires with wide-based single tires carrying the same load would produce four times the fatigue damage and two times the rutting as occurred when dual-wheel tires were used.

Since 1993, the two FHWA ALFs, have been used to assist the highway community in validating Superpave binder tests and specifications, Superpave mixture tests and performance models, and other laboratory tests that have been developed to predict the performances of asphalt mixtures. To accomplish the objective, 48 sites were constructed. The pavements were tested under conditions which promoted either rutting or the formation of fatigue cracks. The asphalt binder and mixture tests were validated using the results from these pavement tests [23].

The ALF Trials in Louisiana

The first ALF trials in Louisiana started in January 1986. The Louisiana pavement research facility in Port Allen uses an ALF machine to simulate traffic loads on several full-scale pavement test sections. The effort was focused on improving pavement base course design. The objective of this trial was to evaluate the performance characteristics of the historically prevalent in-place soil cement stabilized base construction and several promising alternative materials. Nine pavement test sections were constructed. The testing was divided into three phases, each phase consisting three pavement test sections. Phase 1 testing incorporated crushed stone alternatives to soil cement base. Phase 2 was designed to compare the performance of the plant-mixed stabilized soil cement design and construction with that of in-place soil cement. Phase 3 included a comparison of existing in-place soil cement design and construction procedures with that of a plant mixed soil cement process using a reduced cement content [25]. Results from this first ALF experiment can be found in [26], [27], and [28].

The comparative performance of rubberized asphalt hot mix is the second ALF trial at Louisiana. This trial started in March 1999 and ended in December 2000. A detailed description of this trial is presented below.

The third trial currently under testing involves comparing the performance of stone/RAP interlayers, and the fourth trial being planned focuses on SUPERPAVE mixtures.

Pavement Test Lanes

In the field accelerated loading (ALF) evaluation, three test lanes were constructed (Table 4.2). Lane 1 was designed to have a 1.5 inch asphalt rubber HMA

(AR-HMA) wearing course, a 2-inch conventional binder course, and a 3.5 inch conventional Type 5A base course. Lane 2 was designed to have a 1.5 inch conventional wearing course, a 2-inch conventional binder course, and a 3.5 inch AR-HMA base course. Lane 3 was designed as the control lane consisting of a 1.5 inch conventional wearing course, a 2.0 inch conventional binder course, and a 3.5 inch convention Type 5A base course. All three lanes are placed on a 8.5 inch crushed stone subbase course sitting above 10 inches of soil cement with 8% cement [2]. Table 4.2 shows the structure of the cross sections of test lanes.

Table 4.2 Structure of the Planned Test Lanes

Lane 001	Lane 002	Lane 003*
1.5" Wearing Course (Type 8F) Wet Rouse	1.5 Wearing Course (Type 8F)	1.5" Wearing Course (Type 8F)
2.0" Binder Course (Type 8)	2.0" Binder Course (Type 8)	2.0" Binder Course (Type 8)
3.5" Base Course (Type 5A)	3.5" Base Course (Type 5A) Wet Rouse	3.5" Base Course (Type 5A)
8.5" Crushed Stone	8.5" Crushed Stone	8.5" Crushed Stone
10.0" Soil Cement	10.0" Soil Cement	10.0" Soil Cement
38.0" Select Soil/ Embankment	38.0" Select Soil/ Embankment	38.0" Select Soil/ Embankment

*Lane 003 is the Control Section

Description of Pavement Materials

Aggregate

A siliceous limestone aggregate, commonly used in Louisiana, was used in this project. The No.5, No. 67 and No. 78 coarse aggregates and No. 11 screenings were siliceous limestone supplied by Vulcan Materials Company, from Gilbertsville, Kentucky. The coarse siliceous sand was supplied by Quick Sand and Gravel from Waston, Louisiana. Table 4.3 lists the properties of the aggregates.

Asphalt Cement

LaDOTD specifies that PAC-40 asphalt cement, typically modified with an elastomer, be used on high-volume roadways in binder and wearing course mixtures. An AC-30 was used for the conventional Type 5A base course mix and also as the base asphalt cement blended to produce the rubber-modified asphalt. A "wet process" asphalt rubber binder was produced using a No. 80 mesh powdered rubber. The AC-30 met a PG 64-22 specification; the CRM/AC-30 blend met a PG 70-22 specification, as did the PAC-40. Table 4.4 shows the properties of the various binders used in this study.

Mix Design

The mixes were designed using the Marshall mix design procedure. The wearing course mixtures had a nominal maximum aggregate size of 19 mm, the binder and the base courses, 25mm. A similar aggregate structure was used for both the binder course and base course mixtures. All the mixtures contained 20% RAP and the gradations were on the "fine side" of the maximum density line. Table 4.5 shows the properties of the mixes.

Table 4.3 Consensus Aggregate Properties [4]

| Aggregate | | FAA* | Sand | Flat & | CAA** | Friction | LA |
Source	Type	Method	Equiv.	Elong % 5:1	+ two faces	Rating	Abrasion
Limestone	No.5			3	100	II	20.1%
Limestone	No.67			3	100	II	20.1%
Limestone	No.78			2	100	II	20.1%
Limestone	No.11	47	44				
Quick	Coarse sand	43	61				
Mamonth Drive RAP	RAP				100		

FAA: Fine Aggregate Angularity
CAA: Coarse Aggregate Angularity

ALF Loading History and Surface Data Collection

ALF Loading History

To simulate the highway traffic, the ALF loads were applied only in one direction and were normally distributed about a 32-in wheel path. The magnitude of the ALF loading varied with number of loading plates. At the beginning of the test, a 10kip load was applied through dual-wheel tires with tire pressure maintained at 105 psi. The initial 10kip load was applied for a period of time and then the load is increased to 12.3kip, then to 14.4kip at the same tire pressure until the test lanes failed. The loads applied to the three lanes are shown in Table 4.6 with the load history shown in Figure 4.3. The loading was applied alternatively between the test lanes at approximately 25,000 passes to minimize the relative environmental effects occurring during the loading period. Rutting

of 0.50 inches or a decrease in PSI to 2.3 was considered to be the failure criteria for the pavement.

Table 4.4 Binder Test Summary [4]

Description	AC-30	AC-30 w/ CRM	PAC-40	Specs.	AASHTO Method
Original Binder					
Rotational Viscosity; Brookfield, Pas., 135°C	0.463	3.10	1.05	3.0	TP48
Force Ductility, ratio of final/max load	Fail	Fail	Pass	0.3	
Dynamic Shear Rheometer, DSR, G*sinδ, kPa, @10rad/s					
64 °C	1.7274	3.0659		1.0min	TP5
67 °C	1.2146		2.7328	1.0min	TP5
70 °C	0.8405	2.3991	1.8974	1.0min	TP5
76 °C		0.8914	1.0156	1.0min	TP5
RTFO (TFO for AC 30 w/ CRM)					TP240
% Loss		0.1	0.187	1.0max	TP240
64 °C		6.6001	—	2.2min	TP5
67 °C	3.488	4.2759		2.2min	TP5
70 °C	2.2942	3.218	3.2058	2.2min	TP5
76 °C		1.7412	1.8564	2.2min	TP5
PAV					
DSR, G*xsinδ, kPa, @10rad/s (25°C)	3628.3	2122.6	3175.1	5000 max	TP5

Table 4.5 Marshall Properties of the Mixes [4]

TEST DESCRIPTION	ASPHALT MIX DESCRIPTION			
	Type 8 Wearing P40	Type 8 Wearing CRM	Type 5 Base AC30	Type 5 Base CRM
Theoretical SG	2.531	2.531	2.533	2.531
Gmm	2.493	2.509	2.507	2.509
% AC By Weight	4.0	4.0	3.5	3.5
% AC By Volume	9.4	9.4	8.3	8.2
% Voids Total Mix	3.9	4.4	4.0	4.6
%VFA	70.8	68.2	67.5	64.0
%VMA	13.3	13.8	12.3	12.8
Unit Wt. Total Mix, pcf	151.8	151.0	151.8	150.6
Stability, lbs	2430	1904	2711	2455
Flow, 0.001 in.	9	19	10	7

Table 4.6 ALF Passes Applied To Test Lanes

No. of Passes (X 1000)	Total Load, Lbs. *	ESAL Factor	ESALs (X 1000)	Cumalative ESALs	Date Load Applied
0 - 400	9,750	1.377	550.80	550,800	3/5/99
400 - 500	12,050	3.213	321.30	872,100	10/4/99
500 - 650	14,350	6.463	969.45	1,841,550	12/6/99
650 - 750	16,650	11.713	1,171.30	3,012,850	4/14/00
750 - 800	18,950	19.655	982.75	3,995,600	10/9/00
800 - 850	21,250	31.079	1,553.95	5,549,550	12/18/00

* Each addition load increment adds 2,300 lbs to the total load.

Surface Data Collection

Field measurements included the periodic collection of cracking, transverse and longitudinal profile, deflection data, and temperatures. The ALF loading was stopped periodically for maintenance, and surface measurements were made at those times.
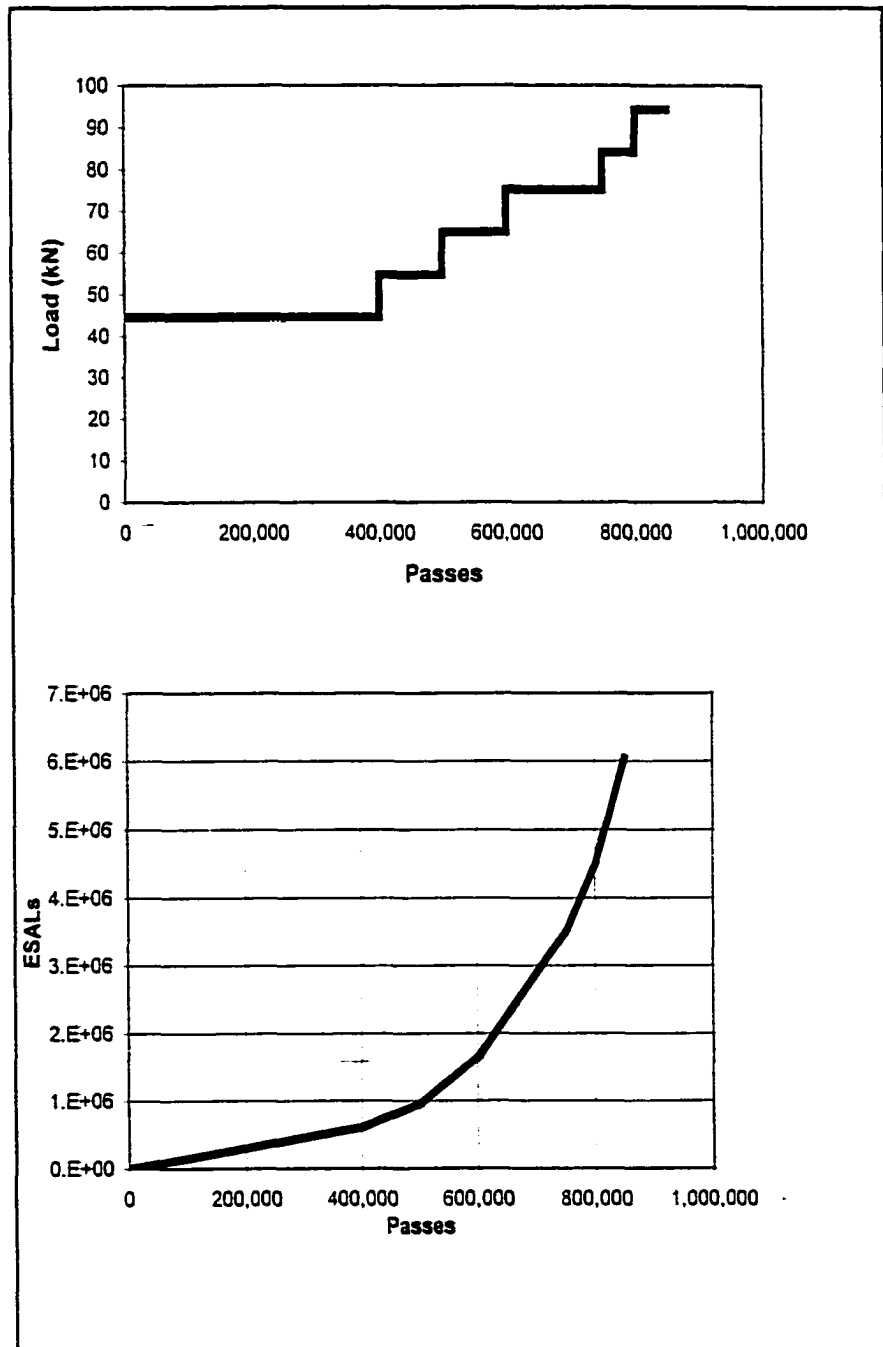
Figure 4.3 ALF Loading History

The transverse profile data were secured using the ALF profilograph, which consists of a linear variable differential transformer (LVDT) mounted on a metal

carriage. It moves transversely across the pavement on a metal frame. The metal frame can be positioned along the pavement section between two rails mounted on the pavement surface, outside the trafficked area. Generally, the profile data were collected approximately every 25,000 passes of ALF machine. For each test lane, measurements were taken at eight stations, 48 inches apart. The average rut depth is calculated from the transverse profile and slope variance is calculated from the longitudinal profile data.

Deflection testing was conducted on a periodic basis using the falling weight deflectometer (FWD). The FWD data were used to backcalculate the moduli of each layer of the test sections. Applying an impulse force generated from two mass assemblies in which the falling weight is dropped onto a second weight/buffer combination created the deflection measurement. The measurements were performed on the centerline of the loading path of each pavement test section at 11 stations spaced at intervals of 5 ft. along the centerline.

The ALF data acquisition system being used for this experiment is capable of measuring 25,000 samples per second. It has up to 512 channels and 64 megabytes of internal non-volatile onboard memory. All the functions are computer controlled [4].

A Campbell Scientific Weather Station was installed at the northeast corner of the test bed to acquire weather data [4]. The weather station updates itself every 10 seconds, records the data every hour, and records: (1) temperature, (2) relative humidity, (3) wind direction and speed, (4) solar radiation in watts per meter squared, (5) barometric pressure, and (6) rainfall.

CHAPTER 5

NUMERICAL SIMULATION OF ALF TEST LANES

Review of Numerical Simulation of Pavement Structures

Numerical simulations of flexible pavements are important for understanding and extending the results of laboratory and field studies [29]. Structural analysis of pavements is usually performed to calculate responses such as stresses, strains and deflections in a layered pavement structure. The methodologies for calculating these pavement responses can be categorized as: multilayered elastic methods, multilayered viscoelastic methods, and the finite element methods.

The multilayered elastic method models a pavement as a series of layers, each of them assumed to be horizontally continuous with materials which are isotropic, homogenous, and elastic. Each layer has definite thickness except for the bottom layer, which is assumed to be semi-infinite in depth. The surface loading is represented by vertical contact pressure uniformly distributed around a circular area. Poisson's ratio and elastic modulus are the two critical material parameters. A number of computer programs, such as BISAR, CHEV and ELSYM5, were designed to calculate stress and strain distributions in the pavement system using this method.

Layered elastic analytical solutions over simplified the asphalt material behavior by assuming linear elasticity. Multilayered viscoelastic methods are similar to the

29

multilayered elastic method, but the material properties are time and temperature dependent. Software such as VESYS includes viscoelastic models for the asphalt concrete and linear elastic or nonlinear elastic models for the base course and subgrade materials [30].

Finite element method (FEM) is another alternative technique in which the body to be analyzed is divided into a set of finite elements connected at their nodal points. The continuous variation of stresses and strains in the body is represented by an assumed linear or quadratic displacement function over each finite element. For a given element geometry and constitutive equation of material behavior, the element stiffness matrix is then established using the principle of virtual work. The global structural stiffness can then be formulated by integrating the individual element stiffness matrices. As a result, a set of simultaneous equations, in terms of a relationship between unknown displacement of nodes and loading force, is formed. Solving these equations using Gaussian elimination produces all of the nodal displacements. With the displacement of all the nodal points known, strains and stresses within each element can then be calculated.

FEM is most useful in calculating the response of pavement structure when pavement material behavior is nonlinear elastic, viscoelastic, or elasto-plastic. Several software programs can be used for the analysis. For example, ABAQUS is a general-purpose finite-element program that can solve problems ranging from relatively simple linear analyses to the most challenging nonlinear simulations. Zaghloul and White [31] applied three dimensional finite element analyses to simulate dynamic traffic loads using ABAQUS. Wathugala and Huang *et al.* [29] analyzed the behavior of geosynthetic-reinforced flexible pavements in a finite element model by using ABAQUS.

ILL-PAVE [32] and FLEXPASS [33] are two software programs which use finite element method to predict pavement structural behavior. Lytton and Tseng calibrated the rutting and fatigue models in FLEXPASS by comparing the actual measurements from 12 AASHO Road Test sections [42] to the predicted distress from FLEXPASS [34]. Hoyt *et al.*, compared predicted performance of asphalt-rubber concrete to that of conventional hot mix asphalt in airfield runways using FLEXPASS [8].

In this study, FLEXPASS is used for pavement performance prediction. It is the only finite element program that has (1) the capabilities to include multiple tire – multiple axle assemblies, (2) the ability to predict distress, and (3) the ability to represent actual tire contact pressure distributions. FLEXPASS has the ability to include seasonal variations of material properties.

Overview of FLEXPASS

FLEXPASS is a finite-element program adapted by Lytton and Tseng of the Texas Transportation Institute to accommodate multiple wheel loads and at the same time employ stress dependent material characterization models. It is an extension of ILLI-PAVE, which was originally developed by Wilson and Duncan and further modified by the Department of Civil Engineering, UIUC in 1982 [33].

FLEXPASS is a finite element program that can analyze flexible pavement responses and predict pavement performance in terms of rutting, fatigue cracking, slope variance and PSI loss. A simplified framework for FLEXPASS is given in Figure 5.1.

The advantages of FLEXPASS are as follows:

* The finite element method permits pavement layers to be described using non-linear stress-strain relationships.

- Interface slip elements are included to model slip between pavement layers.

- The pavement material properties can be varied seasonally.

- The loading configurations can vary from single or dual tires on single or tandem axles.

- The prediction algorithms use calculated responses from the FEM to predict fatigue cracking, rutting, and serviceability loss.

Description of Analytical Model

The development of a numerical simulation of flexible pavements involves many idealizations of the problem, including geometry, loads, material property (constitutive) models, and selection of the numerical technique. In this project, the pavement structure will be modeled three dimensionally by using a 2-D half space of a finite solid of revolution. The half-section structure to be analyzed is divided into a set of quadrilateral finite elements, which are then divided into four triangles by the program to produce a set of elements. The tire contact pressures are assumed to have a vertical uniform distribution over a circular contact area. Material properties such as density, Poisson's ratio, earth-pressure coefficient at rest, and resilient modulus are required as inputs in the program. Two significant material response capabilities, both linear and nonlinear stress-strain relations, are taken into account. The failure criteria for granular and fine-grained soils are considered.

The finite element model used in FLEXPASS is shown Figure 5.2.
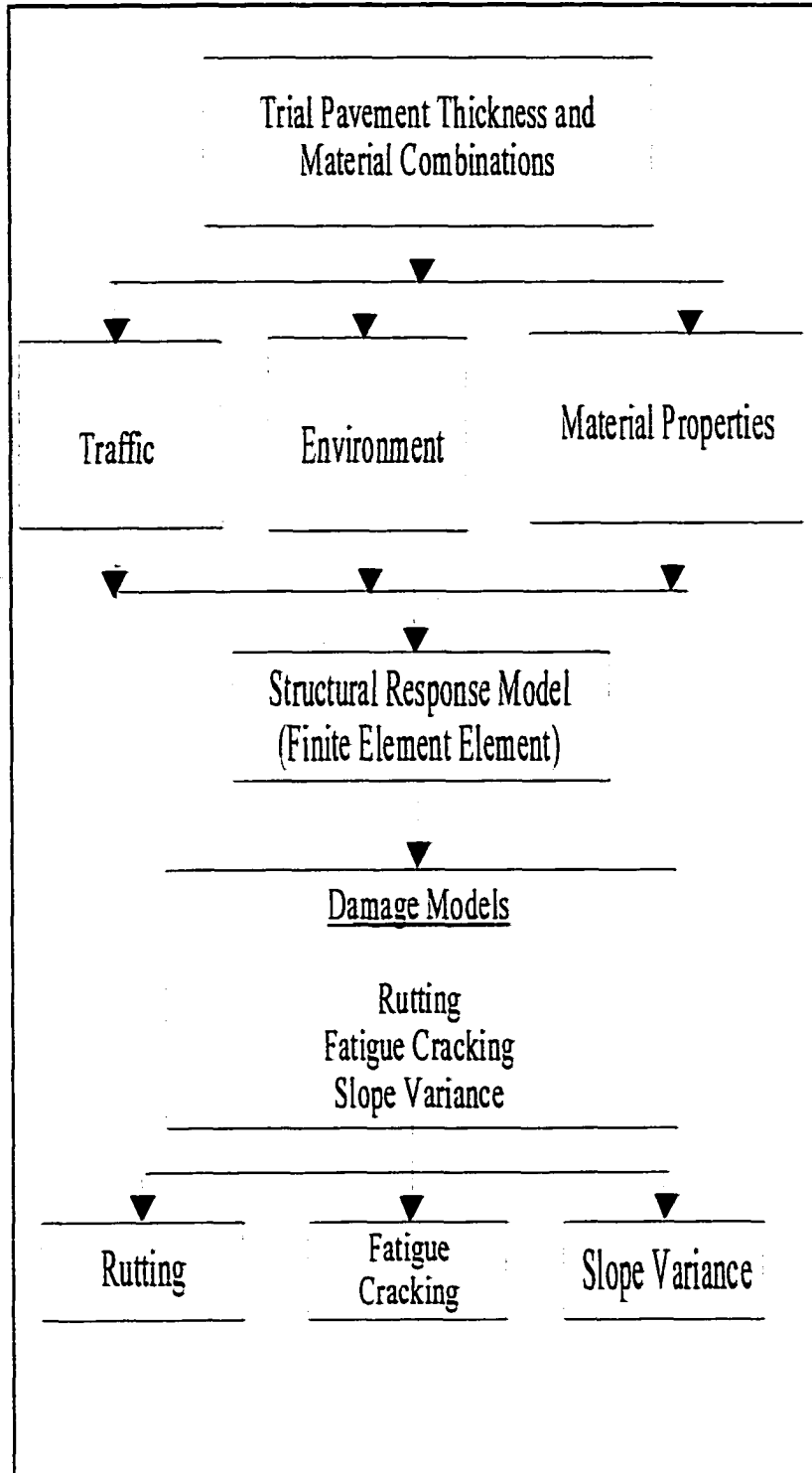
Figure 5.1 Simplified Framework of FLEXPASS [33]
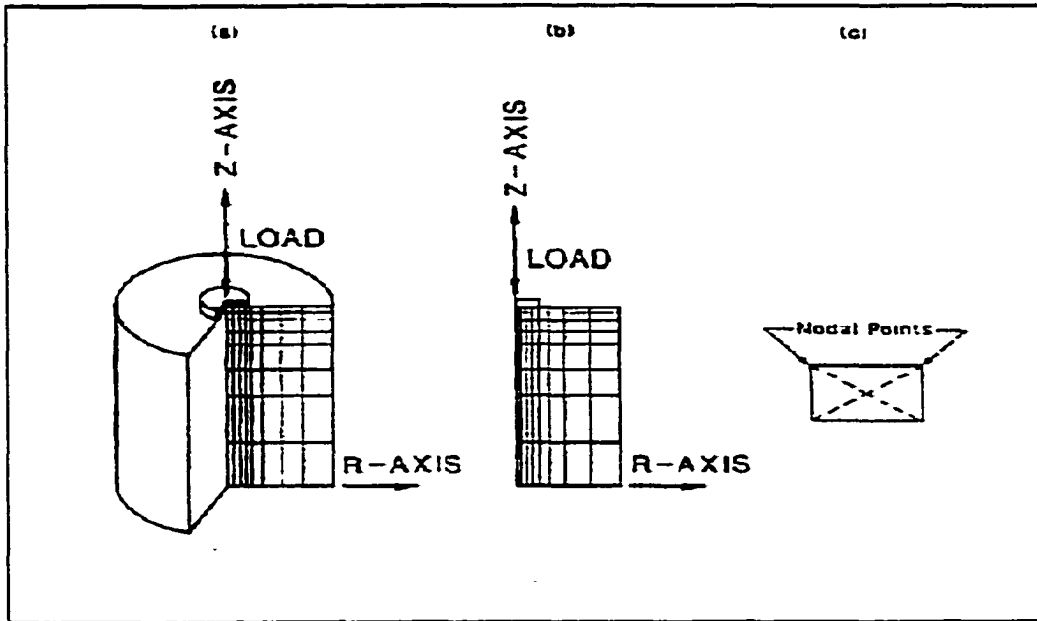
Figure 5.2 Finite Element Model in FLEXPASS: (a) 3-D view, (b) Half-section, (c) Typical Element [35]

Four alternative models are available for describing the resilient modulus of the pavement materials [36]:

1. Linear Resilient Modulus. This model assumes that the material has a linear resilient modulus relationship with temperature. Hot mix asphalt and rubberized HMA are characterized using this model.

2. Bulk Stress Dependent Modulus. This model describes granular materials in which the resilient modulus is a function of bulk stress. The equation is:

$$M_R = K_1(\Theta_3)^{K_2} \qquad (5.1)$$

if $(\sigma_1 / \sigma_3) < K_3$ and $\sigma_3 > K_4$

where

Θ_3 is the bulk stress

K_1, K_2 are the material regression coefficients.

K_3 is the maximum allowable stress ratio, and

K_4 is the minimum horizontal compressive stress ratio.

3. <u>Confining Pressure Dependent Modulus</u>. This model describes the behavior of a granular material in which the modulus is a function of the confining pressure, σ_3, and expressed as

$$E_r = k_1 (\sigma_3)^{k_2} \qquad (5.2)$$

where K_1 and K_2 are regression constants determined from triaxial compression test results.

4. <u>Deviator Stress Dependent Modulus</u>. This model describes a soil material in which the modulus is a function of the deviator stress, and is represented by two intersecting, straight lines The resilient modulus is described by

$$E_r = X_1 + X_3 [\sigma_d - X_1], \text{if } X_1 > (\sigma_1 - \sigma_3) \qquad (5.3)$$
and
$$E_r = X_2 + X_4 [\sigma_d - X_1], \text{if } X_1 < (\sigma_1 - \sigma_3) \qquad (5.4)$$

In which
X_1 = Deviator stress (psi) at the break point
X_2 = Modulus value (psi) at the break point
X_3 = Slope of the left portion of the deviator stress-resilient
      modulus relationship
X_4 = Slope of the right portion of the deviator stress-resilient
      modulus relationship

Besides material modeling with nonlinear stress-dependent relations of pavement materials, a failure criterion based on the Mohr-Coulomb theory for granular materials and fine-grained soils is used to modify the calculated stresses so that they do not exceed the strength of the material. This criterion is accomplished in the program by setting numerical limits on the major and minor principal stresses which can be developed within the material layer. For the next iterative step, the modified stresses are then used in a

stress-dependent resilient modulus relation, and then re-analyzed. A reasonable degree of convergence usually occurs in several iterations.

2-D Finite Element Models by Using FLEXPASS

Geometric Models

Figure 5.3 shows the finite element mesh used in this analysis. A set of quadrilateral finite elements has been used throughout the mesh. The total number of elements is 720, the number of nodal points is 775, the number of columns in the mesh is 24, and the number of rows in the mesh is 30. There are five material layers, namely surface layer, base layer, crushed stone subbase layer, soil cement layer, and embankment/subgrade layer. The number of elements used to model the behavior of each material layer is the surface course, 148; base course, 120; crushed lime stone layer, 120; soil cement layer, 72; embankment layer, 264.

Loading Models

FLEXPASS has a capability of accommodating single, tandem, or triple axles with single or dual tires. Since the ALF load is applied with a single dual-wheel, the tire contact pressures are assumed to have a vertical uniform distribution over a circular contact area. The uniform load is equal to the tire inflation pressure. The traffic applications were input as average 9 kip passes per day (equivalent to one 18 kip single axle load) according to the ALF loading daily report. For the analysis, the 12,050 ~ 21,250 kip ALF wheel loads applied were converted to equivalent 9 kip passes.

Seasonal Pavement Temperatures

As material properties often vary with different seasonal air temperatures, the number of seasons selected should reflect the effect of the environment on the properties
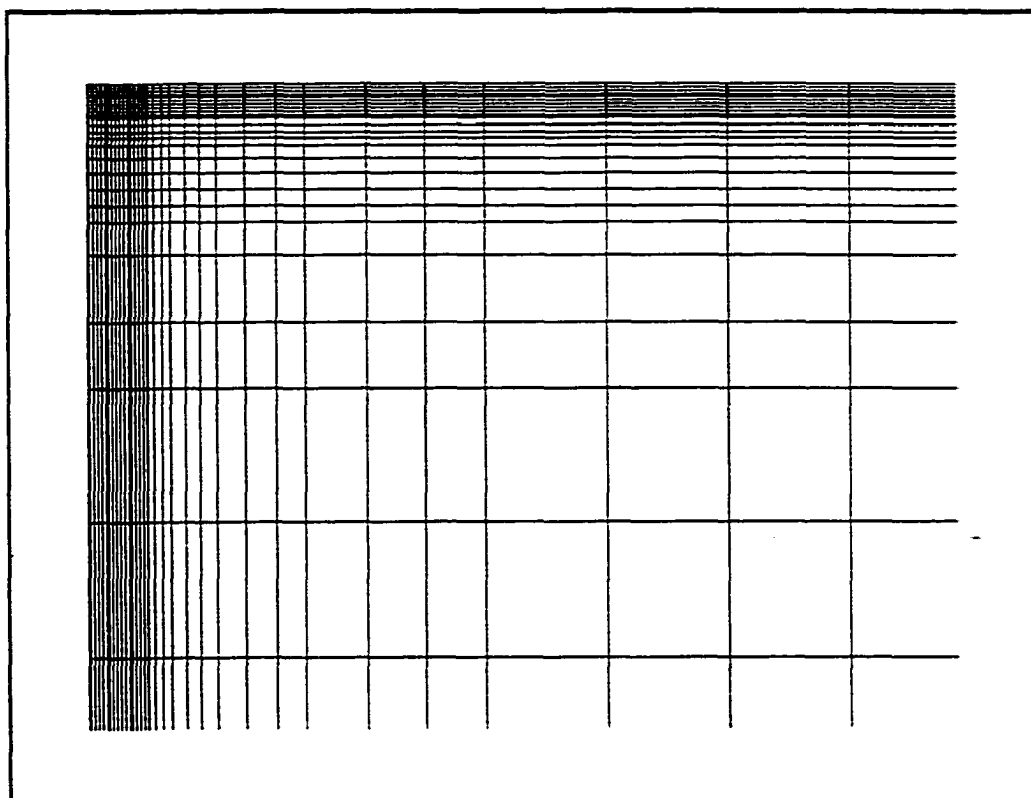
Figure 5.3 The Finite Element Mesh for FLEXPASS

of various pavement materials included in the ALF testing lanes. Some of the procedures

available for calculating pavement temperature include Shell air-HMA temperature chart,

Asphalt Institute charts, and University of Illinois equations. The pavement temperatures

can be determined using any of the above procedures and then input to the program. The

program can accommodate up to 12 different seasonal periods.

Structural Material Properties

      FLEXPASS requires the following material properties inputs: density, Poisson's

ratio, earth-pressure coefficient at rest, and modulus of elasticity for linear or non-linear

stress-strain relationships of each pavement component material. In addition, the program

also requires shear-strength characteristics of the granular and fine-grained materials.

- **Density.** The density of each layer is required to calculate the overburden pressure, i.e., body forces due to gravity. Since the modulus of some materials is stress dependent, the body force due to gravity cannot be neglected.

- **Moisture content.** Moisture-related pavement failures include excessive deflection, reduced load-bearing capacity, raveling and disintegration. Therefore, the moisture content for each season should be estimated and input for each unbound layer.

- **Poisson's ratio.** Poisson's ratio is defined as the ratio of the lateral strain to axial strain. It has an influence on the relative strains of the material in the unstressed and stressed state. In the present model, the value of Poisson's ratio is assumed to be constant for each layer of material.

- **Earth-Pressure Coefficient at Rest.** The earth-pressure coefficient at rest, K_0 is the ratio of lateral pressure to the overburden pressure when there is no resulting expansion or compression in the lateral direction. The use of K_0 in this analysis model is to calculate the lateral pressures, which are the overburden pressures multiplied by earth-pressure (either deviator stress or bulk stress) used to calculate the resilient modulus for the first approximation when the material is stress dependent. For soil material, a good approximation of K_0 is given by

$$K_0 = 1 - \sin\phi \qquad (5.5)$$

where ϕ is the internal friction angle.

- **Moduli of Asphalt Concrete and Asphalt-Rubber Concrete.** As previously mentioned, the modulus of asphalt concrete and asphalt rubber concrete changes

with temperature and frequency of the load. Since the load frequency for the ALF is constant, the resilient modulus is a function of temperature. The modulus-temperature relationships can be developed from a series of repeated load tests or static indirect tensile tests at different temperatures. Figure 5.4 shows typical plots of modulus versus temperature from several asphalt concrete mixes.

- **Modulus of Crushed Limestone Layer.** In this analysis, the crushed limestone layer is characterized by a bulk stress dependent modulus as described by Equation (5.1). Two constants, K_1 and K_2, are determined from a log-log plot of resilient modulus vs. bulk stress or confining pressure where K_1 is the intercept and K_2 is the slope of the linear regression curve. A typical relationship is shown in Figure 5.5.

- **Modulus of the Embankment Subgrade.** The modulus of the fine grained materials is represented by a deviator stress dependent modulus. The relationship was expressed by Equations (5.3) and (5.4). The laboratory tests on fine-grained soils have demonstrated the highly significant effect of deviator stress upon the resilient modulus as shown in Figure 5.6. As shown in Figure 5.6, the resilient modulus decreases rapidly as the deviator stress increases up to the break point of the bilinear curve, then the resilient modulus decreases slightly with a further increase of the deviator stress.

- **Modulus of Soil Cement.** In this analysis, the modulus of soil cement is constant since soil cement has a fairly constant modulus with respect to confining stress.
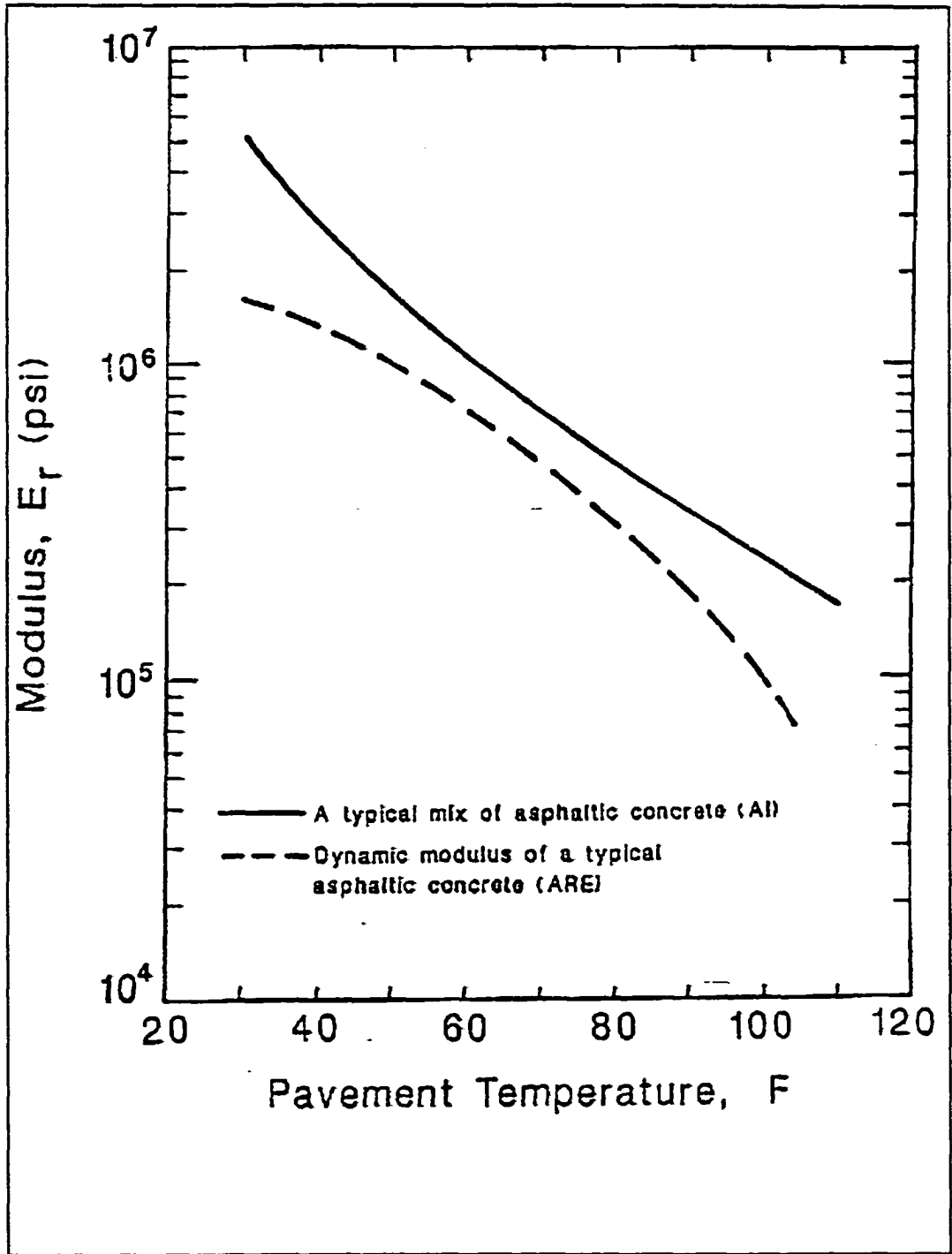
Figure 5.4 Relations Between Asphalt Concrete Modulus and Pavement Temperature [35]
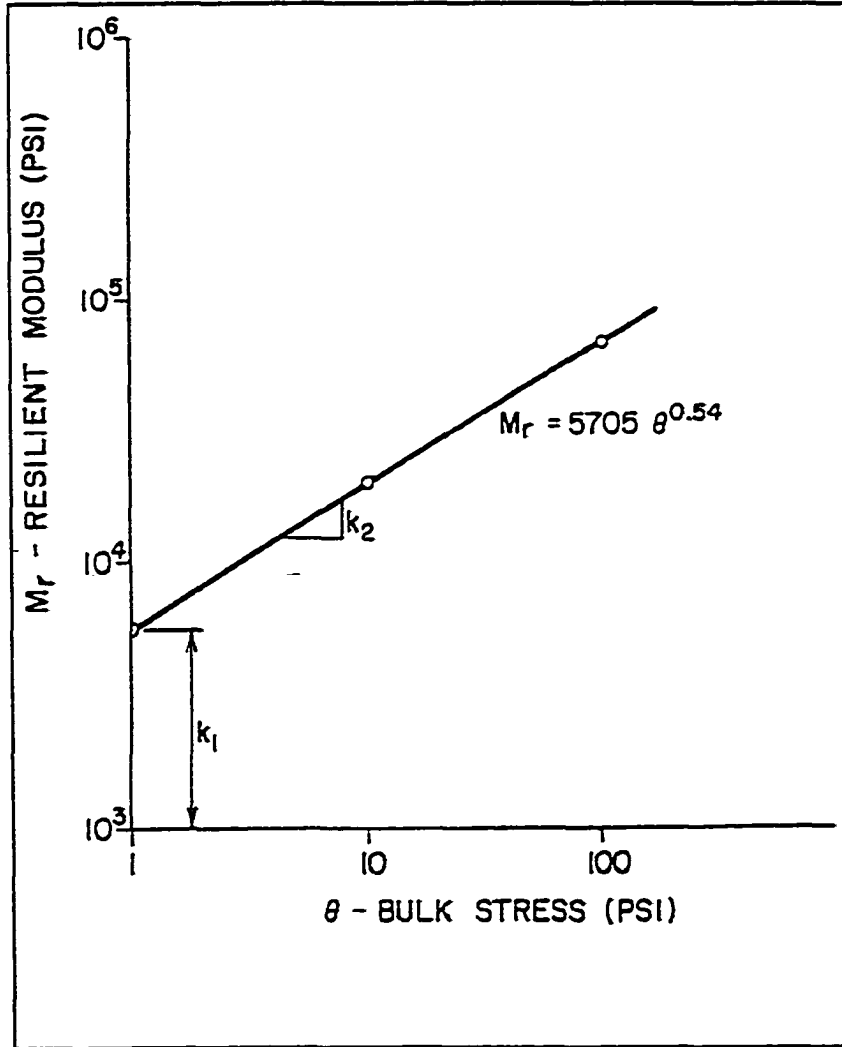
Figure 5.5 Variation of the Resilient Modulus of Granular Materials with Bulk Stress [35]
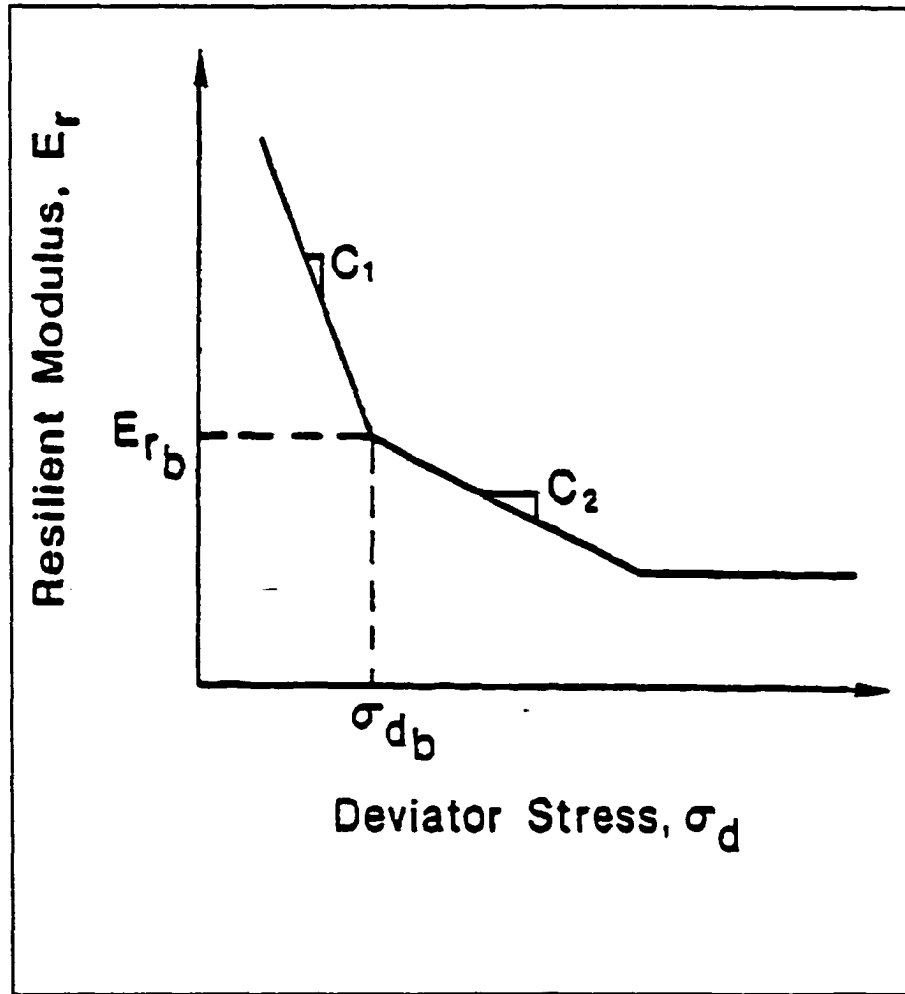
Figure 5.6 Variation of Resilient Modulus with Deviator Stress [35]

CHAPTER 6

SIGNIFICANT DISTRESSES FOR PAVEMENT PERFORMANCE

The structural deterioration of flexible pavement is usually related to two failure criteria, the development of ruts in the wheel paths and the load-induced cracking of the bituminous surface course. Rutting occurs in all layers and results both from permanent vertical strain and from lateral plastic flow in each layer. Fatigue cracking is considered the result of repeated flexural stresses causing large tensile strains at the bottom of the lowest asphalt bound course in the structure.

Rutting in Asphalt Pavements

Rutting is defined as the cumulative permanent deformation in the pavement layers or subgrade caused by consolidation or lateral movement of the materials due to traffic loads [37]. Pavement uplift may occur along the side of the rut. Rutting stems from the permanent deformation in any of the pavement layers or subgrade, usually caused by the consolidation or lateral movement of the materials due to traffic loads [38]. The biggest problem produced by rutting is hydroplaning, a phenomenon in which water in the wheel path causes fast moving vehicles to lose contact between the wheels and pavement surface causing loss of control.

Types of Rutting [36]

Rutting has long been considered as a problem on highway pavements. Rutting reduces road serviceability and causes serious traffic related safety problems. As wheel

loads and tire pressures of truck traffic on highways have increased in recent years, rutting has become more serious.

Rutting in asphalt pavement involves two different mechanisms and is a combination of densification (volume change) and repetitive shear deformation (plastic flow with no volume change). Densification can occur in any part of pavement structure including the asphalt surface layer(s), the base course(s) and the subgrade.

There are four basic causes of rutting [36]. The first type is *shear failure* in the base, subbase, or subbase layers. Based on experiments, Monismith reported that shear deformation is the primary cause of rutting [39]. The second type is *consolidation rutting*, which can occur in any of the pavement layers and can be contributed to poor compaction during construction, to an inadequate mix design, or to poor quality control. The third type is called *plastic flow rutting*, caused by poorly designed mix material being squeezed out from under the load. The fourth type is *pavement surface wear*, caused by abrasion of the surface under repeated wheel loading.

With the advent of higher tire pressures and heavier wheel loads in recent years, permanent deformation potential has increased. Many state DOTs pay special attention to curb rutting when designing and constructing asphalt concrete pavements. The use of asphalt rubber mixture appears to be one way to reduce the rut susceptibility of asphalt concrete mixtures.

Rutting Prediction Approaches

A number of procedures are available to estimate the amount of rutting from repeated traffic loading. They have been divided into three categories [35]:

- The use of elastic theory to predict stresses coupled with permanent strains determined by repeated load laboratory tests. In this approach, the permanent strain is assumed to be functionally proportional to the stress and repeated loadings. Rutting at the surface is calculated as the accumulation of the permanent strain in each layer from the results of structural analysis.

- The use of linear viscoelastic theory together with creep and recovery tests. In this approach, it is assumed that the increment of permanent strain with each load application is approximately equal to a fraction of the resilient strain. The resilient strains are calculated from the viscoelastic analysis of the pavement structure and the fraction of the resilient strain is determined from the creep and recover tests.

- The use of statistical regression analysis. This model is based on the statistical analyses that relate actual rutting which has occurred in a road test to elastic material properties and elastic responses calculated from the multilayered elastic program.

Both of the first two approaches mentioned above are based on the relationship between permanent strain and numbers of load repetitions derived from repeated load axial compression or creep and recovery tests.

Rutting Prediction Model

In this project, non-linear elastic theory will be used to predict stresses coupled with results from the lab repeated loading tests to predict the accumulated permanent strains of the pavement. The model for permanent deformation is based on an evaluation of the vertical resilient strain in each layer by the finite element method and on the

fractional increase of total strains for each material layer of the pavement as determined by the permanent deformation characterization. The finite element analysis is used to take the nonlinear stress-strain behavior of the materials into account.

In general, the relationship between permanent strain and number of load repetitions is represented by a straight-line on the log-log plot of permanent strain versus numbers of load repetitions. Two parameters that characterize this relationship are derived from the slope and the intercept of the straight line and used in the VESYS program [30]. However, it has been shown by other studies [40] that a three-parameter, nonlinear equation more accurately describes asphalt composite behavior due to permanent deformation. The equation relating the permanent strain to loading cycles is given by [35]:

$$\varepsilon_r = \varepsilon_0 e^{-(\rho/N)\beta} \qquad (6.1)$$

where

ε_r = permanent strain

N = number of load cycles

$\varepsilon_0, \rho, \beta$ = model parameters determined by regression from laboratory test data

These model parameters are used to define the permanent deformation properties of each structural layer in the test lanes. They are determined by fitting a curve that relates the cumulative permanent strain to the number of loading cycles from the data obtained from either creep and recovery tests or repeated load triaxial laboratory tests. Typical repeated load test results are shown as Figure 6.1.

According to Tseng [35], the physical meaning of this equation can be explained by the graph in Figure 6.1. The parameter ρ is the scale factor on accumulated permanent strain; a larger ρ means that it takes a large number of load applications to reach a given

level of permanent strain. The parameter β is a shape parameter for the permanent strain curve; values of β greater than 0.5 give a characteristic s-shape while values of β less than 0.5 produce a curve that gradually becomes asymptotic with x-axis.
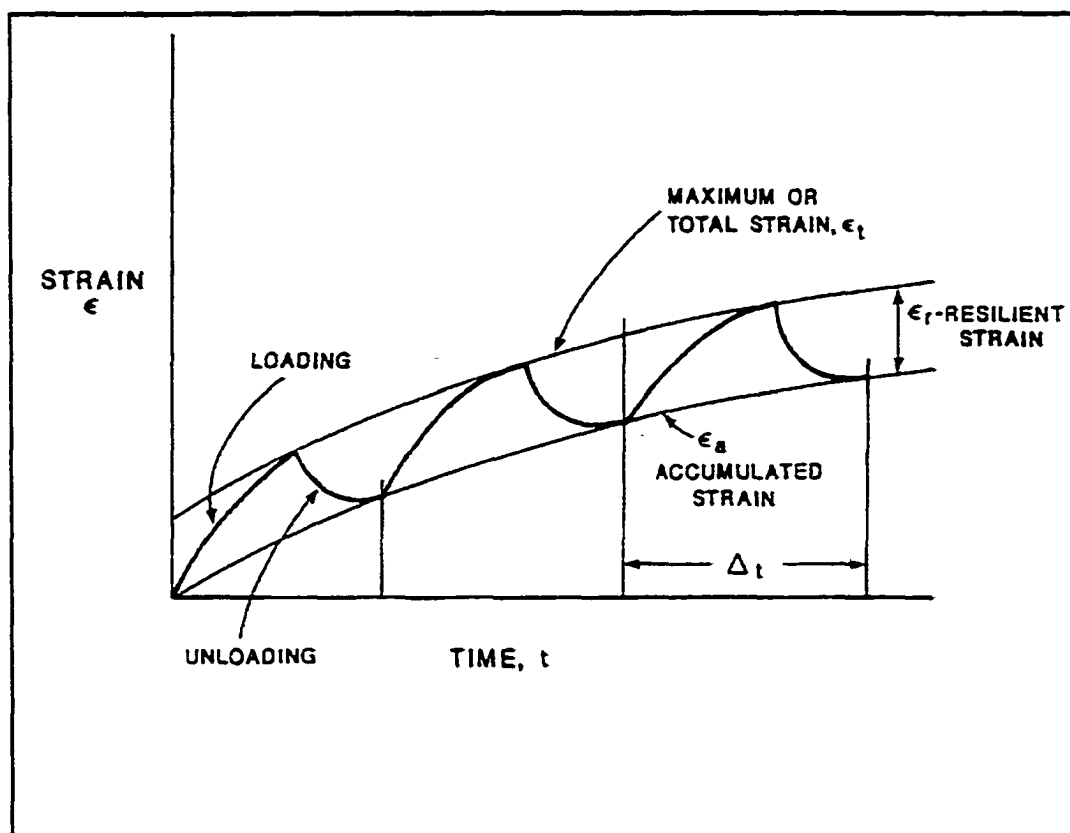
Figure 6.1 Typical Repeated Load Test Results

All curves pass through a common point where $N = \rho$, or at $\varepsilon_a = \varepsilon_0 * e^{-1} = 0.368\varepsilon_0$. Using this equation, the relationship between strain and load cycles becomes non-linear and therefore more accurately represents the material behavior. According to the studies comparing measured deformations and predicted values elsewhere, this model has been found to be applicable to all flexible pavement materials, including asphalt concrete, granular bases, and subgrade soils [39].

To calculate these three parameters for each ALF test material, in this study, repeated load compression tests were performed using the VESYS procedures for direct compression testing [35]. A plot of permanent strain versus loading cycles was made for each mateial tested to determine the shape of the curve and non-linear regression was used to calculate the three parameters. Details of the material permanent deformation characterization testing will be described later.

Fatigue Cracking in Asphalt Pavements

Alligator or fatigue cracking is a series of interconnected cracks caused by fatigue failure of HMA layers under repeated loading. The cracking generally initiates at the bottom of the HMA layer (or stabilized base) where tensile stress and strain are the highest under the wheel load. The cracks propagate to the surface initially as one or more longitudinal parallel cracks. After repeated traffic loading the cracks develop a pattern resembling chicken wire or alligator skin.

The presence of fatigue is an indication of the loss of structural (load-carrying) capacity in the pavement. Once cracking occurs at the bottom of the layer, it develops at an almost exponential rate.

Two different approaches are used to describe the fatigue behavior of HMA using laboratory test results [35]:

- The mechanistic approach.

- The phenomenological approach.

The mechanistic approach is based on the theory of fracture mechanics to arrive at the fatigue characterization. According to fracture mechanics theory, the stress intensity

factor, K, controls the rate of crack propagation since K takes into account the effect of external loads and geometry which, in turn, intensifies the stresses near the crack tip. Also, fatigue life can be described as a process of crack initiation, propagation, and ultimate fracture [35]:

$$\frac{da}{dn} = A(\Delta K)^n \qquad (6.2)$$

where
A and n are the fracture parameters, and
ΔK is the difference of the stress intensity factor that occurs at the crack during one load pass

The number of load cycles to failure, N_f is then expressed by[35]:

$$N_f = \int_{C_0}^{C_f} \frac{da}{A(\Delta K)^n} \qquad (6.3)$$

where C_0 is initial crack length, and C_f is final crack length.

The phenomenological approach is an empirical approach in which the fatigue characteristics of asphalt mixes are described by relationships between initial stress or strain and the number of load repetitions to failure. The fatigue life is measured by laboratory testing of a beam under controlled stress or controlled strain conditions, or by testing of a cylindrical sample loaded repeatedly along its vertical diameter.

In this project, the phenomenological regression approach was used to describe fatigue of the ALF test lane materials. This approach is the most common method for analyzing highway materials [41]. The fatigue cracking of a pavement layer is characterized using [35]:

$$N_f = K_1 (\frac{1}{\varepsilon})^{K_2} \qquad\qquad (6.4)$$

where

N_f = number of load applications to failure

ε = tensile strain at the bottom of the asphalt layer

K_1, K_2 = parameters of the fatigue model

This equation describes a straight line on a log-log plot of cycles to failure versus bending strain, where log K_1 is the intercept of the y-axis, and $-K_2$ is the slope of the straight line. K_1 and K_2 are influenced by such factors as the type of load, dimensions of the test specimen, loading rate, test type, temperature, and the properties of the mix, including air voids, aggregate gradation and type, asphalt content and viscosity, etc. K_1 and K_2 of each asphalt material is determined by the laboratory fatigue testing using the indirect tensile fatigue test at constant strain conditions [41]. This approach provides a reasonably simple procedure which has gained wide acceptance.

Slope Variance in Asphalt Pavements

Slope variance is defined as the variance of the slopes along the longitudinal profile of the roadway. A method to calculate the slope variance is based on the assumption that slope variance is a function of the spatial variations in the properties and thickness of the layer materials [35]. From this assumption, an auto correlation function of the permanent surface deformation is assumed. Kenis expressed the auto correlation function in terms of pavement deflection response and material variability [30] and showed that slope variance is equal to the negative second derivative of the auto

correlation function. The expression for the slope variance in terms of the variation of the load deflection response, rutting, and variance of rutting can be developed as [35]:

$$E[sv] = \frac{2B}{C^2} \text{var}[\delta_a]$$ (6.5)

where

$E[sv]$ = expected value of slope variance,

$\text{var}[\delta_a]$ = variance of rut depth, and

B and C = roughness properties.

Present Serviceability Index

The present serviceability index, PSI, as an indicator of pavement performance, was developed at the AASHO Road Test [42]. This index was predicted from measurements taken on the pavement surface, including rutting, slope variance, and cracking and patching. PSI was predicted from the following equation [35]:

$$PSI = 5.03 - 1.91 \log(1 + sv) - 1.38(\delta_a)^2 - 0.01\sqrt{\bar{c} + p}$$ (6.6)

where p is the area of patching in square feet per 1000 square feet.

$\bar{c}$ is the cracked area in square feet per 1000 square feet.

sv is the slope variance.

δ_a is the average rut depth, in.

CHAPTER 7

LABORATORY CHARACTERIZATION OF ALF TEST LANE MATERIALS

This chapter presents the laboratory testing program conducted to determine the material characteristics of conventional asphalt materials and rubber asphalt materials used for ALF test lanes. These material properties are used as input in the performance predictions of the ALF test lanes.

Overall Testing Objectives

As mentioned earlier, the material parameters must be defined for the rutting and the fatigue prediction models used in the analysis. Tests performed to measure these properties include:

- Repeated Load Compression Test (Permanent Deformation Prediction)

- Repeated Loading Indirect Tension Test (Fatigue Prediction)

Four materials were tested:

- T8WC (Conventional Type 8 Wearing Course)
- T8WC-CRM (AR-HMA Type 8 Wearing Course)
- T5A (Conventional Type 5A Base Course)
- T5A-CRM (AR-HMA Type 5A Base Course).

The tests on each of the four mixes were conducted to measure the properties of the materials at a range of temperatures and typical loading rates in order to simulate the seasonal temperature changes and different axle loads that occurred during the ALF

52

testing. Each of the tests will be described followed by typical test results for each of the four mixes tested. All of the specimen preparation and testing were conducted in the Engineering Materials Characterization and Research Facility (EMCRF) at LTRC.

The specimen preparation and testing were performed to obtain the material parameters needed in the performance prediction models so that a realistic comparison could be made between the performance of the AR-HMA and that of the conventional HMA and to evaluate the optimal position of AR-HMA in the pavement structure.

Specimen Preparation

Specimens were prepared using the Superpave Gyratory Compactor (SGC) from plant produced materials. All specimens of these four mixture materials prepared for testing were compacted in accordance with the standard procedures followed in the laboratories of LTRC. The specimen preparation facilities will be described in detail below.

The Superpave gyratory compactor (SGC) is a laboratory compaction device used in the Superpave mix design system. The SGC mold is 150-mm in diameter The SGC consists of the following main components as shown in Figure 7.1:

- Reaction frame, rotating base, and motor;

- Loading system, loading ram, and pressure gauge;

- Height measuring and recording system; and

- Mold and base plate.

In developing a mixture design, specimens are first mixed in a mixing bowl (Figure 7.2), mixing bucket (Figure 7.3) or a mini-pugmill mixer (Figure 7.4). Two

Superpave gyratory compactors (SGC), a Pine Instrument Model AFGC125X (Figure

7.5), and a Troxler Model 4140 (Figure 7.6) are available to compact the specimens.
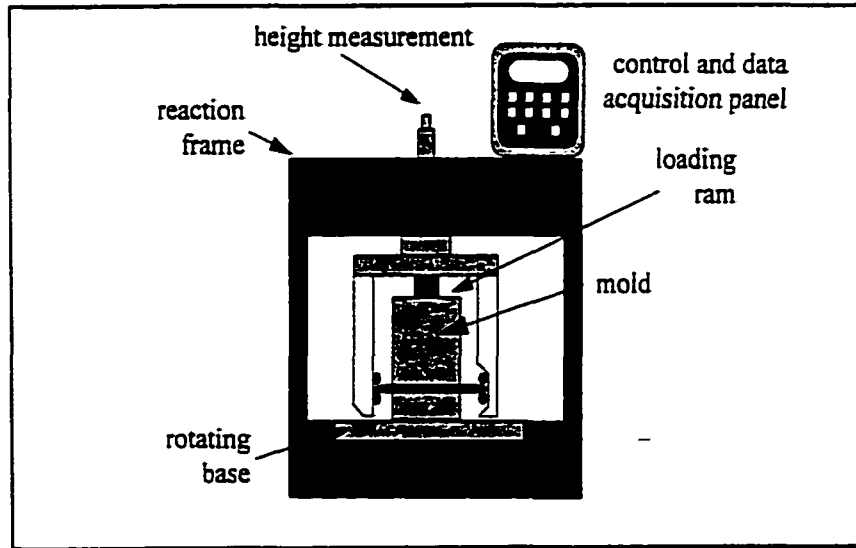
**Figure 7.1 Components of Superpave Gyratory Compactor
(Asphalt Institute, 1994)**
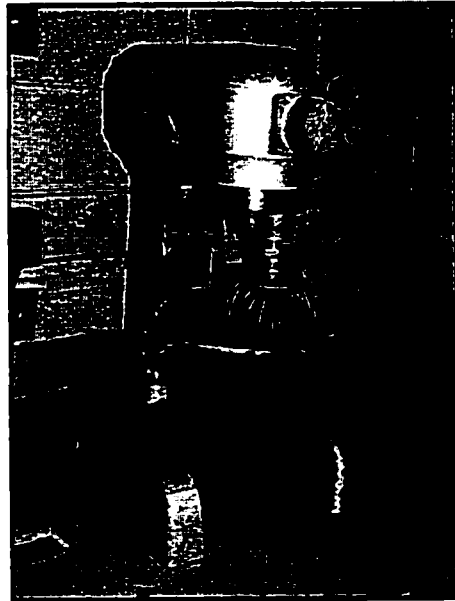
Figure 7.2 Mixing Bowl

Figure 7.3 Mixing Bucket

Figure 7.4 PTI Double Pugmill Mixer
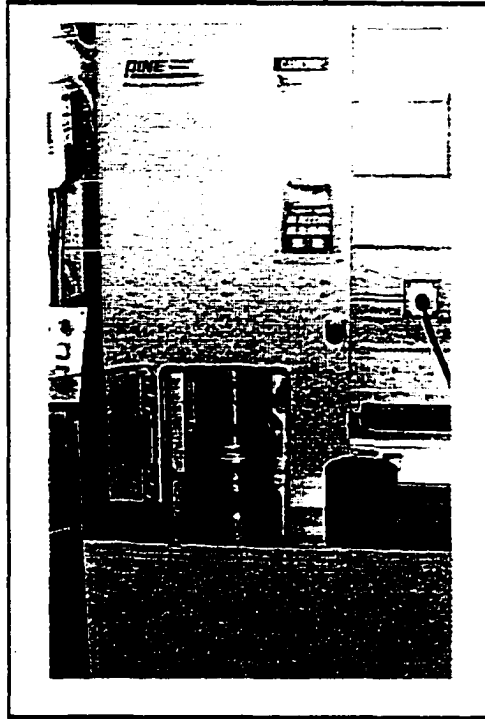
Figure 7.5 Pine Instrument Superpave Gyratory Compactor

Figure 7.6 Troxler Superpave Gyratory Compactor

Figure 7.7 shows the configuration of a SGC mold, which has an inside diameter of 150 mm and a nominal height of 250 mm. A base plate fits in the bottom of the mold to confine the specimen during compaction.
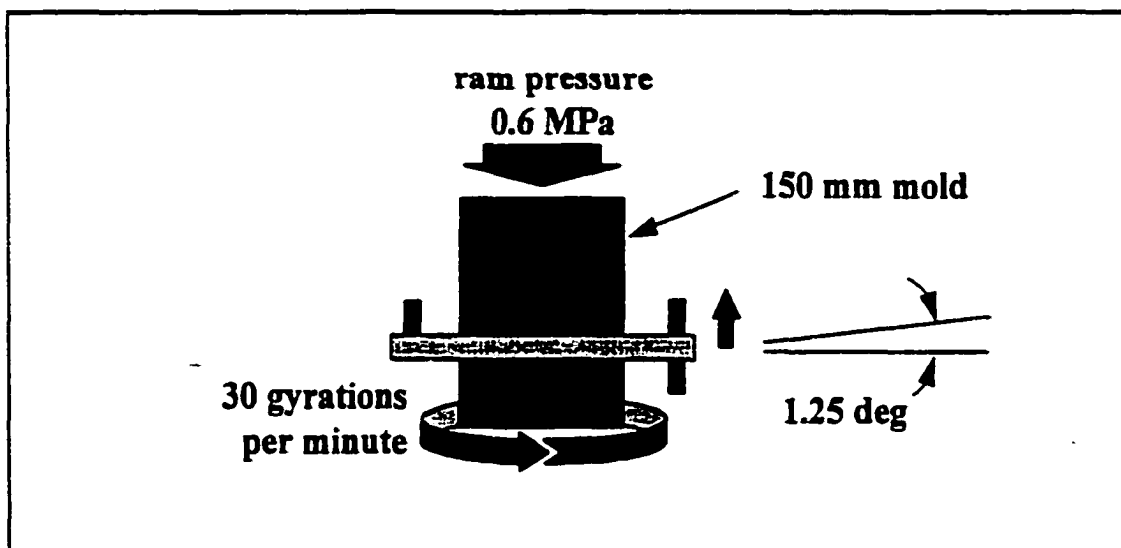
Figure 7.7 SGC Mold Configuration and Compaction Parameters

For this experimental program, since the asphalt mixtures were plant produced, laboratory mixing was not required. Mixtures were reheated in the oven and compacted using the SGC.

Design of the Experiments

All specimens were cylindrical samples. There were two types of specimen sizes: 4 inches in diameter by 6 inches in height made for Repeated Load Compression (RLC) Testing, as shown in Figure 7.8, and 4 inches in diameter by 2 ½ inches in height made for Indirect Tensile Fatigue (ITF) Testing, as shown in Figure 7.9.

The Repeated Load Compression (RLC) Test was conducted at three temperatures: 40°F (4°C), 77°F (25°C), and 104°F (40°C). Three replicates were tested for each combination of material and temperature.

Indirect Tensile Fatigue (ITF) Tests were conducted at two temperatures: 77ᵒF (25ᵒC), and 104ᵒF (40ᵒC). Three replicates were tested for each combination of material and temperature.

Table 7.1 shows the tests performed for each mixture. A detailed description of each test is presented below.

Table 7.1 Test Factorial

Tests	Sample Size (D X H, in.)	Test Temperature (ᵒF)	Mixtures			
			18WC	18WC-CRM	15A	15A-CRM
ITF	4 X 2 ½	40, 77, 104	3, 3, 3*	3, 3, 3	3, 3, 3	3, 3, 3
RLC	4 X 6	40, 77	3, 3	3, 3	3, 3	3, 3

*The number represents the replicas for each combination of temperature and mixture.

Repeated Load Compression (RLC) Test

Permanent deformation parameters are needed to characterize the rutting susceptibility of each asphalt material. In this study, repeated load tests were performed to provide data to calculate the three material parameters needed to predict rutting using FLEXPASS.
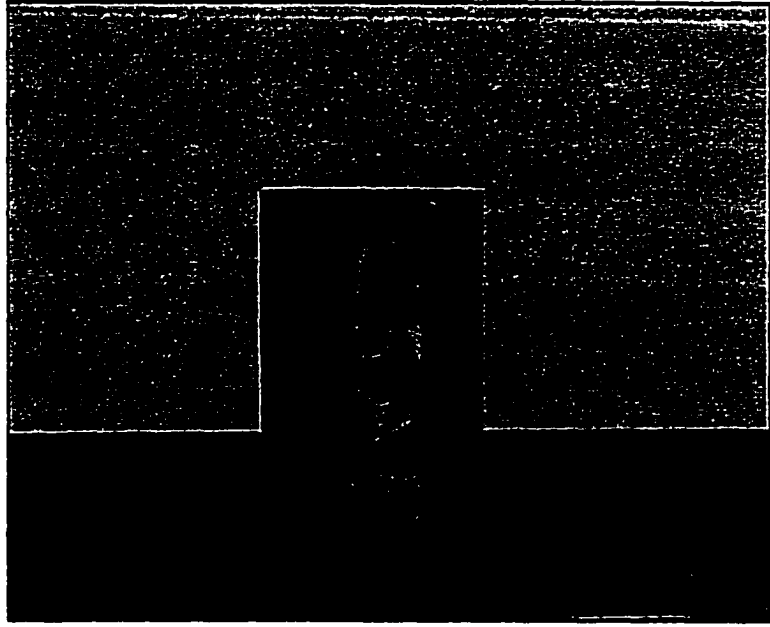
Figure 7.8 Specimen Prepared for the Repeated Load Compression (RLC) Test
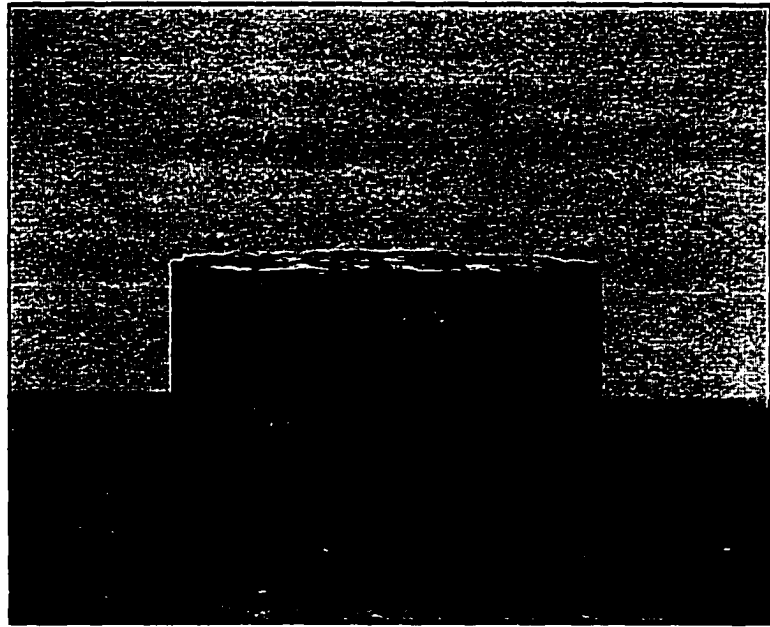
Figure 7.9 Specimen Prepared for the Indirect Tensile Fatigue (ITF) Test

Test Equipment

A Cox and Sons CS7500 Axial Testing and Environmental System was used for the Repeated Load Compression (RLC) Test. It is a versatile, fully automated, single axis, closed-loop hydraulic testing system specifically designed to perform tests on soils and asphalt concrete mixtures over a wide range of stresses and frequencies. The equipment has sufficient flexibility to perform special or standard tests under different environmental temperatures. The system is rated for 55 kips. It has digital controller operated under IBM OS/2 and MTS testing software for data acquisition and equipment control. Several user-friendly menu-driven software systems were developed to conduct tests on asphalt concrete specimens.

The system software features custom test templates that automatically perform SHRP and AASHTO tests, analyze the results and present the data in the report-ready format. The system software incorporates standard test and data acquisition templates to perform tests that may be required for various research projects including the following tests:

- Dynamic Test (sine, square and triangular wave);

- Creep;

- Repetitive loading (haversine);

- Constant rate (ramp);

- Fatigue;

- Random loading;

- Custom software templates for other tests are made available for tests that fall within the static and dynamic capabilities of the system.

The system consists of (a) the load frame, (b) an environmental chamber, (c) hydraulic power supply, and (d) the micro console as shown in Figure 7.10.
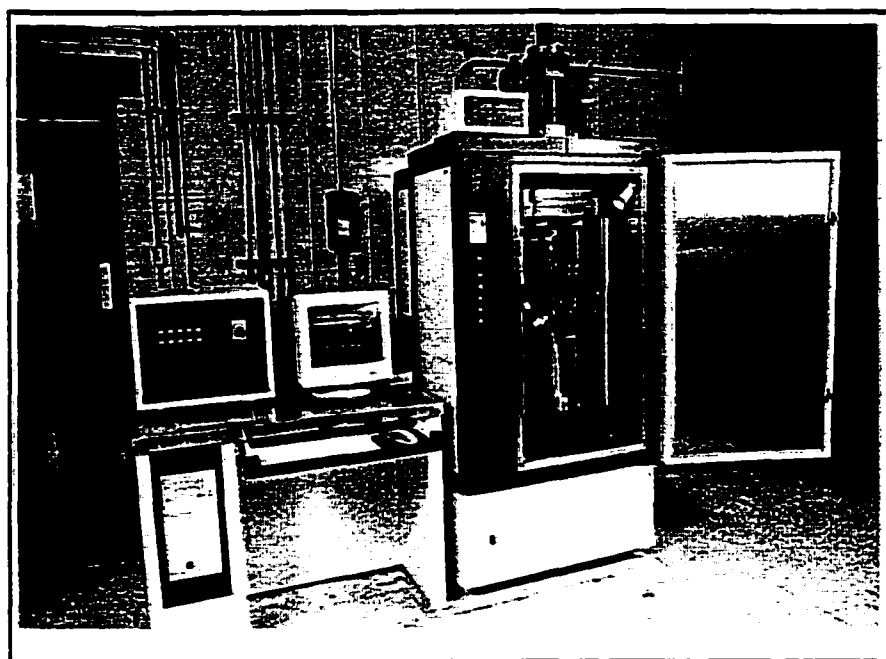
Figure 7.10 Cox and Son CS7500 Axial Testing and Environmental System

The environmental chamber allows testing over a range of temperature representing those experienced by in-service pavements. The chamber temperature is controlled by a microprocessor based controller with an operating range of -100 oF (-73 oC) to 600 oF (356 oC). The micro console displays various information about the system. Controlled stress tests were performed with programmed load control. The system measures deformation via output from a linear voltage displacement transducer (LVDT) located within the system actuator. The resulting deformation data were recorded with a PC using a data acquisition software called Automated Testing System software (ATS).

Designed by SHRP Equipment Corporation. ATS is a comprehensive computer software package that automates material testing and facilitates data analysis. ATS can

automatically control any testing process, be programmed for standard testing sequences, or used to create special testing procedures. The ATS Report module allows viewing of test results in spreadsheet format in a matter of seconds. ATS runs under Microsoft Windows environment. The minimum system requirements for ATS operations includes the following:

- Processor Based Computer (IBM_AT compatible with a Clock Speed higher than 33 MHz)

- Microsoft Windows compatible mouse

- Microsoft Windows compatible monitor and video card

- 12Mb or above memory RAM

- Hard disk

Faster operations occur with a Pentium processor based computer with at least 99 MHz clock speed.
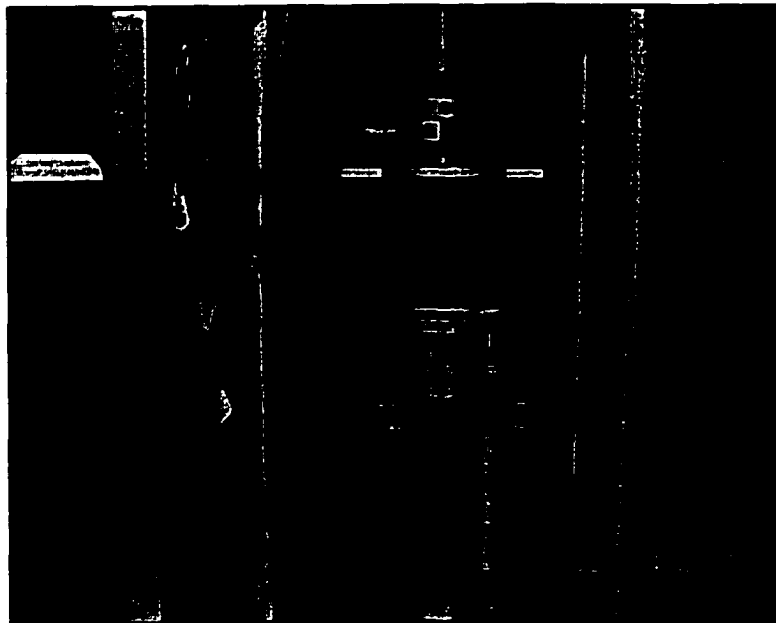
Figure 7.11 Loading Frame and Specimen of RLC Test
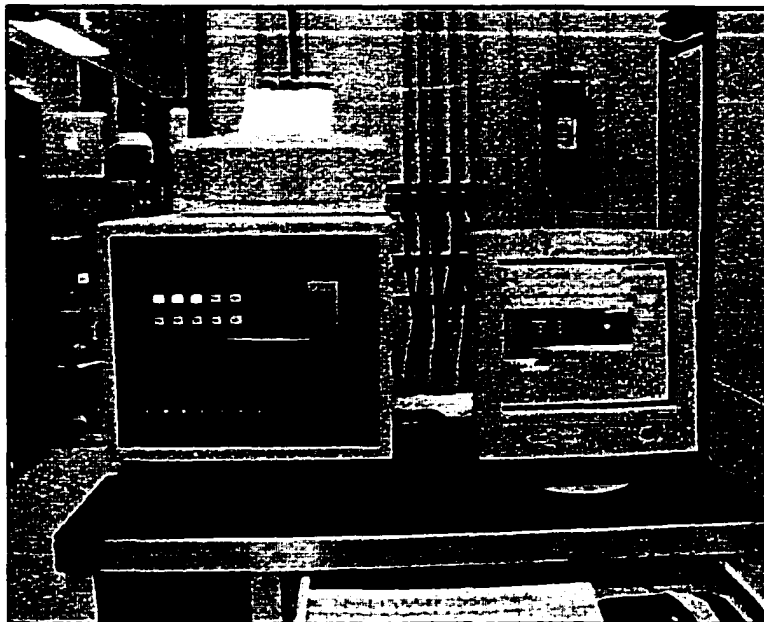
Figure 7.12 Micro Console, and Personal Computer

Deformation Measurement

The direction, magnitude, duration, and frequency of loads were programmed at the micro console. The starting position of the actuator was recorded for each test. During the axial loading, the current position of actuator is constantly measured so that the corresponding axial displacement can be calculated. The strains were calculated by dividing the displacement by the original specimen height. Specimen height was input as the average of four measurements made 90° apart.

The direction, magnitude, duration, and frequency of loads were programmed at the micro console. Displacements of the actuator were transmitted to the computer so that deformation measurement could be calculated at specified intervals.

Loading Procedure

The repeated compression tests were conducted following the VESYS procedures for direct compression testing [30], but the minimum loading cycles were 10,000 rather

than 100,000 in the manual. One test was performed for each mixture material at every temperature. Repeated haversine loads were applied with a 1.0 second axial load cycle time (a load duration of a 0.1 second and a 0.9-second rest period). After applying a minimum of 10,000 load applications, the accumulated deformation was measured at 1, 10, 100, 200, 1,000, and 10,000 load repetitions. The peak-to-peak strain was measured at the 200th cycle. The load was released after 10,000 repetitions and the rebound was measured after 15 minutes and the specimen removed.

Figure 7.13 shows the phase schematic of the test. Appendix 1 provides a detailed description of the test procedure.

Loading Condition

Stress level, frequency, and temperature greatly affect the magnitude of the permanent deformation parameters. The laboratory testing had to be performed with an applied load much lower than that which occurs in the field. A 4-inch diameter cylindrical laboratory tested specimen would fail at much lower stress level than field material supported laterally by surrounding material. Since the top layers of the pavement structure contribute the most to rutting, the influence of lateral support is often neglected. Table 7.2 shows the stress levels applied at the different testing temperatures.

Specimen Temperature Control

The specimen temperature control was provided by an environmental chamber previously described. Specimens were placed in the chamber for a minimum of 24 hours before testing to stabilize temperature within the specimen.
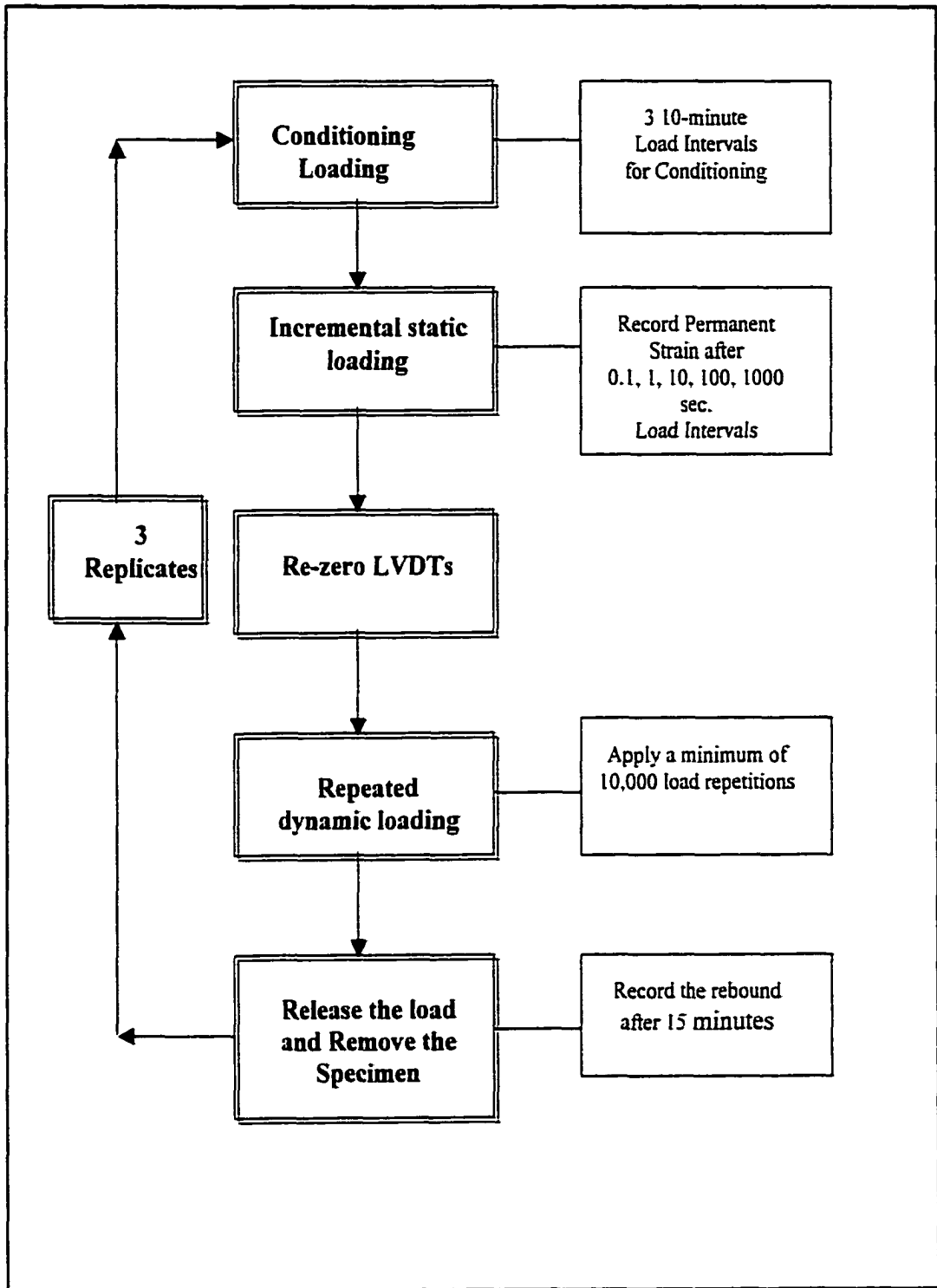
Figure 7.13 Repeated Compression Loading (RCL) Test Phase Schematic

Table 7.2 Stress Level of RLC Test

Material Type	Temperature (°F)	Stress Level (psi)
T8WC	40	20
	77	20
	104	10
T8WC-CRM	40	20
	77	20
	104	10
T5A	40	20
	77	20
	104	10
T5A-CRM	40	20
	77	20
	104	10

Data Recording and Processing

As mentioned previously, repeated haversine loadings were applied with the same 1.0 second load cycle time (a load duration of a 0.1 second and a 0.9-second rest period). The accumulated deformation was measured at 1, 10, 100, 200, 1,000, and 10,000 load repetitions. The machine made 100 records of the deformation during the 1.0 second load cycle time with 30% of them in the 0.1 second load period and 70% of them in the 0.9 second rest period. The records were not only made at the specified number of repetitions but also one cycle ahead of and one cycle after the specific cycle. The records of these

three cycles were averaged to minimize the influence of the noise in the data. Figure 7.14 shows the typical haversine loadings versus cycles, and Figure 7.15 shows the stroke position of the actuator versus loading cycles. The permanent strains recorded from the results of the test for each specimen of the four materials at the testing temperatures are listed in Appendix 2.

Test Results and Analysis

A plot of permanent strain versus load cycles was made for each specimen tested to determine the shape of the curve and if the three-parameter equation suitably describes the material behavior. Figure 7.16 shows a typical plot.

Because the operator of the tests was inexperienced, many variation occurred in the test data. To minimize this influence, some of the test results were eliminated by considering the field data for exclusion of bad results. The remaining test data are averaged for each test material at each of the three test temperatures, and these results are listed in Appendix 3. Figures A3.1 through A3.12 show an arithmetical plot of the permanent strain versus load cycles for each material at each of the three test temperatures, and Figures A3.13 through A3.24 show the log plot of the permanent strain versus load cycles for each material at each of the three test temperatures.

A Non-Linear regression procedure (NLIN) from the S.A.S package was used to analyze the sample averages for each material at each specific temperature. The NLIN procedure produces the least square or weighted least-squares estimates of the parameters of a nonlinear model. The procedure uses an iterative process in which the regression expression must be declared, the derivatives of the model with respect to the parameters are specified, and an initial starting value for each parameter is input. Several iterative

methods are available in this procedure. For this analysis, the modified Gauss-Newton method was selected. In the Gauss-Newton method, the residuals were regressed onto the partial derivatives of the model with respect to the parameters until the iterations converged. The iterations are said to have converged if

$$(SSE_{i-1} - SSE_i)/(SSE_i + 10^{-6}) < 10^{-8}$$, where i is the number of iterations.

Tables 7.3 through 7.6 contain the predicted permanent deformation parameters for each of the materials. Figures A4.1 to A4.12 of Appendix 4 show the plots of actual test data (A) versus predicted results (P). The permanent deformation parameters versus temperature relationships are included in Appendix 5.

Table 7.3 Predicted Permanent Deformation Parameters for T8WC
(Conventional AC Wearing Course)

Temperature (°F)	$\varepsilon_0/\varepsilon_r$	ρ	β	$Log(\varepsilon_0/\varepsilon_r)$	$Log\,\rho$	$Log\,\beta$
40	0.63	89.64	1.3474	-0.20066	1.952502	0.129497
77	1.77	144.6	0.5223	0.247973	2.160168	-0.28208
104	21.85	5.52E+10	0.0849	1.339451	10.74194	-1.07109

Table 7.4 Predicted Permanent Deformation Parameters for T8WC-CRM
(AR-HMA Wearing Course)

Temperature (°F)	$\varepsilon_0/\varepsilon_r$	ρ	β	$Log(\varepsilon_0/\varepsilon_r)$	$Log\,\rho$	$Log\,\beta$
40	0.66	315.4	0.4165	-0.18046	2.498862	-0.38038
77	1.8	410.6	0.3284	0.255273	2.613419	-0.4836
104	253.2	1.01E+17	0.0583	2.403464	17.00432	-1.23433

Table 7.5 Predicted Permanent Deformation Parameters for T5A
(Conventional Black Base Course)

Temperature (°F)	$\varepsilon_0 / \varepsilon_r$	ρ	β	$\text{Log}(\varepsilon_0/\varepsilon_r)$	$\text{Log}\,\rho$	$\text{Log}\,\beta$
40	1.11	164.2	0.81	0.045323	2.215373	-0.09151
77	1	38.326	0.6116	0	1.583493	-0.21353
104	196.5	1.49E+21	0.0467	2.293363	21.17319	-1.33068

Table 7.6 Predicted Permanent Deformation Parameters for T5A-CRM
(AR-HMA Base Course)

Temperature (°F)	$\varepsilon_0 / \varepsilon_r$	ρ	β	$\text{Log}(\varepsilon_0/\varepsilon_r)$	$\text{Log}\,\rho$	$\text{Log}\,\beta$
40	1	304.8	0.3513	0	2.484015	-0.45432
77	1.5	27.9573	0.3772	0.176091	1.446495	-0.42343
104	50	1.84E+17	0.0537	1.69897	17.26482	-1.27003
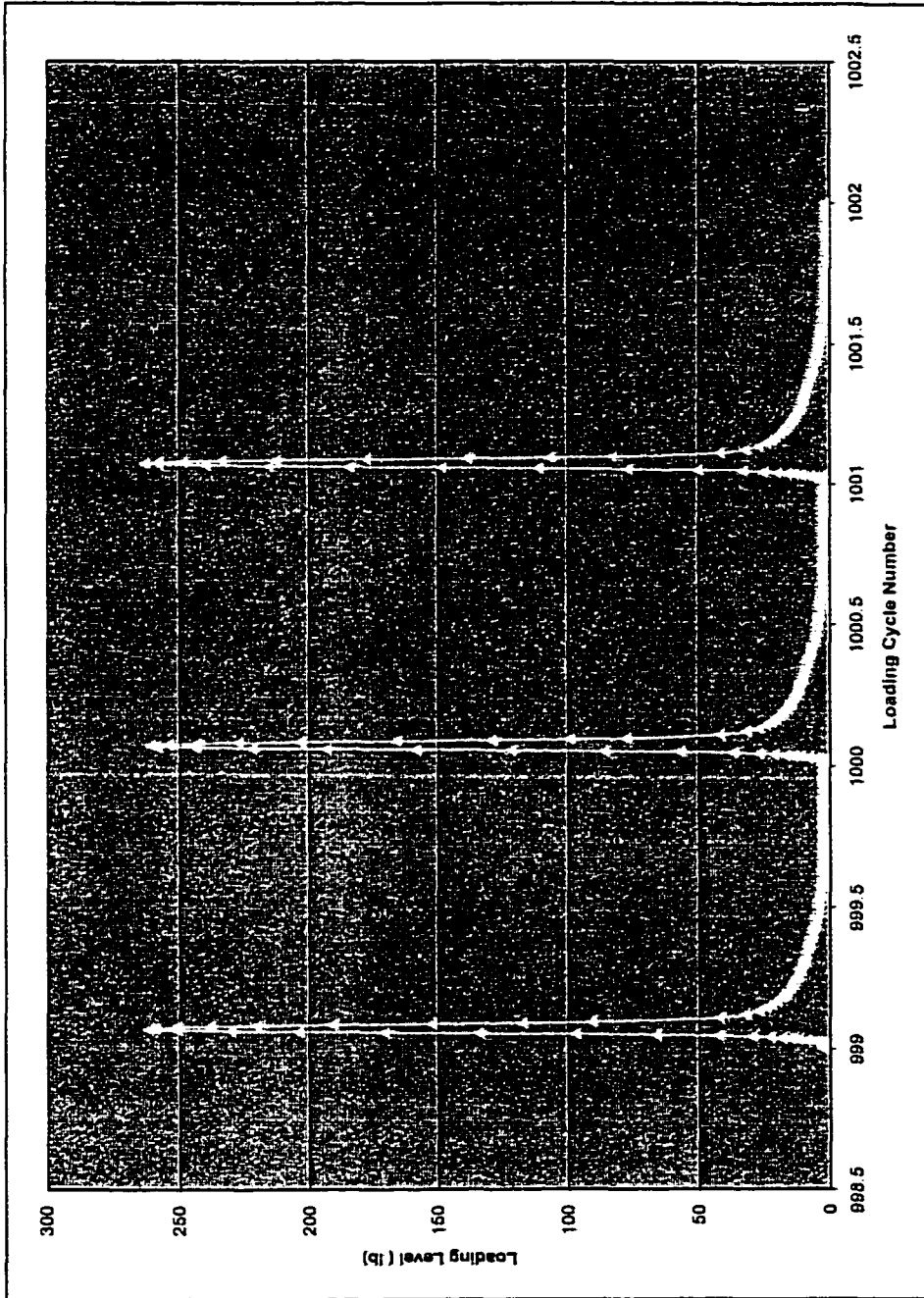
Figure 7.14 Typical Haversine Loading versus Loading Cycles for RCL Test
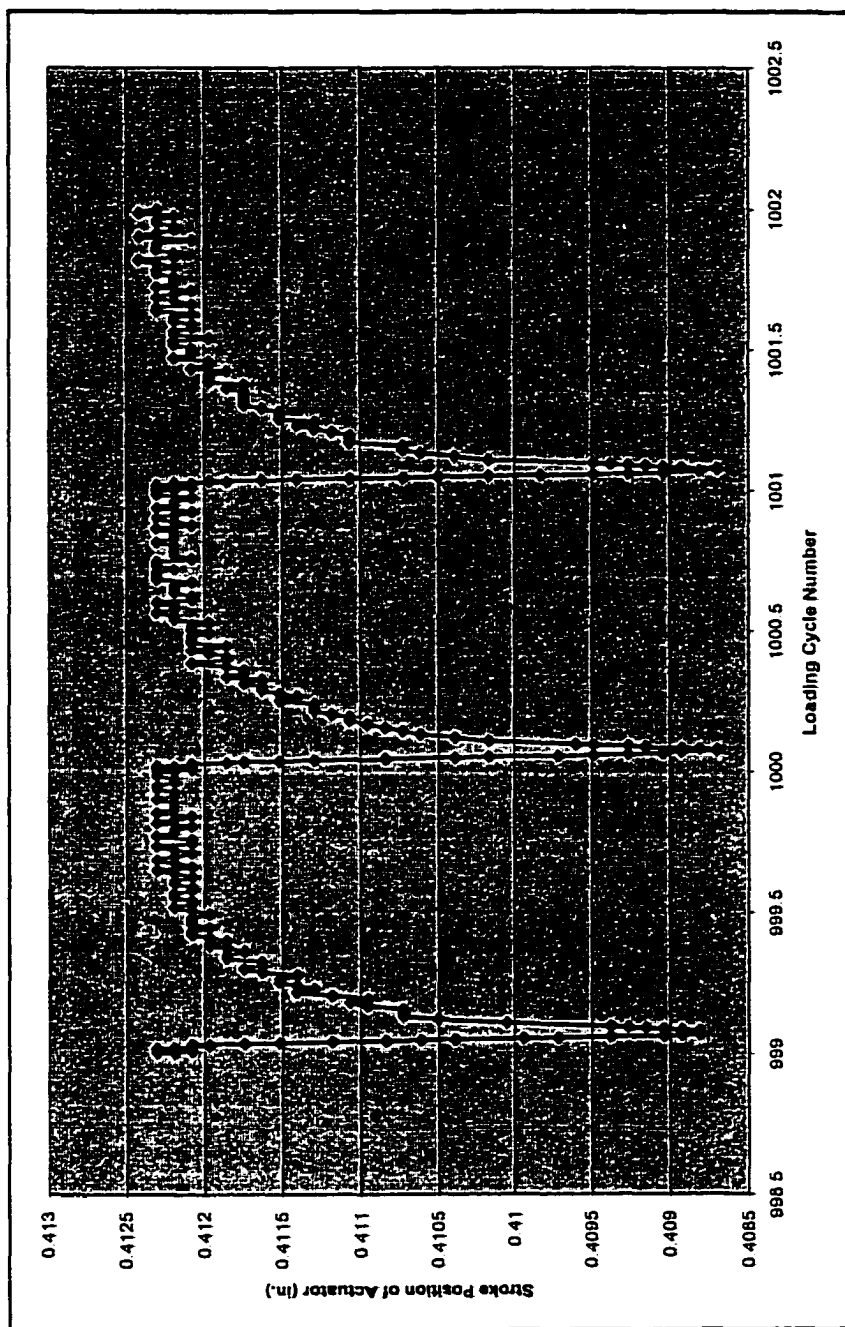
Figure 7.15 Position of Actuator versus Load Cycles
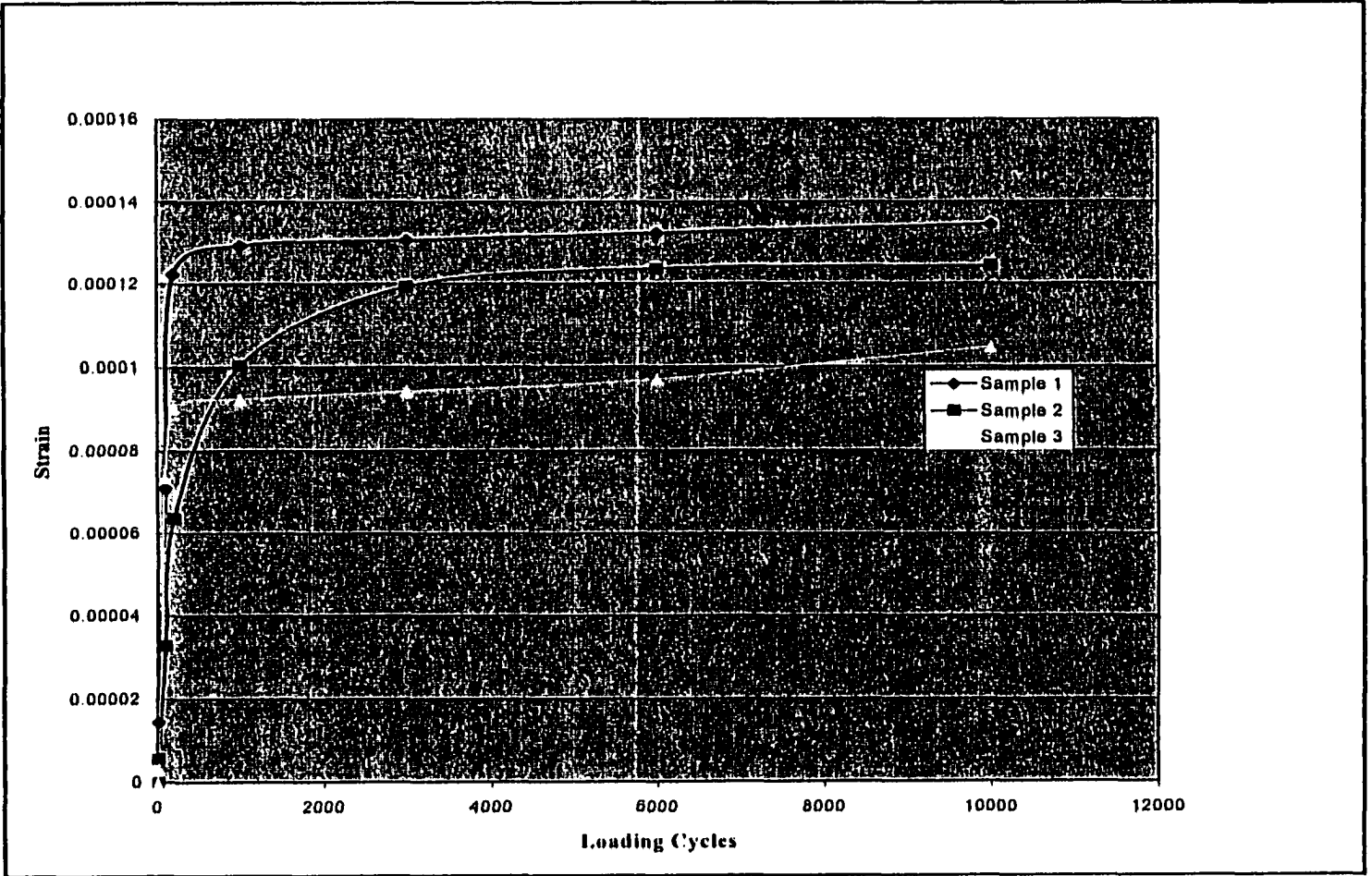
Figure 7.16 Typical Plot of Permanent Strain vs. Loading Cycles for Test Specimen

CHAPTER 8

FLEXPASS INPUTS FOR PERFORMANCE PREDICTION OF ALF TEST LANE

Type and Volume of Traffic

Table 8.1 shows the ALF load history for the test lanes:

Table 8.1 ALF Passes Applied to Test Lanes

No. of Passes x 1000	Total Load, Lbs. **	ESAL Factor	ESALs x 1000	Cumulative ESALs	Date of First Load Application
0 - 400	9,750	1.377	550.80	550,800	3/5/99
400 - 500	12,050	3.213	321.30	872,100	10/4/99
500 - 650	14,350	6.463	969.45	1,841,550	12/6/99
650 - 750	16,650	11.713	1,171.30	3,012,850	4/14/00
750 - 800	18,950	19.655	982.75	3,995,600	10/9/00
*800 - 850	21,250	31.079	1,553.95	5,549,550	12/18/00

* Testing on Lane 2-2 only.
** Each increment represents an additional Load of 2,300 Lbs.

For the analysis, all of the ALF wheel load passes were converted to equivalent 9 kip wheel load passes or to 18 kip equivalent single-axle loads (ESALs). The number of ALF passes applied for each lane and the ESAL conversion factors are shown in Table 8.1.

Since the ALF field testing lasted for almost two years and the average loading days for each lane is 110 days per year, the average daily passes were calculated as the

sum of equivalent 9 kip passes divided by 220, which was 13,100 passes. The tire contact pressure was assumed to be uniform and applied at 105 psi on a circle area of 5.44- inch radius. The load geometry input parameters are shown in Table 8.2.

Table 8.2 Load Geometry Parameters Input

Load Parameter	Value
Number of Axles	1 (single)
Radius of the Load Area (inches)	5.44
Spacing between Tires (inches)	13.5
Tire Inflation Pressure (psi)	105

Seasonal Pavement Temperatures

Ullidtz and Larsen [1983] proposed the following equation for predicting the asphalt pavement temperature using the air temperature:

$$T_{asp} = 1.2T_{air} + 3.2 \qquad (8.1)$$

$$T_{air} = \frac{T_1 + T_2}{2} + \left[\frac{T_1 + T_2}{2}\right]\cos\left[\frac{U - U_0}{26}\right]\pi \qquad (8.2)$$

Where:

T_{asp} = asphalt temperature, in °C

T_{air} = mean weekly air temperature, in °C

T_1 = maximum temperature during the year, in °C

T_2 = minimum temperature during the year, in °C

U = week number (counted from January)

U_0 = number of weeks from the beginning of the year to the week of maximum temperature

This method predicted the asphalt temperature at mid depth of the whole asphalt bound layers for the ALF lanes. During the loading, the lane being tested was shaded and the measurements by PRC staff showed that the pavement temperature for the lane being tested was 20° F cooler than adjacent lanes subjected to solar radiation. Therefore the shield temperature effect should be considered to adjust the temperature predictions for the ALF test lanes. The whole year (1999) air temperature record was used. Table 8.3 provides the results of these calculations.

Table 8.3 Calculation Result of Asphalt Temperature of Test Lanes

# Week	$\dfrac{T_1+T_2}{2}$ (°C)	$\cos\left[\dfrac{U+U_0}{26}\right]\pi$	T_{air} (°C)	T_{asp} (°C)	T_{asp} (°F)	T_{asp}-Shield_Adj $(T_{asp}-20)$ (°F)
1	17.7389	-0.99291	0.126	3.351	38.03	18.03
2	17.7389	-1	2.250	3.200	37.76	17.76
3	17.7389	-0.99252	0.133	3.359	38.05	18.05
4	17.7389	-0.97059	0.522	3.826	38.89	18.89
5	17.7389	-0.93452	1.162	4.594	40.27	20.27
6	17.7389	-0.88483	2.043	5.652	42.17	22.17
7	17.7389	-0.82225	3.153	6.984	44.57	24.57
8	17.7389	-0.7477	4.476	8.571	47.43	27.43
9	17.7389	-0.66225	5.991	10.390	50.70	30.70
10	17.7389	-0.56716	7.678	12.414	54.34	34.34
11	17.7389	-0.4638	9.512	14.614	58.31	38.31
12	17.7389	-0.35369	11.465	16.958	62.52	42.52
13	17.7389	-0.23842	13.510	19.411	66.94	46.94
14	17.7389	-0.11969	15.616	21.939	71.49	51.49
15	17.7389	0.000796	17.753	24.504	76.11	56.11
16	17.7389	0.121266	19.890	27.068	80.72	60.72
17	17.7389	0.23997	21.996	29.595	85.27	65.27
18	17.7389	0.355178	24.040	32.047	89.69	69.69
19	17.7389	0.465211	25.991	34.389	93.90	73.90
20	17.7389	0.568468	27.823	36.587	97.86	77.86
21	17.7389	0.663444	29.508	38.609	101.50	81.50
22	17.7389	0.748754	31.021	40.425	104.77	84.77
23	17.7389	0.823158	32.341	42.009	107.62	87.62
24	17.7389	0.88557	33.448	43.338	110.01	90.01
25	17.7389	0.935081	34.326	44.391	111.91	91.91
26	17.7389	0.970971	34.963	45.155	113.28	93.28
27	17.7389	0.992716	35.349	45.618	114.11	94.11
28	17.7389	1	35.478	45.773	114.39	94.39
29	17.7389	0.992716	35.349	45.618	114.11	94.11
30	17.7389	0.970971	34.963	45.155	113.28	93.28
31	17.7389	0.935081	34.326	44.391	111.91	91.91

Table 8.3 Continued

32	17.7389	0.88557	33.448	43.338	110.01	90.01
33	17.7389	0.823158	32.341	42.009	107.62	87.62
34	17.7389	0.748754	31.021	40.425	104.77	84.77
35	17.7389	0.663444	29.508	38.609	101.50	81.50
36	17.7389	0.568468	27.823	36.587	97.86	77.86
37	17.7389	0.465211	25.991	34.389	93.90	73.90
38	17.7389	0.355178	24.040	32.047	89.69	69.69
39	17.7389	0.23997	21.996	29.595	85.27	65.27
40	17.7389	0.121266	19.890	27.068	80.72	60.72
41	17.7389	0.000796	17.753	24.504	76.11	56.11
42	17.7389	-0.11969	15.616	21.939	71.49	51.49
43	17.7389	-0.23842	13.510	19.41	66.94	46.94
44	17.7389	-0.35369	11.465	16.96	62.52	42.52
45	17.7389	-0.4638	9.512	14.62	58.31	38.31
46	17.7389	-0.56716	7.678	12.41	54.34	34.35
47	17.7389	-0.66225	5.991	10.39	50.70	30.70
48	17.7389	-0.7477	4.476	8.57	47.43	27.43
49	17.7389	-0.82225	3.153	6.98	44.57	24.57
50	17.7389	-0.88483	2.043	5.65	42.17	22.13
51	17.7389	-0.93452	1.162	4.59	40.27	20.27
52	17.7389	-0.97059	0.522	3.83	38.89	18.89

* $T_1 = 37.7222$, $T_2 = -2.2444$

** $U = 52$, $U_0 = 12$

The distribution of the adjusted asphalt temperature along the whole year is shown in Figure 8.1. Because the number of seasons for material characterization was limited to 6, the period from the beginning of the year to the time of the highest pavement temperature was divided into three seasonal intervals using the following weekly average temperatures: $<= 40$ °C, $40°$ ~ 70°C, and $>= 70$ °C. The period from the time with the highest temperature to the end of the year was divided into another three seasonal intervals according to the same standard mentioned above. The average temperature of each interval was used as the input pavement temperature of that season, as shown in Table 8.4.

Table 8.4 Pavement Seasonal Temperature Selected

Num. Of Week (from New Year)	Time Interval (Months)	Temp. Interval (°F)	Average Temp. (°F)
1~11	0.79	<=40	24.6
12~18	0.40	40~70	56.1
19~28	0.90	>=70	86.9
29~37	0.70	>=70	86.1
38~44	0.30	70~40	56.1
44~52	0.61	<=40	27.1
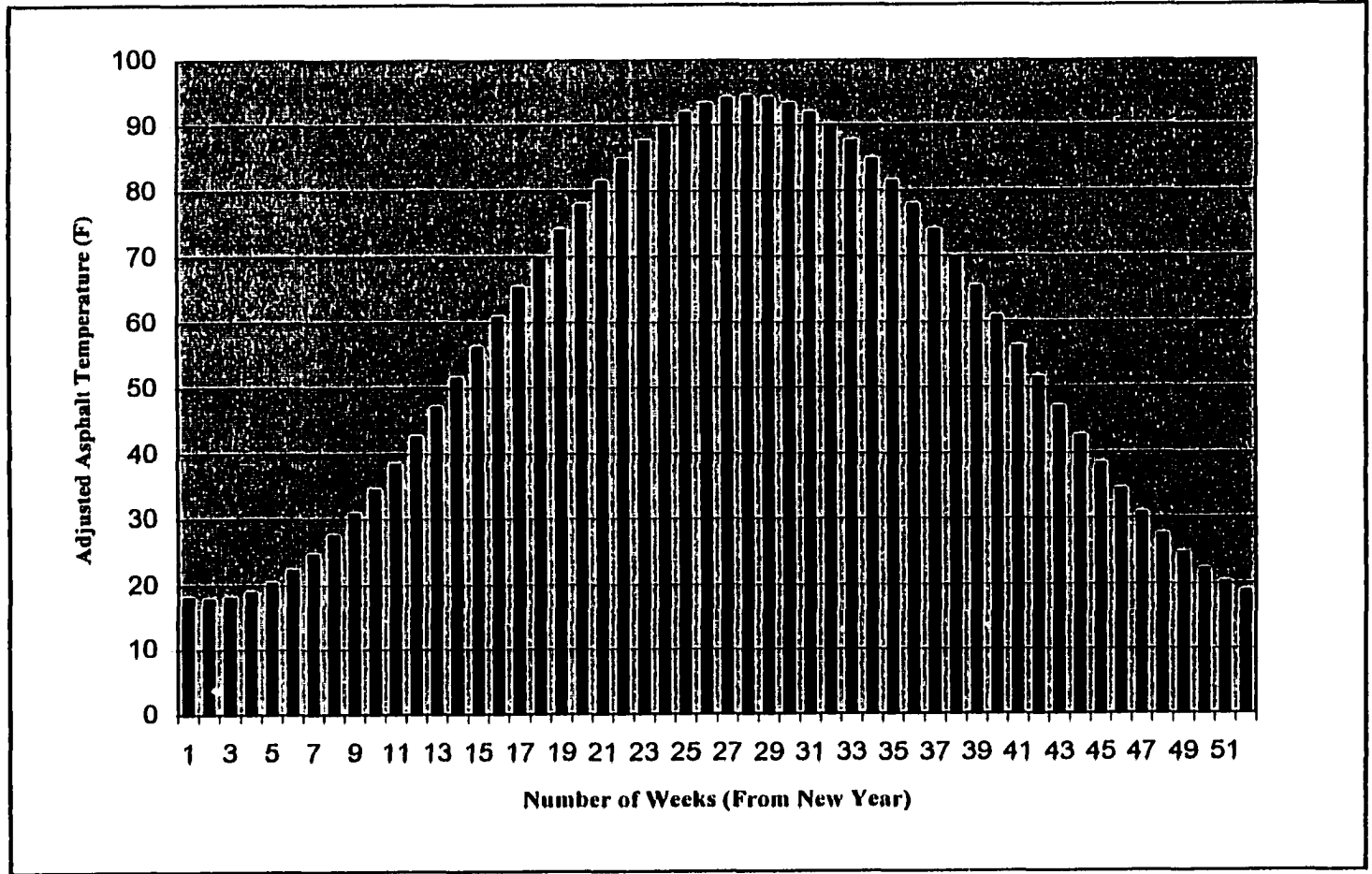
Figure 8.1 Distribution of Pavement Temperature along a Whole Year

Structural Material Properties

The cross-section of the three ALF test lanes used for FLEXPASS was given in Figure 8.2. As the maximum number of pavement layers in FLEXPASS was limited to 5, the wearing course and binding course of the test lanes had to be combined as one layer for the performance predictions. According to construction report of the ALF test lanes [4], the construction thickness along the test section was different, and therefore the actual average thickness of each course for each test lane in this analysis, as shown in the Figure 8.2.

Lane 2-1	Lane 2-2	Lane 2-3 (Control)
4.2" Type 8F Wet Rouse Surface Course	4.6" Type 8F Course	4.0" Type 8F Course
2.6" Type 5A Base Course	3.3" Type 5A Wet Rouse Base Course	3.2" Type 5A Base Course
8.5" Crushed Stone	8.5" Crushed Stone	8.5" Crushed Stone
10.0" Soil Cement	10.0" Soil Cement	10.0" Soil Cement
38.0" Select Soil	38.0" Select Soil	38.0" Select Soil

Figure 8.2 Layer Structures of ALF Test Lanes for FLEXPASS

The test lanes were modeled using a two-dimensional half space of a finite solid of resolution. The half-section structure to be analyzed was divided into a set of quadrilateral elements which were then divided into four triangles by the program to produce a set of elements like those shown in Figure 5.2 of Chapter 5. The density of the various layer materials used was determined from the laboratory moisture density

relationships provided by Louisiana Transportation Research Center (LTRC). The Poisson's ratio is assumed equal to the typical value of the Poisson's ratio of corresponding materials for all layers. The earth pressure coefficient at rest was calculated using equation (5.5). The moisture content for the base layer was assumed equal to the optimum moisture content for all the seasons. For the sub-base and sub-grade layers the approximate moisture content reported by the field engineers at the ALF site was used. The moisture content was assumed constant for the test period selected. The structural material properties used in the modeling are tabulated in Table 8.5.

Table 8.5 Material Characteristics for Various Materials Used in ALF Test Lanes

Layer Component	Density (pcf)	Poisson's Ratio	Moisture/Asphalt Content (%)
T8F WC	141.80	0.35	4.0 (Asphalt Content)
T8F WC-CRM	141.80	0.30	4.0 (Asphalt Content)
T5A Base	140.00	0.35	3.5 (Asphalt Content)
T5A-CRM Base	140.00	0.30	3.5 (Asphalt Content)
Crushed Stone	129.37	0.35	6.0
Soil Cement	120.00	0.20	25.0
Select Soil	101.86	0.45	30.0

Resilient Modulus

Resilient Modulus of Asphalt Concrete

Indirect tensile resilient tests were performed on each asphalt mixture at 40 °F, 77 °F, and 104 °F in the LTRC laboratory [2]. Indirect tensile resilient modulus (M_R) represents the elastic property of the asphalt mixture at the test temperature. Table 8.6

presents the test results for mean indirect tensile resilient modulus (M_R) at 40, 77, and

104°F.

Table 8.6 Indirect Tensile Resilient Modulus (M_R) of Asphalt Mixtures

Temperature	M_R for Each Mixture, psi			
	T8F WC	T8F WC-CRM	T5A	T5A-CRM
40 °F (4 °C)	6.34E+05	6.25E+05	6.28E+05	6.37E+05
77 °F (25 °C)	4.64E+05	4.48E+05	5.53E+05	4.81E+05
104°F (40 °C)	2.86E+05	2.45E+05	3.25E+05	3.25E+05

The temperature versus measured resilient modulus is plotted in Figures 8.3

through 8.6 respectively. The linear regression method was used to predict the

relationship between resilient modulus (M_R) and pavement temperatures. The resilient

modulus for the seasonal pavement temperatures were calculated using the regression

equations in Table 8.7 with the results tabulated in Tables 8.8 through 8.11.

Resilient Modulus of Crushed Stone Material

The modulus relationship for the crushed stone layer was modeled as bulk stress

dependent as given by equation (5.1). Resilient modulus tests were not performed on the

crushed stone material. Hence, the material parameters of a similar material were chosen

to model the resilient modulus for the crushed stone layer [43]. The material modulus

parameters selected for crushed stone layer are tabulated in Table 8.12.

Resilient Modulus of Soil Cement

The soil cement resilient modulus was assumed to remain constant during the

loading period at 450,000 psi.
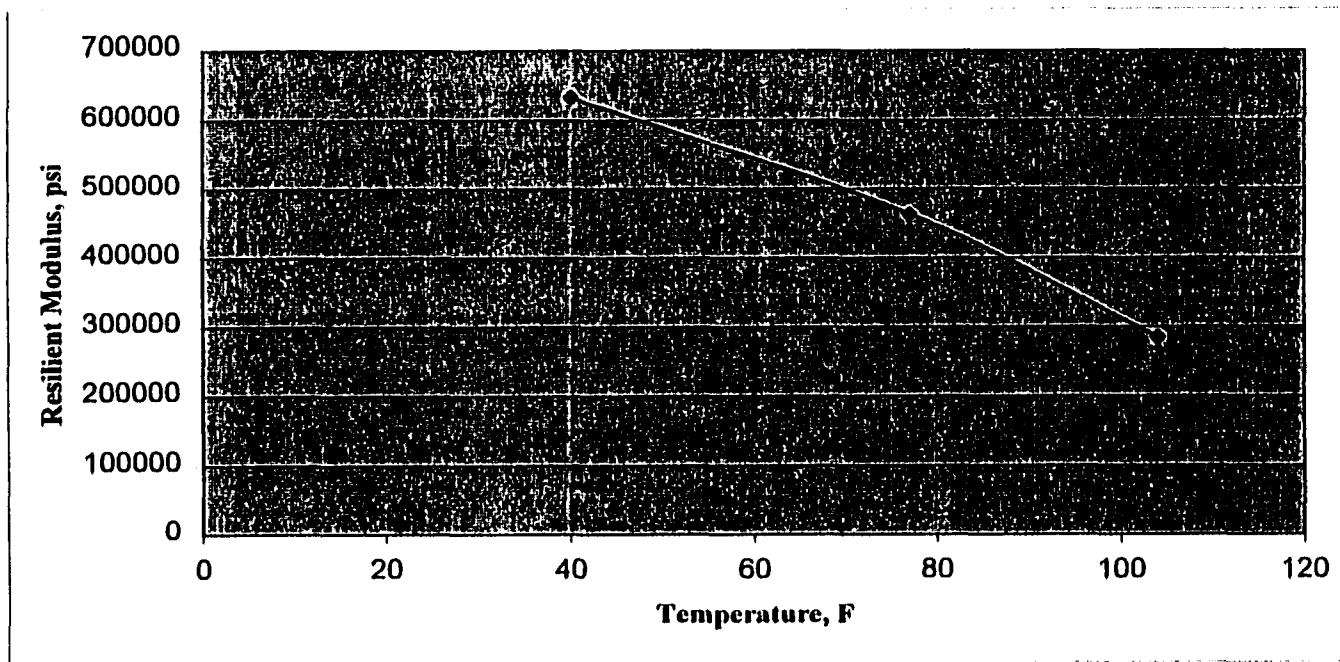
Figure 8.3 Plot of Resilient Modulus versus Temperature for T8F Wearing Course
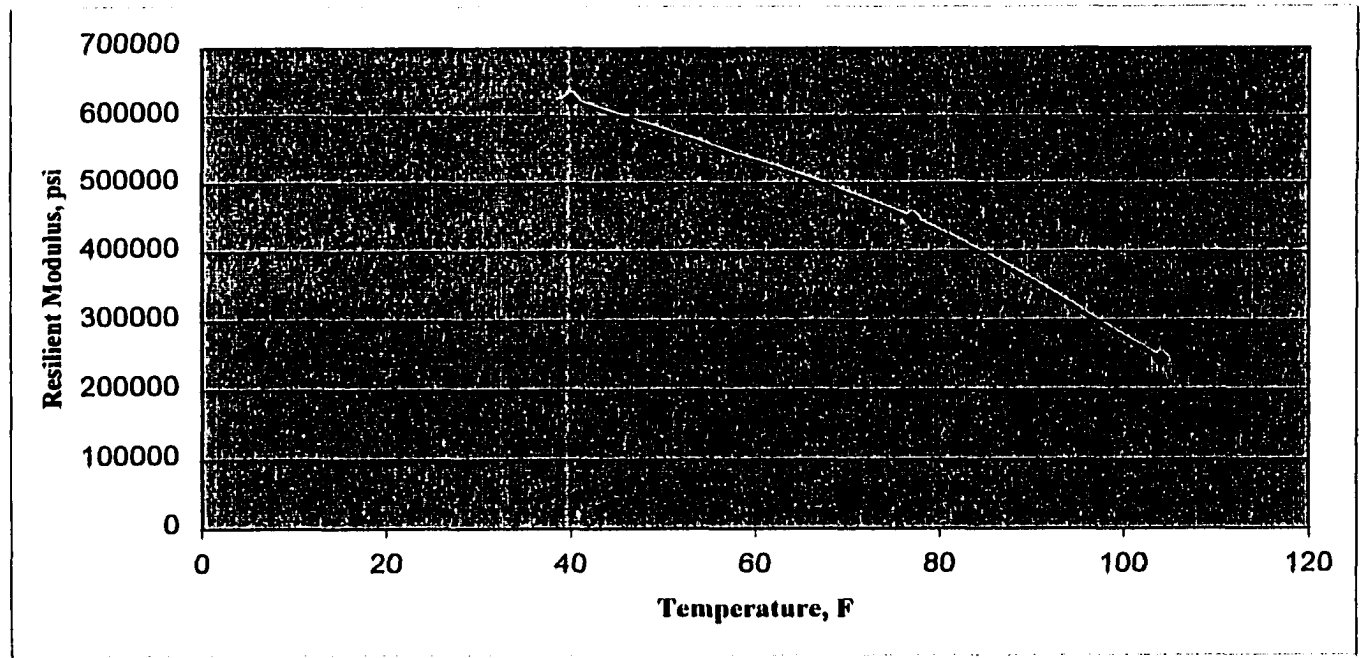
Figure 8.4 Plot of Resilient Modulus versus Temperature for T8F-CRM Wearing Course
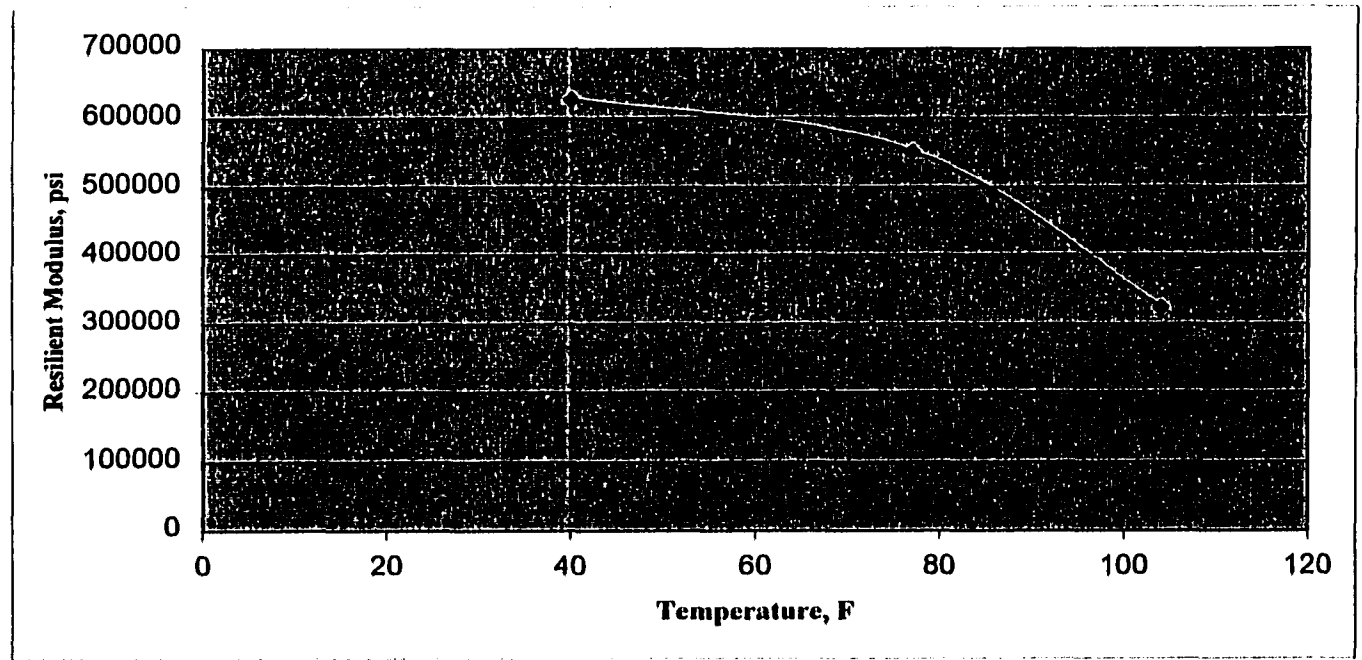
Figure 8.5 Plot of Resilient Modulus versus Temperature for T5A Black Base
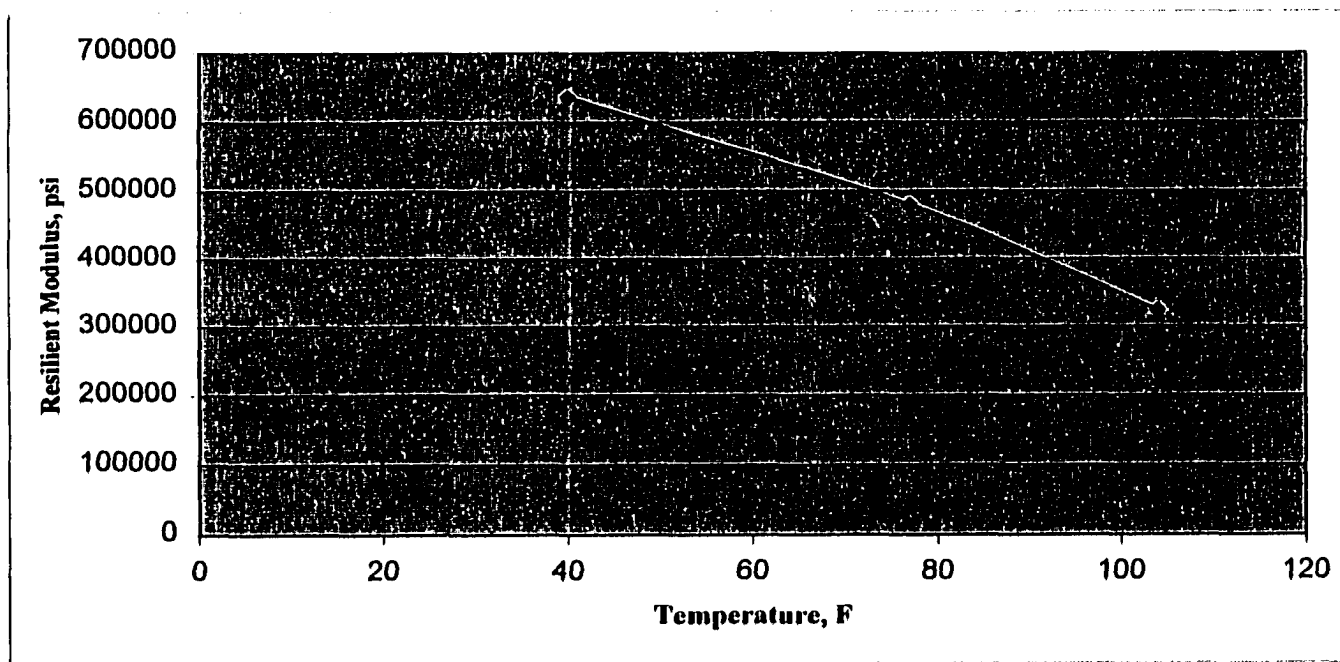
Figure 8.6 Plot of Resilient Modulus versus Temperature for T5A-CRM Base

Table 8.7 Regression Equations to Predict Resilient Modulus

T8F Wearing Course	$M_R = 158.3241 - 0.00018\ T_{asp}$	(8.3)
T8F-CRM Wearing Course	$M_R = 147.3 - 0.00017\ T_{asp}$	(8.4)
T5A Black Base	$M_R = 168.846 - 0.00019\ T_{asp}$	(8.5)
T5A-CRM Base	$M_R = 172.32 - 0.00021\ T_{asp}$	(8.6)

Table 8.8 M_R of T8F Wearing Course for Each Season

Season #	Average Temp. (° F)	Modulus (ksi)
1	24.6	743
2	56.1	568
3	86.9	397
4	86.1	401
5	56.1	568
6	27.1	729

Table 8.9 M_R of T8F-CRM Wearing Course for Each Season

Season #	Average Temp. (° F)	Modulus (ksi)
1	24.6	722
2	56.1	536
3	86.9	355
4	86.1	360
5	56.1	536
6	27.1	707

Table 8.10 M_R of T5A Black Base Course for Each Season

Season #	Average Temp. (° F)	Modulus(ksi)
1	24.6	759
2	56.1	593
3	86.9	431
4	86.1	435
5	56.1	593
6	27.1	746

Table 8.11 M_R of T5A-CRM Base Course for Each Season

Season #	Average Temp. (° F)	Modulus (ksi)
1	24.6	703
2	56.1	553
3	86.9	407
4	86.1	411
5	56.1	553
6	27.1	692

Table 8.12 Material Input Parameters for Crushed Stone Layer

Parameter	Value
Modulus at Failure (psi)	65000
Coefficient K_1	14030
Coefficient K_2	0.37

Resilient Modulus of Select Soil Embankment

The select soil embankment layers were modeled as a fine-grained soil where resilient modulus is a function of deviator stress as given by Equations (5.4) and (5.5). For the subgrade, the parameters were determined from the test data provided by LTRC. The input parameters for the subgrade layer are given in Tables 8.13, and 8.14, respectively.

Table 8.13 Resilient Modulus Test Results on Field Core Samples of Subgrade Soil

Confining pressure (psi)	Deviator stress (psi)	Resilient modulus (psi)
6.05*	2.03*	4900*
6.05	0.99	5700
6.05	2.05	5000
6.05	3.06	4300
2.97	0.99	5100
2.99	2.05	4400
2.99	3.06	3800
0.17	0.97	4100
0.19	2.03	3500
0.19	3.05	3000

* pre loading

Table 8.14 Input Parameters for the Subgrade Layer

Input Variables	Subgrade
x1	2
x2	4896
x3	-650
x4	-650
Resilient modulus after failure, psi	4308
Deviator stress upper limit	3.00
Deviator stress lower limit	1.00
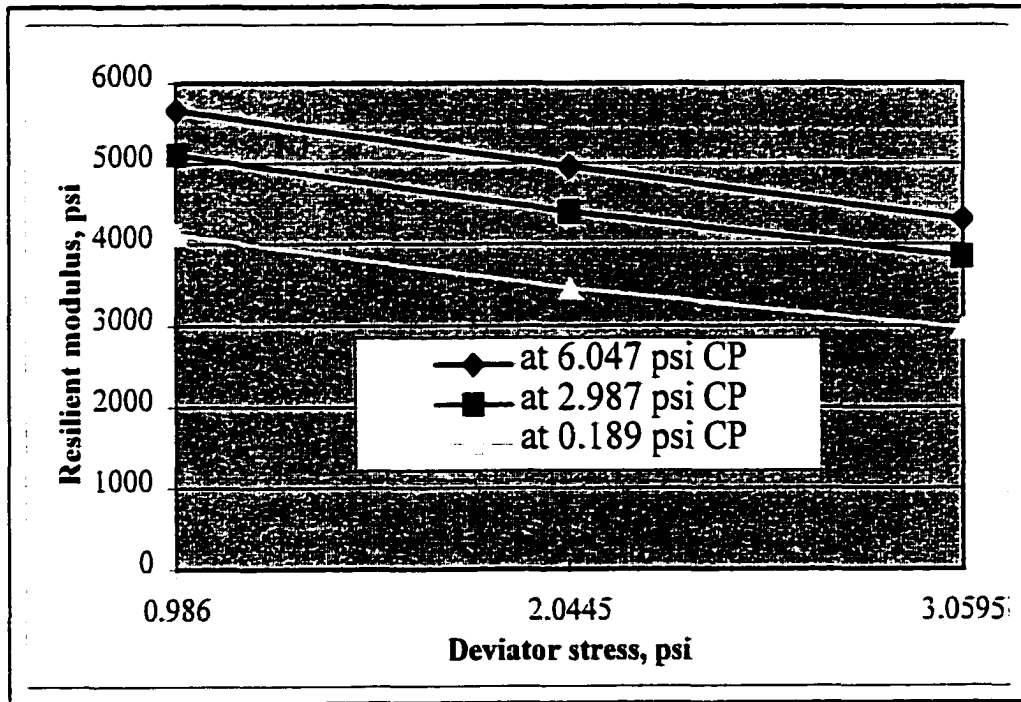
Figure 8.7 Deviator Stress vs. Resilient Modulus for Field Cores of Subgrade Soil Tested at Different Confining Pressures

Material Distress Characterization Parameters

Permanent Deformation Parameters

The three-parameter permanent deformation model of Equation (6.1) was the basis for predicting the permanent deformation performance in this study. Repeated load compression tests described in Chapter 7 were performed and the three parameters for each of the four materials tested at three different temperatures were developed and included in Tables 7.3 through 7.6.

In this study, the input parameters for the seasonal pavement temperatures were interpolated from the test results and shown in Tables 8.15 through 8.18 for the four surface and base materials.

Table 8.15 Permanent Deformation Parameters of T8F Wearing Course for FLEXPASS Input

Temperature (°F)	$\varepsilon_0 / \varepsilon_r$	ρ	β	$Log(\varepsilon_0 / \varepsilon_r)$	$Log \rho$	$Log \beta$
24.6	0.6300	89.64	1.3474	-0.20066	1.952502	0.129497
56.1	0.9882	110.3878	0.891854	-0.00532	2.042921	-0.04971
86.9	4.4606	207182.4	0.267756	0.649395	5.316353	-0.57226
86.1	4.1290	112860.7	0.283135	0.615842	5.052543	-0.54801
56.1	0.9878	110.3878	0.891854	-0.00532	2.042921	-0.04971
27.1	0.6300	89.64	1.3474	-0.20066	1.952502	0.129497

Table 8.16 Permanent Deformation Parameters of T8F-CRM Wearing Course for FLEXPASS Input

Temperature (°F)	$\varepsilon_0 / \varepsilon_r$	ρ	β	$Log(\varepsilon_0 / \varepsilon_r)$	$Log\,\rho$	$Log\,\beta$
24.6	0.6600	315.4000	0.4165	-0.18046	2.498862	-0.38038
56.1	1.0216	353.7859	0.375557	0.009263	2.548741	-0.42532
86.9	11.1002	80551394	0.1739	1.045329	7.906073	-0.7597
86.1	9.5344	29086138	0.183391	0.979293	7.463686	-0.73662
56.1	1.0216	353.7859	0.375557	0.009263	2.548741	-0.42532
27.1	0.6600	315.4	0.4165	-0.18046	2.498862	-0.38038

Table 8.17 Permanent Deformation Parameters of T5A Black Base Course for FLEXPASS Input

Temperature (°F)	$\varepsilon_0 / \varepsilon_r$	ρ	β	$Log(\varepsilon_0 / \varepsilon_r)$	$Log\,\rho$	$Log\,\beta$
24.6	1.1100	164.2	0.81	0.045323	2.215373	-0.09151
56.1	1.0607	87.14638	0.716734	0.025589	1.940249	-0.14464
86.9	6.9735	6.14E+08	0.237468	0.843448	8.788147	-0.6244
86.1	5.9285	1.53E+08	0.257008	0.772948	8.185946	-0.59005
56.1	1.0607	87.14638	0.716734	0.025589	1.940249	-0.14464
27.1	1.1100	164.2	0.81	0.045323	2.215373	-0.09151

Table 8.18 Permanent Deformation Parameters of T5A-CRM Base Course for FLEXPASS Input

Temperature (°F)	$\varepsilon_0 / \varepsilon_r$	ρ	β	$Log(\varepsilon_0 / \varepsilon_r)$	$Log\,\rho$	$Log\,\beta$
24.6	1.0000	304.8	0.3513	0	2.484015	-0.45432
56.1	1.193084	107.7143	0.362351	0.076671	2.032273	-0.44087
86.9	5.447186	18370575	0.184167	0.736172	7.264123	-0.73479
86.1	4.890551	5995920	0.195541	0.689358	6.777856	-0.70876
56.1	1.193084	107.7143	0.362351	0.076671	2.032273	-0.44087
27.1	1.0000	304.8	0.3513	0	2.484015	-0.45432

Asphalt Concrete Fatigue Parameters

In this study, the model described by equation (6.2) was used for predicting the occurrence of load-induced cracking. The parameters of K_1 and K_2 were developed from beam fatigue results from a study conducted by Hoyt, Lytton, and Roberts [8] for the Federal Aviation Administration (FAA) and shown in Table 8.19. The test followed the procedures for fatigue testing described in the VESYS IIM User's manual [30]. In the test, a device was used to apply a repeated tension-compression load in the form of a haversine wave for 0.1 second duration with 0.4 second rest periods. Tests were performed at temperatures of 34 °F, 68 °F and 104 °F respectively. A regression method was used to calculate parameters of K_1 and K_2. The parameters calculated from the laboratory tests were summarized in Table 8.19. To use the laboratory results in a comparative analysis which was sensitive to the difference due to both material and temperature, a double regression procedure was applied to the lab data — $|\log K_1|$ versus $\log T$ (where T is the temperature in Fahrenheit degrees) was plotted and a linear regression was performed to produce a set of regression equations where temperature was the independent variable and K_1 was the dependent variable. Then K_2 versus $\log K_1$ was plotted and a linear regression performed for each material, which yielded a set of equations with $\log K_1$ as the independent variable and K_2 as the dependent variable. Using this equation, the fatigue parameters could be calculated for any temperature. The equations thus derived are shown in Equations 8.7 through 8.10 in Table 8.20.

Table 8.19 Fatigure Parameters Calculated from Laboratory Fatigue Tests Performed in Reference [8]

Material	Temperature °F	Number of Samples	R	K1	K2	log K1
AC-10	104	8	-0.89	3.21E-3	2.35	-2.49
	68	8	-0.95	9.48E-12	4.69	-11.02
	34	7	-0.63	1.43E-6	2.92	-5.85
ARC-Medium	104	10	-0.85	2.82E-6	3.47	-5.55
	68	9	-0.98	3.16E-5	2.82	-4.50
	34	9	-0.86	9.91E-10	4.04	-9.00

Table 8.20 Regression Equations Generated from Laboratory Data in Reference [8] and Used to Predict Fatigue Parameters for Any Temperature (°F)

$|\log K_1|$ versus $\log T(°F)$		
AC-10 Control	$|\log K1| = 14.630 - 4.558 \log T$	(8.7)
ARC-Medium	$|\log K1| = 20.483 - 7.879 \log T$	(8.8)
K_2 versus $|\log K_1|$		
AC-10 Control	$| K_2| = 1.512 - 0.28 \log K1$	(8.9)
ARC-Medium	$| K_2| = 1.900 - 7.879 \log K1$	(8.10)

For the ALF test lane pavement structures, fatigue cracking would start in the base course. Therefore, the input fatigue parameters for FLEXPASS were those for the base course materials. Using the equations mentioned above, the input fatigue parameters for the base course materials were calculated and tabulated in Tables 8.21 and 8.22.

Table 8.21 Fatigue Parameters of T5A Black Base for FLEXPASS Input

Material	Season #	Temperature °F	LOGK1	K1	K2
T5A	1	24.59	-9.52521	2.98E-10	4.17906
	2	56.11	-6.70231	1.99E-07	3.388647
	3	86.93	-5.20428	6.25E-06	2.969199
	4	86.10	-5.23711	5.79E-06	2.978391
	5	56.11	-6.70231	1.98E-07	3.388647
	6	27.08	-9.19516	6.38E-10	4.086645

**Table 8.22 Fatigue Parameters of T5A-CRM Base for
FLEXPASS Input**

Material	Season #	Temperature °F	LOGK1	K1	K2
T5A-CRM	1	24.59	-8.29092	5.12E-09	3.833458
	2	56.11	-6.65787	2.20E-07	3.376205
	3	86.93	-5.79126	1.62E-06	3.133554
	4	86.1	-5.81026	1.55E-06	3.138872
	5	56.11	-6.65787	2.20E-07	3.376205
	6	27.08	-8.09999	7.94E-09	3.779996

Stochastic Coefficients

Coefficient of variation of K1, K2 and correlation between K1 and K2 are
selected as 0.2, 0.04 and –0.9 respectively, which are the typical values recommended in
the FLEXPASS manual.

Initial Serviceability Index

In this study, the initial serviceability index for all test lanes was assumed to be
4.2.

CHAPTER 9

DISCUSSION OF RESULTS AND CONCLUSIONS

ALF Field Results

Observed Field Rutting

The transverse profile taken for each station was used to calculate rut depth of the test lanes. For each test lane, transverse measurements were taken at eight stations over a length of 30 ft. within the 38-ft. loading area. Table 9.1 shows the transverse profile of the test lanes at the end of ALF loadings. Eight transverse profiles were measured after every 25,000 ALF load applications. The average of rut depth from each of these 8 measurements is reported and used to compare with the FLEXPASS predictions. The history of the average rut depths for the test lanes are included in Tables 9.2 through 9.4. Figure 9.2 shows the average rut depths versus accumulated 18 kip ESALs for all three test lanes. The results showed that rutting began very early for lane 2-3 (control lane) with 0.12 inch rut depth at about 35,000 18-kip ESALs, while the other two lanes showed very little rutting (around 0.03 inch) at this loading stage. The rutting developed at a much faster rate in lanes 2-3 and 2-1 than in lane 2-2. All three lanes experienced a uniform rate of rutting until around 500,000 ESALs when the rutting rate reduced dramatically in all lanes. During the first half million ESALs, rutting development in lane 2-3 was the fastest and the rut depth was the largest, whereas rutting development in lane

95

2-2 was the slowest and the rut depth was about 35% lower than the other two lanes. All three lanes showed little additional rut depth development between 500,000 and 2,100,000 ESALs. During this loading period, the wheel load was increased from 9,750 lbs. to 14,350 lbs. After that, the rut development began to increase again until the end of loading. The final measured rut depth for lane 2-1 and lane 2-3 were 0.56 inch and 0.55 inch respectively, both were about 55% higher than the rutting of lane 2-2 (0.36 inch).

Table 9.1 Transverse Profile of the Test Lanes at the end of ALF Loading

Transverse Dist. (in.)	Lane2-1	Lane2-2	Lane2-3	Transverse Dist. (in.)	Lane2-1	Lane2-2	Lane2-3
0	-0.075	0	-0.05	48	-1	-0.475	-0.85
2	-0.125	0	-0.05	50	-1.025	-0.45	-0.875
4	-0.15	0	-0.05	52	-1.025	-0.475	-0.85
6	-0.2	0	-0.05	54	-1	-0.475	-0.875
8	-0.25	0	-0.1	56	-0.95	-0.475	-0.85
10	-0.275	-0.025	-0.1	58	-0.9	-0.45	-0.8
12	-0.25	-0.075	-0.1	60	-0.8	-0.425	-0.8
14	-0.275	-0.1	-0.175	62	-0.725	-0.425	-0.8
16	-0.325	-0.15	-0.2	64	-0.6	-0.375	-0.725
18	-0.325	-0.15	-0.2	66	-0.55	-0.3	-0.675
20	-0.4	-0.15	-0.2	68	-0.475	-0.25	-0.6
22	-0.45	-0.175	-0.225	70	-0.425	-0.2	-0.575
24	-0.5	-0.2	-0.25	72	-0.375	-0.15	-0.5
26	-0.6	-0.225	-0.325	74	-0.375	-0.15	-0.5
28	-0.7	-0.25	-0.4	76	-0.375	-0.125	-0.475
30	-0.75	-0.275	-0.45	78	-0.325	-0.1	-0.45
32	-0.8	-0.325	-0.525	80	-0.275	-0.1	-0.45
34	-0.9	-0.4	-0.6	82	-0.25	-0.1	-0.4
36	-0.975	-0.425	-0.675	84	-0.225	-0.1	-0.325
38	-1	-0.5	-0.725	86	-0.165	-0.075	-0.275
40	-1	-0.5	-0.75	88	-0.2	-0.05	-0.25
42	-1.025	-0.5	-0.775	90	-0.15	-0.05	-0.225
44	-1.05	-0.475	-0.825	92	-0.15	0	-0.225
46	-1.075	-0.5	-0.85	94	-0.115	0	-0.175
				96	-0.1	0	-0.175

**Table 9.2 Average Rut Depth Measured for Lane 2-1
with Asphalt Rubber Wearing Course**

DATE	PASS NO.	Cumulative 18Kip ESAL	AVG RUT
2/2/99	0	0	0.00
3/18/99	25000	34425	0.12
3/29/99	50000	68850	0.17
4/8/99	75000	103275	0.18
4/22/99	100000	137700	0.19
5/17/99	150000	206550	0.27
5/27/99	175000	240975	0.29
6/10/99	200000	275400	0.30
6/22/99	225000	309825	0.33
7/20/99	275000	378675	0.36
8/9/99	300000	413100	0.37
8/23/99	325000	447525	0.40
9/8/99	350000	481950	0.41
9/22/99	375000	516375	0.41
10/4/99	400000	550800	0.41
10/21/99	425000	631050	0.41
12/6/99	500000	871800	0.41
12/20/99	525000	952050	0.43
1/11/00	550000	1194800	0.44
2/7/00	600000	1517800	0.44
5/1/00	675000	2133650	0.44
10/9/00	750000	3012200	0.56
11/27/00	800000	3994700	0.56

Table 9.3 Average Rut Depth Measured for Lane2-2
with Asphalt Rubber Base Course

DATE	PASS NO.	Cumulative ESAL	AVG RUT
2/2/99	0	0	0.00
3/18/99	25000	34425	0.04
3/29/99	50000	68850	0.10
4/8/99	75000	103275	0.10
4/22/99	100000	137700	0.10
5/17/99	150000	206550	0.13
5/27/99	175000	240975	0.14
6/10/99	200000	275400	0.18
6/22/99	225000	309825	0.19
7/20/99	275000	378675	0.22
8/9/99	300000	413100	0.22
8/23/99	325000	447525	0.24
9/8/99	350000	481950	0.25
9/22/99	375000	516375	0.26
10/4/99	400000	550800	0.26
10/21/99	425000	631050	0.26
12/6/99	500000	871800	0.26
12/20/99	525000	952050	0.26
1/11/00	550000	1194800	0.26
2/7/00	600000	1517800	0.26
5/1/00	675000	2133650	0.26
10/9/00	750000	3012200	0.36
11/27/00	800000	3994700	0.36
12/31/00	850000	4977200	0.36

Table 9.4 Average Rut Depth Measured for Lane2-3 with Conventional HMA

DATE	PASS NO.	Cumulative ESAL	AVG RUT
2/2/99	0	0	0.00
3/18/99	25000	34425	0.03
3/29/99	50000	68850	0.07
4/8/99	75000	103275	0.10
4/22/99	100000	137700	0.12
5/17/99	150000	206550	0.19
5/27/99	175000	240975	0.22
6/10/99	200000	275400	0.23
6/22/99	225000	309825	0.27
7/20/99	275000	378675	0.32
8/2/99	300000	413100	0.35
8/23/99	325000	447525	0.35
9/8/99	350000	481950	0.38
9/22/99	375000	516375	0.39
10/4/99	400000	550800	0.39
10/20/99	425000	631050	0.39
12/20/99	525000	952050	0.39
1/11/00	550000	1194800	0.39
2/7/00	600000	1517800	0.40
5/1/00	675000	2133650	0.40
10/9/00	750000	3012200	0.55
11/27/00	800000	3994700	0.55
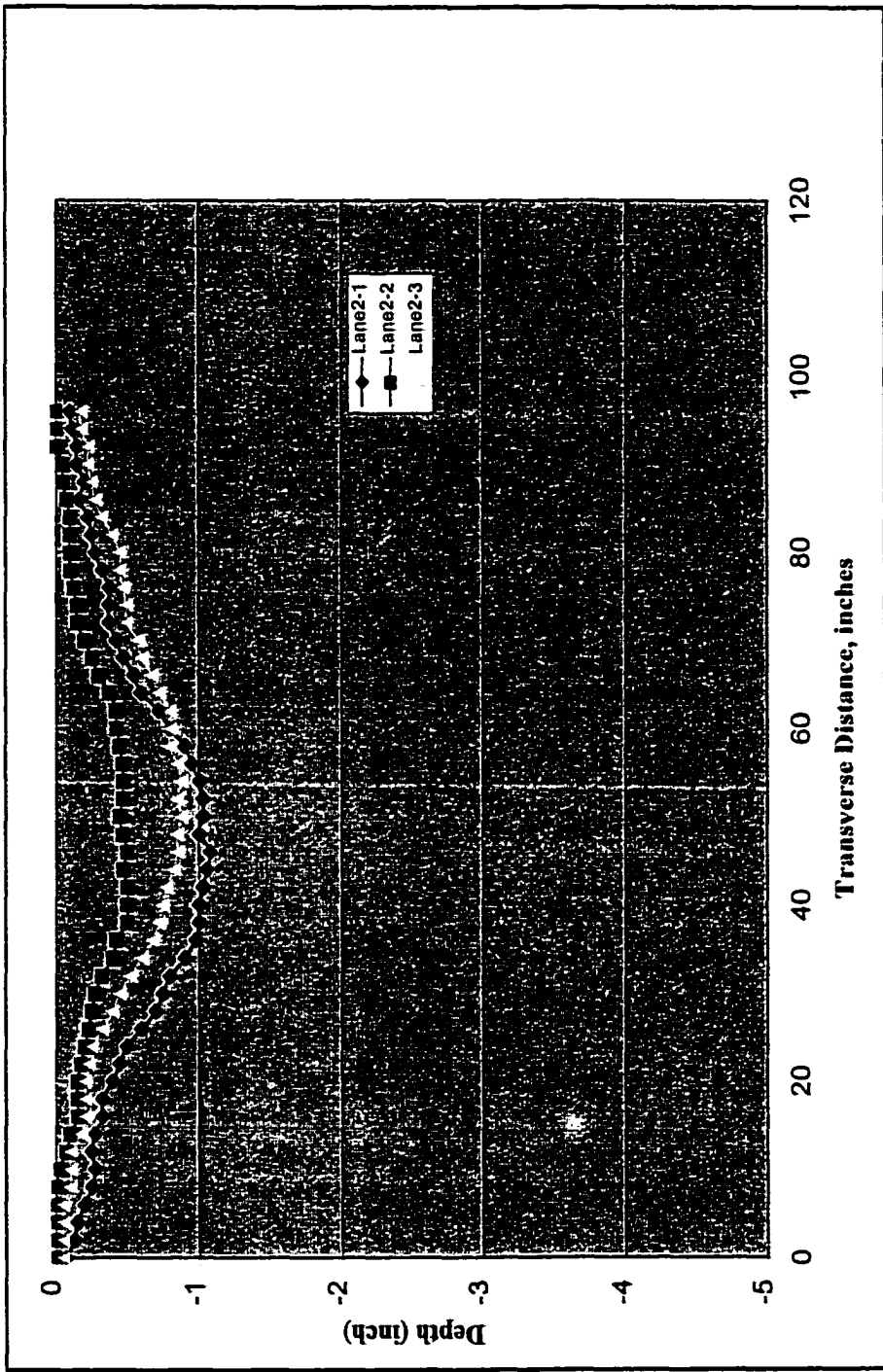
Figure 9.1 Transverse Profile for All Test Lanes at the End of ALF Testing
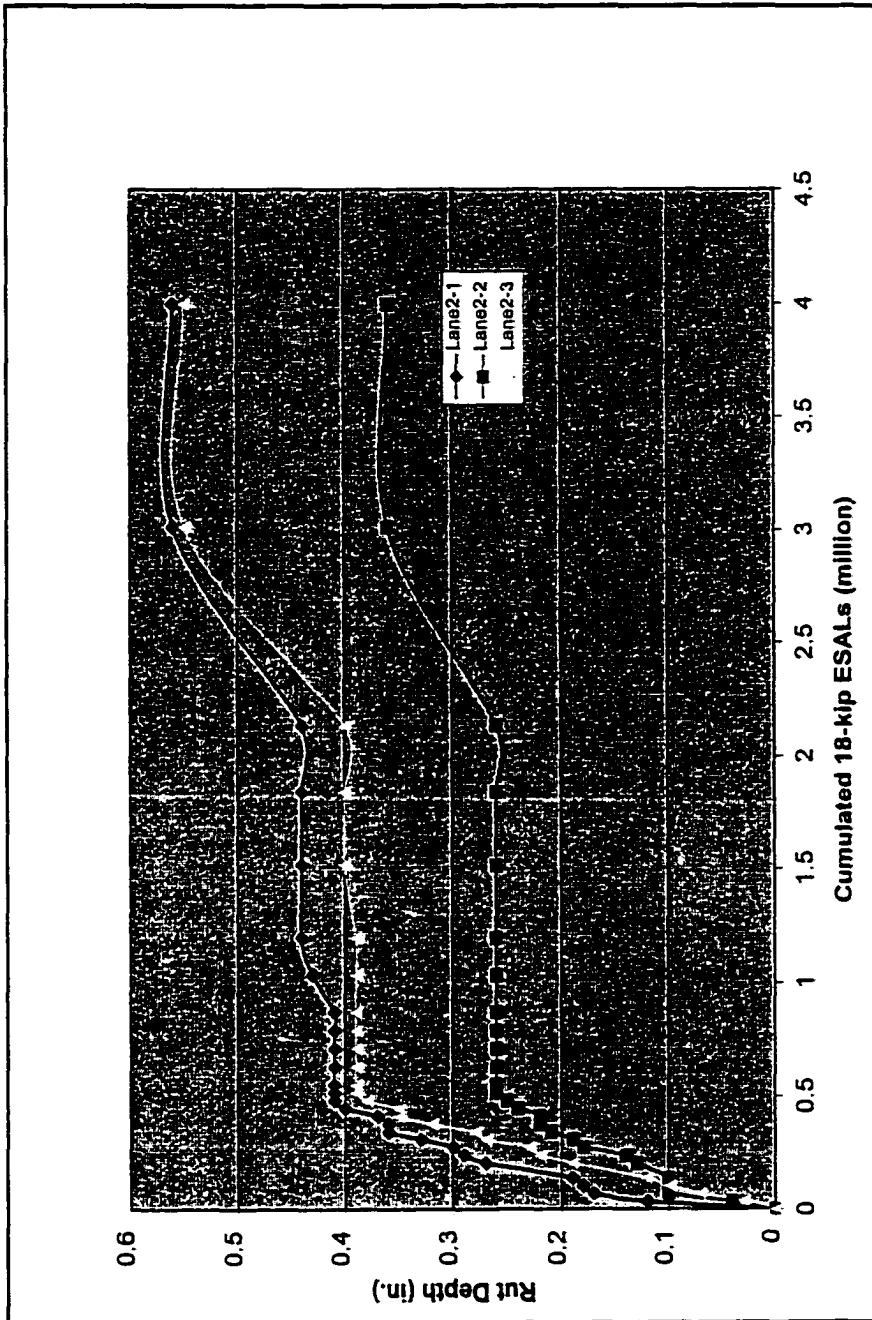
Figure 9.2 Observed Rut Depth versus Cumulative 18-kip ESALs of ALF Test Lanes

Observed Fatigue Cracking

The pavement surface was examined every 25,000 passes for evidence of cracking. There were no observed fatigue cracks in any of the lanes during the entire ALF loading history. In fact, no cracks of any type occurred in any of the test lanes.

Performance Prediction of Actual Sections from FLEXPASS Model

Rut Depth Predictions

Figure 9.3 shows the FLEXPASS rutting predictions using the constructed cross sections for all 3 lanes as shown in Figure 8.2. The predicted rut depths for lanes 2-1 and 2-3 are similar. These results are consistent with the field observations and also with the laboratory material characterization, which showed that the properties of the wearing course with or without crumb rubber were similar [2]. Lanes 2-1 and 2-3 showed no difference in the rut depth development up to 500,000 ESALs. After that, the rut depth development rate slowed down for all three lanes for the load interval between 500,000 and 1,500,000 ESALs. The rate of rut depth development began even smaller after 1.5 million ESALs until the end of loading. The final predicted rut depth for lane 2-1 was 0.67 inch, for lane 2-2 was 0.31 inch, and for lane 2-3 was 0.64 inch. The trends for these observations are consistent with the ALF field data while the FLEXPASS predictions were about 20% higher than the field values for lane 2-1 and 2-3 and about 15% lower than the field value for lane 2-2.

Slope Variance

Figure 9.4 shows the FLEXPASS predicted roughness for all the test lanes. The predicted slope variance developed at a rapid rate before 500,000 ESALs for all three lanes; then the development slowed down for the balance of the loading. The slope variance of lane 2-2 was the lowest, but the other two lanes showed similar slope variance development curves.

Fatigue Cracking

FLEXPASS did not predict any fatigure cracking development for any of the test lanes, a result consistent with the field observations.

Present Serviceability Index

Figure 9.5 shows the predicted PSI for all three test lanes. The initial PSI was assumed to be 4.2. The comparison showed that the PSI of lane 2-3 decreased faster than the other two lanes. Since no fatigue cracking occurred, the predicted PSI at the end of loading for all three test lanes was higher than the terminal value of 2.5.
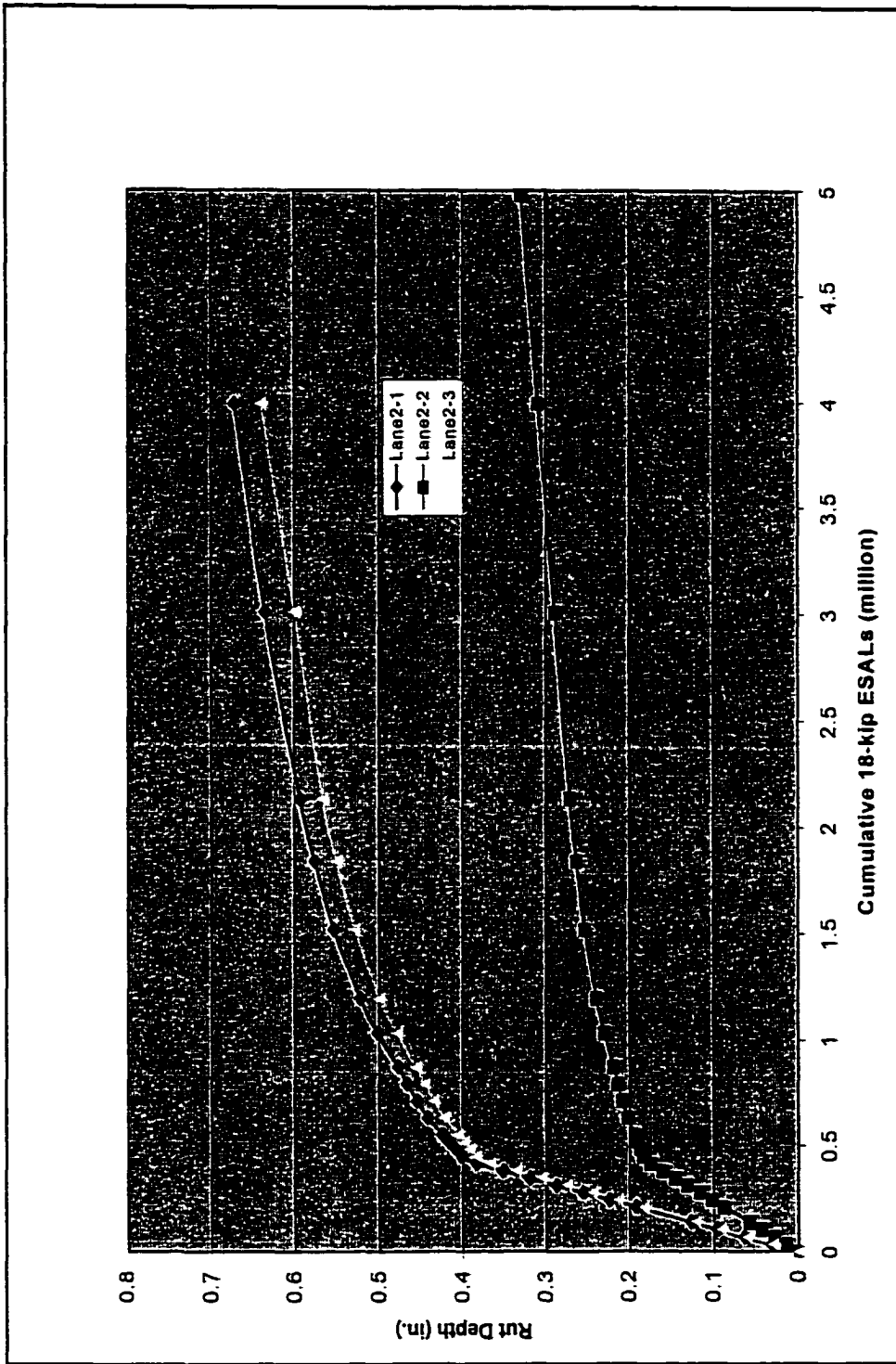
Figure 9.3 Comparison of Predicted Rut Depth for All ALF Test Lanes
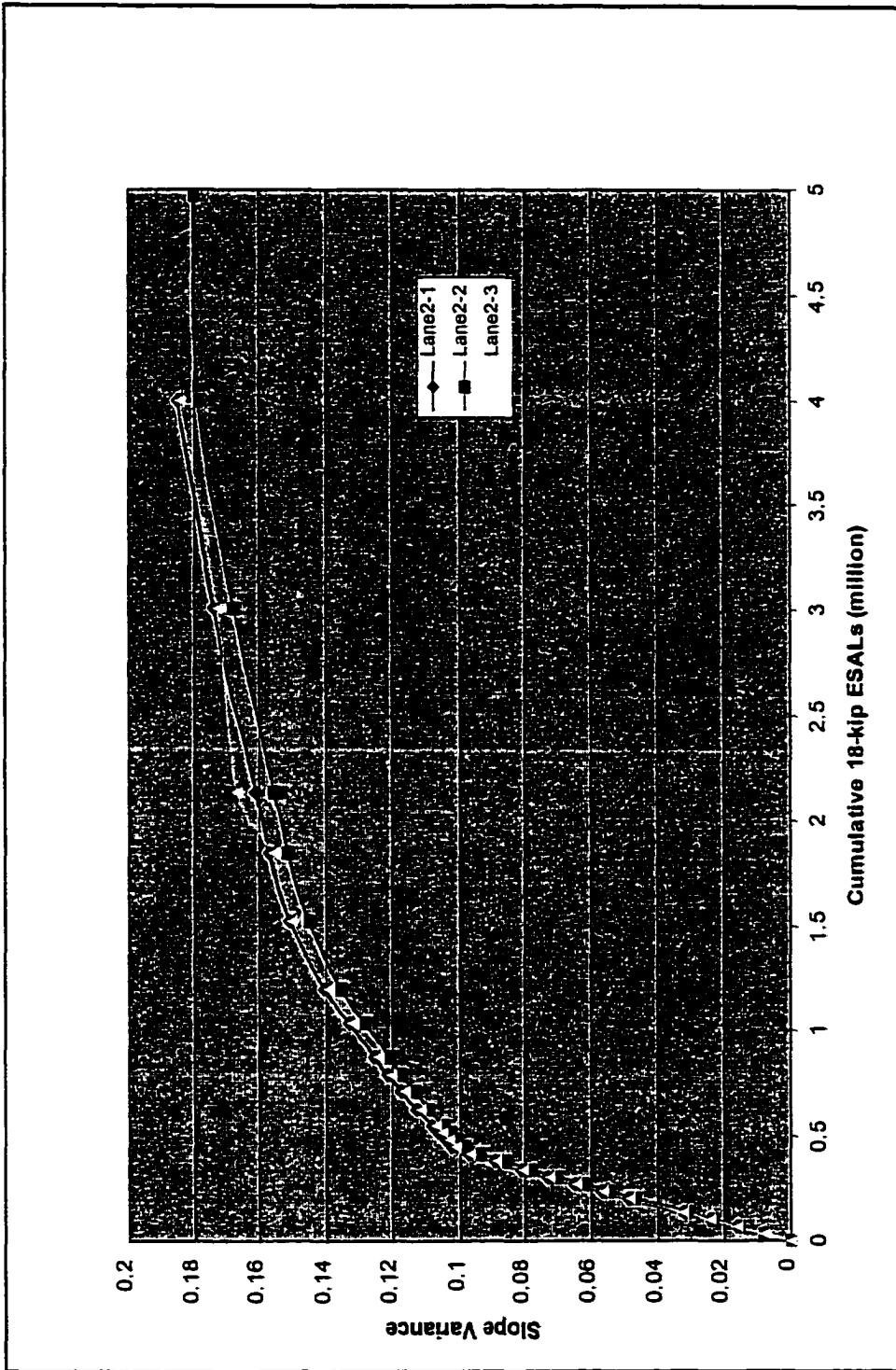
Figure 9.4 FLEXPASS Predicted Slope for All ALF Test Lanes
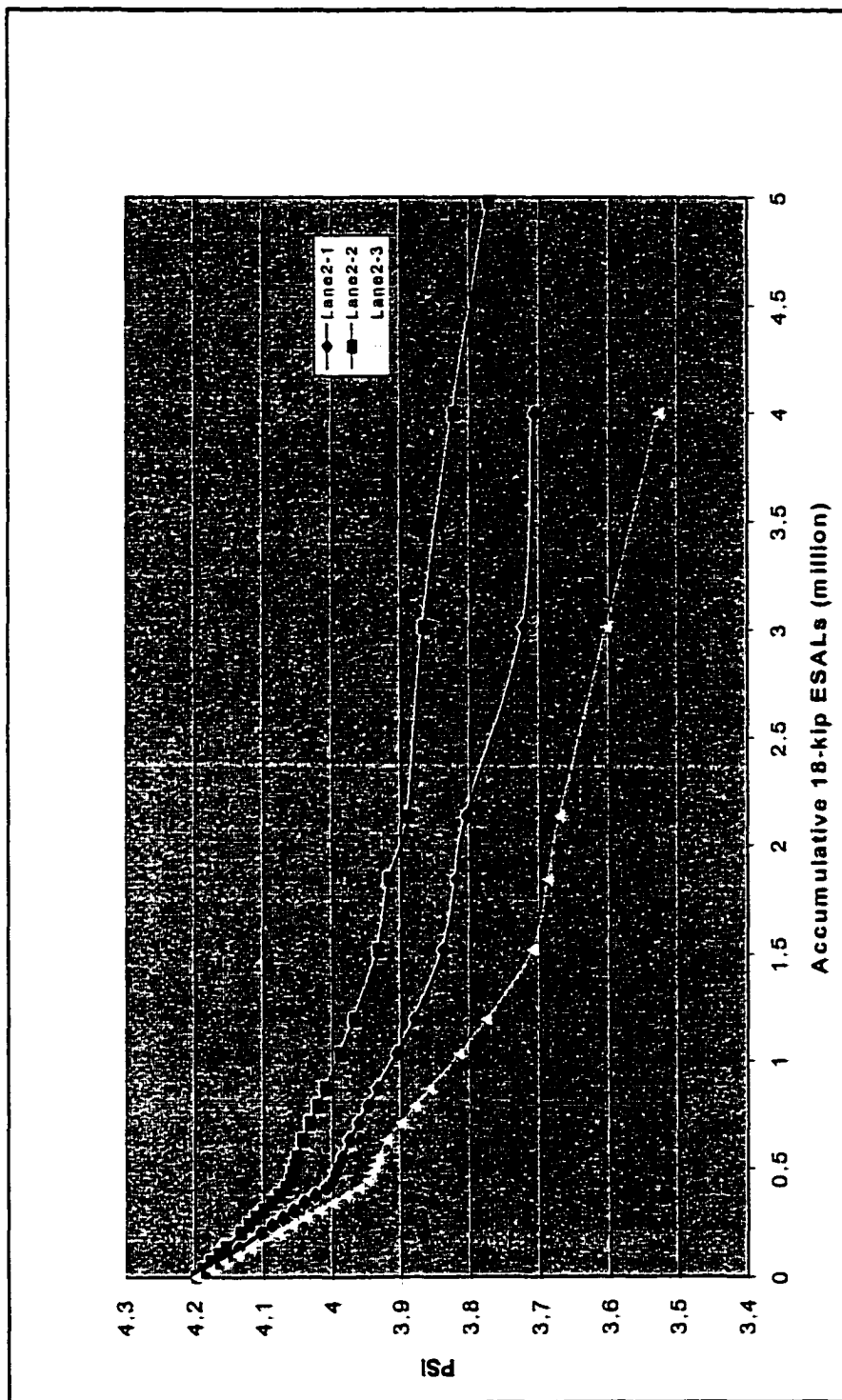
Figure 9.5 FLEXPASS Predicted PSI for All Test Lanes

Comparison between Predicted Distress and Observed Distress

Because the only observed distress was rutting, the only comparison will be that between predicted and observed rutting. Figure 9.6 shows the rutting development for FLEXPASS prediction as well as the measured observations for lane 2-1. Field rutting began at 34,425 18-kip ESALs and increased rapidly to around 0.40 inch at about 500,000 18-kip ESALs. The rut depth remained relatively constant until at about 2 million 18-kip ESALs. After 2 million ESALs, the rut depth began to increase sharply as the half axle load increased above 14.35 kips. The observed performance of lane 2-1 shows the three typical phases of rutting which are observed in HMA pavements. In phase I, the initial rutting increases at a rapid rate early in the life of the pavement, in Figure 9.6 from zero to about 500,000 ESALs. Phase II is the stable region of performance where the slope of the rutting curve is fairly flat. The length of phase II varies and in Figure 9.6 lasts from about 500,000 ESALs until about 2,200.000 ESALs corresponding to wheel loads increasing from 9,750 lbs to 14,350 lbs on the half single axle. In phase III, there is a very rapid increase in the rate of rutting as the HMA material experiences rapid shear flow typically associated with low air void contents. Figure 9.6 shows a rapid increase in rutting starting at about 2,200,000 ESALs and continuing as the wheel load increases from 14,350 lbs to 16,650 lbs at 3 million ESALs. This trend continued as the wheel load increased to 18,950 lbs until testing was terminated at 4 million ESALs for lane 2-1. It should be noted that while the rate of rutting increased as the wheel loads increased from 14,350 to 18,950 lbs, there was no evidence of shear flow adjacent to the wheel loaded area. As a result of this observation, the authors believe that section 2-1 pavements were still behaving in the phase II region of rutting. The

FLEXPASS prediction also showed that rutting increased rather rapidly at the early loading stage until at about 450,000 18-kip ESALs, where the rate of rutting development decreased. The predicted rut depth was about 20% more than the measured field data. The pattern of predicted behavior from FLEXPASS is typical of that obtained from computer programs which include material characterizations using creep tests to model the behavior of materials in phases I and II of rutting. The traffic loadings in FLEXPASS are in terms of 18 kip ESALs so the effect of increasing the axle load is reflected by an increased rate of ESALs per traffic period. Since this traffic is applied when the rutting behavior is nearly flat, the effect of these loads is less in the predictions than is shown in the field data.

Figure 9.7 show the comparison of rutting development for FLEXPASS prediction and field measurements for test lane 2-2, which includes the AR Type 5A base. The field results showed that rutting began at 34,425 18-kip ESALs and increased rapidly to around 0.26 inch at about 500,000 18-kip ESALs. But then the rutting remained constant until about 2,100,000 18-kip ESALs where the load was 14,350 lbs. After that, the rut depth increased rapidly. The FLEXPASS prediction also showed that rutting increased rather quickly at the early loading stage until 0.20 inch at about 550,000 18-kip ESALs. Then the rate of rutting development began decreasing. The FLEXPASS prediction is less than the field result, but as the axle loads increased, the predicted and observed rut depths were very similar.

Figure 9.8 shows the comparison of rutting development for FLEXPASS prediction and field measurement of ALF test lane 2-3, the conventional HMA and control section. The field results showed that rutting began at very early loading level and

increased rapidly to around 0.41 inch at about 450,000 18-kip ESALs. The rut pattern for the conventional materials showed a rapid rise in rutting with each increase in axle load, but then rutting leveled off. The FLEXPASS prediction also showed that rutting increased more steeply at the early loading stage until 0.40 inch at about 550,000 18-kip ESALs. Then the rate of rutting development slowed down, but rutting developed gradually as the wheel loads increased because the number of 18 kip ESALs per axle pass increased as the loads increased. The predicted rutting was less than the field rutting until around 500,000 18 kip ESALs. After that loading level, the predicted rutting exceeded the observed rutting. The predicted rut depth was about 15% larger than the observed field rutting when testing terminated.

Discussion of Differences between Predicted and Observed Distresses

At the early loading level, both field measurement and predictions showed a similar trend of rut development even though FLEXPASS tends to underestimate the rut depth. After the early rut development, both the predicted and observed rate of rutting began to slow down, and the observed rutting was lower than the predicted rutting. This pattern can be attributed to several things. First, the FLEXPASS model is based on the finite element method for a depth-limited multilayer system over a rigid base. The test lane is considered to be a depth-limited continuum over a rigid layer, and the nodes at the bottom of the model are considered to be fixed in both the horizontal and vertical directions. As a result, the vertical deformation will be restrained during the early loading stages when the materials still show elastic characteristics. Second, the FLEXPASS model was calibrated to predict the normal service behavior of pavements and not those experiencing short term accelerated loading. The magnitude of wheel loads on the ALF

test lanes was so large and applied so intensively that once distress occurred, there was no chance for the pavement to experience the recovery and healing which occurs in normal service. The net effect is that at the early loading stages, FLEXPASS predictions are less severe than observations of field performance. Third, the ALF field test ESAL data were recorded sequentially as the axle loads were applied. However, in the FLEXPASS model, the load applications were grouped according to several temperatures. For example, all the days when ALF loads were applied were assigned to one of six seasonal temperatures. When all days had been assigned, the ESALs for each season were determined by adding up the daily values. Since only 6 seasonal temperatures could be input into FLEXPASS and the testing period occurred over 2 years, it was not possible to input the loading sequence as it occurred. The similarity of result for fatigue cracking predictions of FLEXPASS with the field data indicates that the material modeling for FLEXPASS is consistent with the field materials.

Overall the fact that the FLEXPASS model predictions compared favorably with observed field data indicates that no further adjustments or modification are needed to calibrate the model.

The following observations were made:

- The numerical simulation model created by FLEXPASS is sufficient and adequate to predict the performance of the three test lanes under ALF loading.

- The rut depth of the lane with conventional materials was similar to that of the lane with CRM-HMA Type 8F wearing course.

- The lane with CRM-HMA Type 5A base course had the lowest rut depth both in the ALF field test and in the FLEXPASS prediction.

- The lane with CRM-HMA Type 5A base course worked better in resisting rutting development than the lane with all conventional materials. It shall be noted that the conventional Type 5A base was constructed with an AC 30 asphalt cement while the asphalt rubber binder had similar characteristics to that of the PAC 40 binder, see Table 4.4. One implication of this observation is that improved performance occurs when more strain-tolerant materials are included in the base.

- The lane with CRM-HMA Type 5A base course showed higher PSI than the lanes with all conventional materials or with the CRM-HMA Type 8 wearing course.

- No fatigue cracking occurred for all three test lanes in the ALF field test or in the FLEXPASS prediction during the loading history.
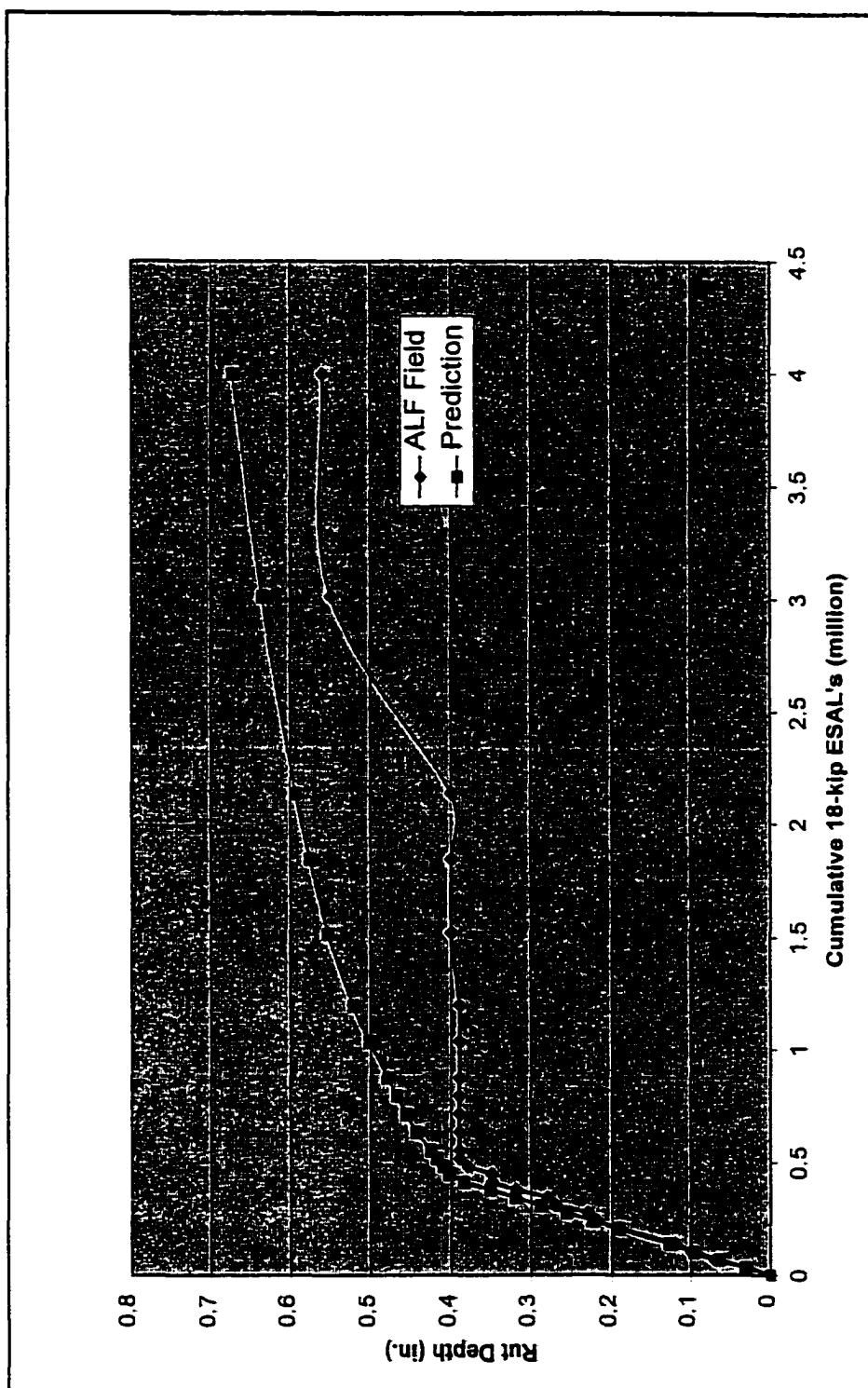
Figure 9.6 Rut Depth Comparison between Field and Prediction Data for Lane 2-1
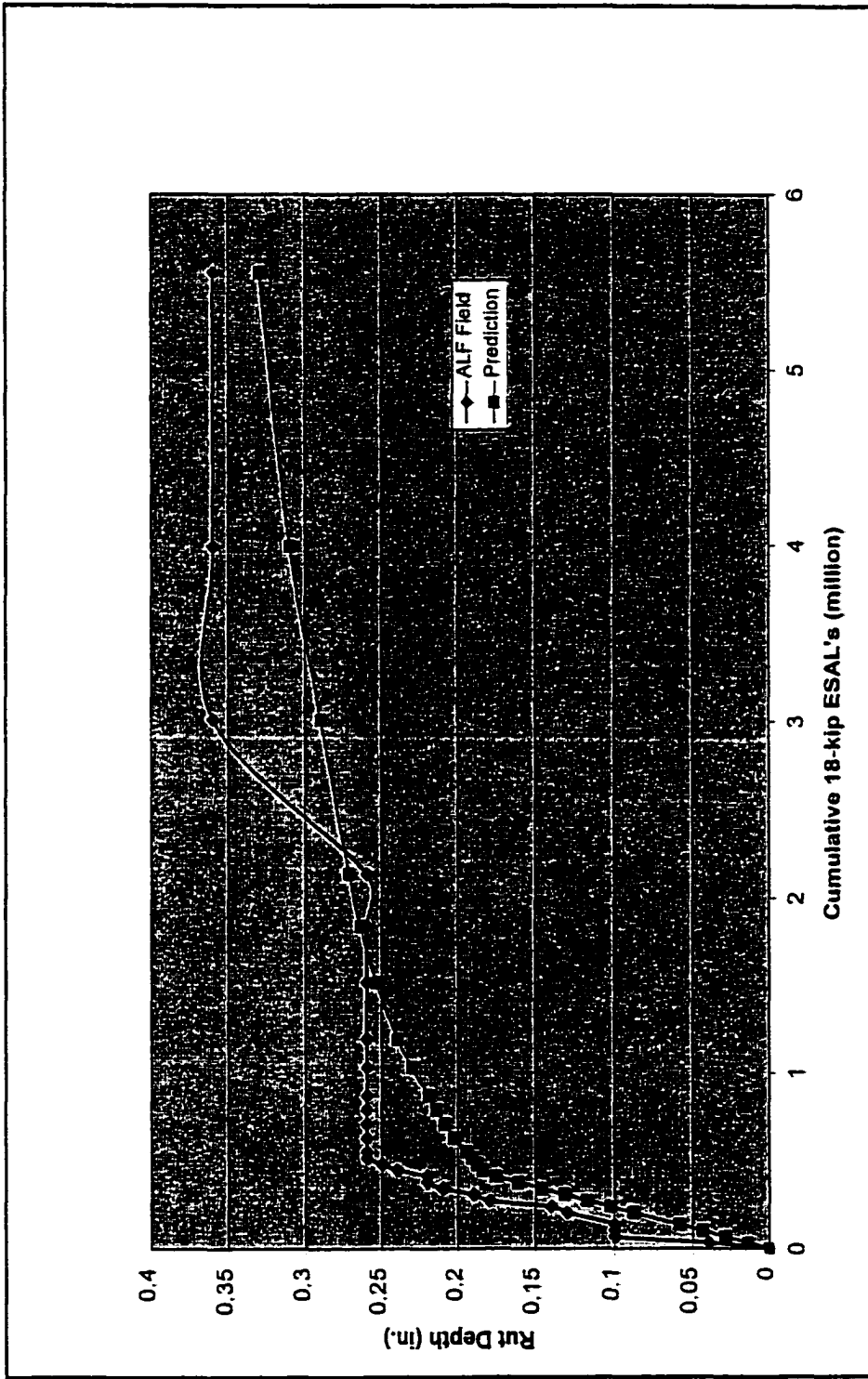
Figure 9.7 Rut Depth Comparison between Field and Prediction Data for Lane2-2
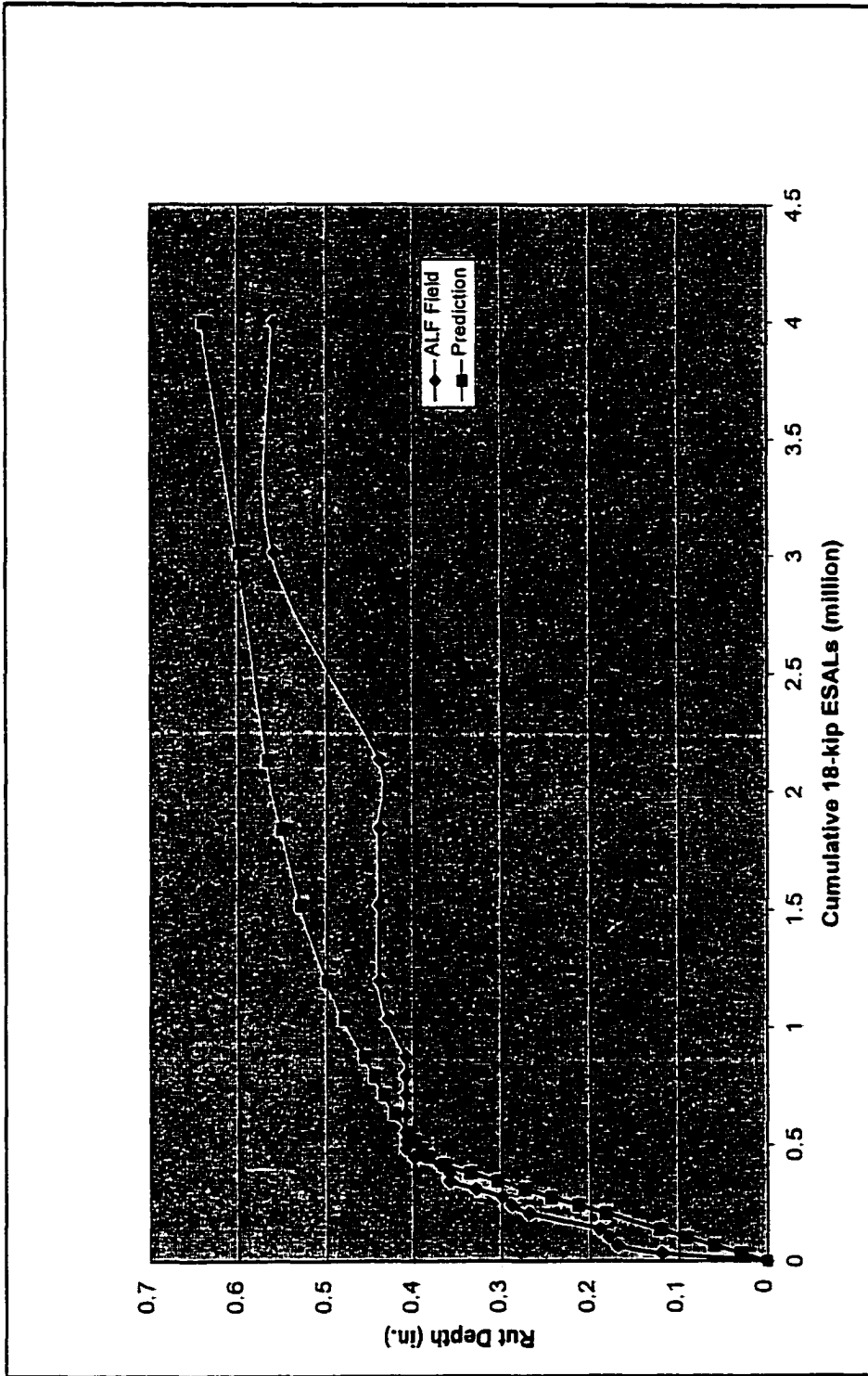
Figure 9.8 Rut Depth Comparison between Field and Prediction Data for lane2-3 (Control Lane)

Conclusions

The purpose of this project was to test, evaluate, and compare the performance of HMA and asphalt rubber materials used in the construction of three test lanes at the PRF. Numerical simulations of the same three test lanes were also generated to determine if computer models could be used to extend the application of the field studies. The following conclusions were made after comparing the results from the ALF field measurement with those from the FLEXPASS numerical predictions:

1. Based on the results from this study, one may observe that there is good agreement between FLEXPASS predictions and observed field performance and conclude that FLEXPASS can be used to successfully model Louisiana flexible pavements.

2. DOTD should consider extending the use of modified binders in all flexible pavement layers in the light of the superior performance of the AR Type 5A base section.

3. DOTD should consider adding asphalt rubber materials to its list of available base course materials.

APPENDIX A

LOADING PROCEDURE FOR REPEATED LOAD COMPRESSION (RLC) TEST

116

1. Place test specimens in the controlled temperature cabinet and bring it to the specified test temperature. Center the specimen under the loading apparatus in the controlled temperature cabinets.

2. Extend the lower LVDT clamp and slide it carefully down over the specimen to approximately the lower quarter point of the specimen. Repeat for the upper clamp, placing it at the upper quarter point. Ensure that both clamps lie in horizontal planes and that the holes in the clamps are properly aligned. Place the precalibrated LVDTs into position in the clamps. Connect the LVDTs to the recording unit. Determine to the nearest 0.01inch (0.25mm), the vertical spacing between the LVDT clamps and record this value.

3. For conditioning, apply a 20 psi ramp load and hold for 10 minutes duration, and unload. If deformation during the initial load exceeds 2,500 micro units of strain, reduce stress by 5 psi and repeat until strain level remains below 2,500 micro units. Unload and immediately apply a second conditioning load at the same level for 10 minutes. Release 2nd load and immediately apply a third conditioning load for 10 minutes. Followed by a 10-minute unload period; re-zero LVTDs.

4. Incremental static loading.

   a. At the test temperature, apply one ramp load at the level identified in step 3 to the specimen as quickly as possible and hold loading for 0.1 second. Release the load and measure total permanent deformation after 2 minutes of unload. See figure 5.4 for a description of the loading function. [Note: If at any time the deformation under load starts to exceed 2,500 micro units of strain, immediately reduce the maximum stress level by 5 psi. If the deformation starts to exceed 2,500 micro

strain, then reduce the stress level by another 5 psi. Wait 30 minutes and repeat Step 4a. at this level.]

b. Apply a second ramp load to the specimen at the same stress level used above and hold for 1 second. Release the load and measure the total permanent deformation after 2 minutes of unload.

c. Apply a third ramp load to the specimen at the stress level used in step 4a and hold for 10 seconds. Release the load and measure the total permanent deformation after 2 minutes of unload or when rebound becomes negligible.

d. Apply a fourth ramp load to the specimen at the level used in step 4a above and hold for 100 seconds. Release the load and measure the total permanent deformation remaining after 4 minutes of unload or when rebound becomes negligible.

e. Apply a fifth ramp load to the specimen at the level used in step 4a above and hold for 1,000 seconds. Measure the magnitude of the creep deformation during loading after 0.03, 0.1, 0.3, 1.0, 3.0, 10.0, 30.0, 100.0, and 1,000.0 seconds. Release the load and measure the total permanent deformation after 8 minutes of unload or when rebound becomes negligible.

f. Re-zero LVDTs.

5. Repeated dynamic loading.

Apply repeated haversine loading to the specimen at the test temperature such that each load application has a magnitude equal to the stress level used in step 4a above and each load application has a load duration of a 0.1 second. A 0.9-second rest period follows each load application. Apply a minimum of 10,000 load applications

and measure the accumulated deformation at 1, 10, 100, 200, 1,000, and 10,000 repetitions. Read the peak-to-peak strain at the 200th cycle.

6. Release the load after 10,000 repetitions, record the rebound for a period of 15 minutes and remove the specimen.

7. Using new specimens, repeat steps 1 through 8 for another specified temperature. Note that the 104F level loads may have to be decreased in accordance with Table 5.2.

8. Repeat step 1 through 9 for at least two more replicates for each specified temperature.

APPENDIX B

RESULTS OF REPEATED COMPRESSION TESTS

120

Table B.1 T8F Wearing Course at 40 °F

Specimen	Cycle	Stroke	Deformation	Strain	Log(Strain)
1a#	1	0.417893	0	0	
	10	0.417806	8.64E-05	1.45E-05	-4.83805
	100	0.41747	0.000423	7.1E-05	-4.14869
	200	0.417164	0.000729	0.000122	-3.91197
	1000	0.417122	0.00077	0.000129	-3.88802
	3000	0.417115	0.000778	0.000131	-3.88382
	6000	0.417105	0.000788	0.000132	-3.87827
	10000	0.417092	0.0008	0.000134	-3.8714
2a#	1	0.415838	0	0	
	10	0.415804	3.38E-05	5.68E-06	-5.24553
	100	0.415643	0.000195	3.28E-05	-4.48377
	200	0.415459	0.000379	6.38E-05	-4.19545
	1000	0.415241	0.000597	0.0001	-3.99838
	3000	0.415128	0.00071	0.000119	-3.92331
	6000	0.415102	0.000736	0.000124	-3.90752
	10000	0.415098	0.00074	0.000124	-3.90531
3a#	1	0.479322	0	0	
	10	0.479302	2.03E-05	3.41E-06	-5.46738
	100	0.478885	0.000437	7.35E-05	-4.13382
	200	0.478783	0.000539	9.05E-05	-4.04323
	1000	0.478772	0.00055	9.24E-05	-4.03423
	3000	0.478761	0.000561	9.43E-05	-4.02543
	6000	0.478744	0.000578	9.72E-05	-4.01254
	10000	0.478699	0.000623	0.000105	-3.97993

Table B.2 T8F Wearing Course at 77 °F

Specimen	Cycle	Stroke	Deformation	Strain	Log(strain)
3#	1	0.41476	0	0	
	10	0.414752	7.51E-06	1.26E-06	-5.89948
	100	0.414704	5.63E-05	9.45E-06	-5.02441
	200	0.41464	0.00012	2.02E-05	-4.69536
	1000	0.414565	0.000195	3.28E-05	-4.4845
	10000	0.414437	0.000323	5.42E-05	-4.26601
4#	1	0.412108	0	0	
	10	0.412012	9.58E-05	1.61E-05	-4.79251
	100	0.411331	0.000778	0.000131	-3.88308
	200	0.410829	0.001279	0.000215	-3.66693
	1000	0.41017	0.001938	0.000326	-3.4864
	10000	0.409742	0.002366	0.000398	-3.3997
5#	1	0.412142	0	0	
	10	0.412022	0.00012	2.02E-05	-4.6939
	100	0.411832	0.00031	5.22E-05	-4.28259
	200	0.411462	0.00068	0.000114	-3.94137
	1000	0.411177	0.000965	0.000163	-3.78911
	10000	0.410737	0.001405	0.000236	-3.62617

Table B.3 T8F Wearing Course at 104 °F

Specimen	Cycle	Stroke	Deformation	Strain	Log (strain)
2#	1	0.405894	0	0	
	10	0.405888	5.63E-06	9.47E-07	-6.02368
	100	0.405802	9.2E-05	1.55E-05	-4.81061
	200	0.405775	0.000118	1.99E-05	-4.70147
	1000	0.40564	0.000254	4.26E-05	-4.37047
	3000	0.40552	0.000374	6.28E-05	-4.20195
	6000	0.405347	0.000547	9.19E-05	-4.03691
	10000	0.405227	0.000667	0.000112	-3.95058
6#	1	0.402462	0	0	
	10	0.402417	4.51E-05	7.58E-06	-5.12059
	100	0.40235	0.000113	1.89E-05	-4.72265
	200	0.402274	0.000188	3.16E-05	-4.50081
	1000	0.402143	0.000319	5.37E-05	-4.27036
	3000	0.402057	0.000406	6.82E-05	-4.16635
	6000	0.401921	0.000541	9.09E-05	-4.04141
	10000	0.401891	0.000571	9.6E-05	-4.01793

Table B.4 T8F-CRM Wearing Course at 40 °F

Specimen	Cycle	Stroke	Deformation	Strain	Log (strain)
1a#	1	0.416086	0	0	
	10	0.416052	3.38E-05	5.68E-06	-5.24553
	100	0.415815	0.00027	4.55E-05	-4.34244
	200	0.415549	0.000537	9.03E-05	-4.04444
	1000	0.415158	0.000928	0.000156	-3.80708
	3000	0.414978	0.001108	0.000186	-3.72995
	6000	0.414873	0.001213	0.000204	-3.69057
	10000	0.414863	0.001223	0.000205	-3.68722
2a#	1	0.415103	0	0	
	10	0.415077	2.59E-05	4.36E-06	-5.36093
	100	0.414929	0.000174	2.93E-05	-4.53326
	200	0.41482	0.000283	4.76E-05	-4.3224
	1000	0.414587	0.000516	8.67E-05	-4.06179
	3000	0.414516	0.000587	9.87E-05	-4.00554
	6000	0.414508	0.000595	1E-04	-4.00002
	10000	0.414504	0.000599	0.000101	-3.99729
3a#	1	0.417576	0	0	
	10	0.417547	2.91E-05	4.89E-06	-5.31047
	100	0.417457	0.000119	2E-05	-4.69803
	200	0.417389	0.000187	3.14E-05	-4.50298
	1000	0.417209	0.000367	6.17E-05	-4.20966
	3000	0.417134	0.000442	7.43E-05	-4.12882
	6000	0.416991	0.000585	9.83E-05	-4.00735
	10000	0.416927	0.000649	0.000109	-3.96236

Table B.5 T8F-CRM Wearing Course at 77 °F

Specimen	Cycle	Stroke	Deformation	Strain	Log (strain)
1#	1	0.415034	0	0	
	10	0.414993	4.13E-05	6.94E-06	-5.15838
	100	0.414441	0.000593	9.97E-05	-4.00112
	200	0.413994	0.00104	0.000175	-3.7573
	1000	0.413445	0.001589	0.000267	-3.57344
	10000	0.412844	0.00219	0.000368	-3.43411
2#	1	0.407127	0	0	
	10	0.407116	1.13E-05	1.9E-06	-5.72229
	100	0.406985	0.000143	2.4E-05	-4.61963
	200	0.406722	0.000406	6.82E-05	-4.16599
	1000	0.406324	0.000804	0.000135	-3.869
	10000	0.405933	0.001194	0.000201	-3.69698
7#	1	0.413892	0	0	
	10	0.413885	7.51E-06	1.26E-06	-5.89875
	100	0.413825	6.76E-05	1.14E-05	-4.9445
	200	0.413761	0.000131	2.21E-05	-4.65571
	1000	0.413719	0.000173	2.9E-05	-4.53702
	10000	0.413472	0.000421	7.07E-05	-4.15056

Table B.6 T8F-CRM Wearing Course at 104 °F

Specimen	Cycle	Stroke	Deformation	Strain	Log (Strain)
4#	1	0.404606	0	0	
	10	0.404577	2.91E-05	4.89E-06	-5.31047
	100	0.404491	0.000116	1.94E-05	-4.71193
	200	0.404446	0.000161	2.7E-05	-4.56884
	1000	0.404314	0.000292	4.91E-05	-4.30908
	3000	0.404228	0.000378	6.36E-05	-4.19653
	6000	0.404055	0.000551	9.26E-05	-4.0332
	10000	0.403953	0.000653	0.00011	-3.95985
5#	1	0.403048	0	0	
	10	0.403003	4.51E-05	7.59E-06	-5.11986
	100	0.402988	6.01E-05	1.01E-05	-4.99493
	200	0.402981	6.76E-05	1.14E-05	-4.94377
	1000	0.402951	9.77E-05	1.64E-05	-4.78407
	3000	0.402909	0.000139	2.34E-05	-4.63084
	6000	0.402755	0.000293	4.93E-05	-4.30695
	10000	0.402601	0.000447	7.52E-05	-4.1235
6#	1	0.405749	0	0	
	10	0.405741	7.51E-06	1.26E-06	-5.89875
	100	0.405629	0.00012	2.02E-05	-4.69463
	200	0.405621	0.000128	2.15E-05	-4.6683
	1000	0.405572	0.000177	2.97E-05	-4.52768
	3000	0.405452	0.000297	4.99E-05	-4.30215
	6000	0.405283	0.000466	7.83E-05	-4.10635
	10000	0.405073	0.000676	0.000114	-3.9445

Table B.7 T5A Black Base Course at 40 °F

Specimen	Cycle	Stroke	Deformation	Strain	Log (strain)
1a#	1	0.408967	0	0	
	10	0.408848	0.000119	2E-05	-4.69803
	100	0.408483	0.000484	8.13E-05	-4.09003
	200	0.408232	0.000735	0.000124	-3.90807
	1000	0.407507	0.00146	0.000245	-3.61011
	3000	0.407484	0.001483	0.000249	-3.60345
	6000	0.407475	0.001492	0.000251	-3.60075
	10000	0.407462	0.001505	0.000253	-3.5969
2a#	1	0.413573	0	0	
	10	0.413483	9.01E-05	1.52E-05	-4.81956
	100	0.412949	0.000624	0.000105	-3.97967
	200	0.412645	0.000928	0.000156	-3.80708
	1000	0.412476	0.001097	0.000184	-3.73439
	3000	0.412311	0.001262	0.000212	-3.67344
	6000	0.412104	0.001469	0.000247	-3.6076
	10000	0.411894	0.001679	0.000282	-3.54947
3a#	1	0.409297	0	0	
	10	0.40928	1.66E-05	2.79E-06	-5.55464
	100	0.409136	0.000161	2.7E-05	-4.5688
	200	0.408975	0.000321	5.4E-05	-4.26781
	1000	0.408615	0.000682	0.000115	-3.9409
	3000	0.408374	0.000922	0.000155	-3.80972
	6000	0.408337	0.00096	0.000161	-3.79239
	10000	0.408232	0.001065	0.000179	-3.74722

Table B.8 T5A Black Base Course at 77 °F

Specimen	Cycle	Stroke	Deformation	Strain	Log (strain)
2#	1	0.40889	0	0	
	10	0.408825	6.46E-05	1.09E-05	-4.96388
	100	0.408791	9.84E-05	1.66E-05	-4.78111
	200	0.408694	0.000196	3.3E-05	-4.48174
	1000	0.408682	0.000207	3.49E-05	-4.45747
	10000	0.408352	0.000538	9.05E-05	-4.04347
5#	1	0.413261	0	0	
	10	0.413175	8.64E-05	1.46E-05	-4.8371
	100	0.412544	0.000717	0.000121	-3.91779
	200	0.412405	0.000856	0.000144	-3.84089
	1000	0.412356	0.000905	0.000152	-3.81681
	10000	0.412044	0.001217	0.000205	-3.68828

Table B.9 T5A Black Base Course at 104 °F

Specimen	Cycle	Stroke	Deformation	Strain	Log (strain)
3#	1	0.399882	0	0	
	10	0.399837	4.51E-05	7.58E-06	-5.12059
	100	0.399795	8.64E-05	1.45E-05	-4.83805
	200	0.399728	0.000154	2.59E-05	-4.58699
	1000	0.399641	0.00024	4.04E-05	-4.3936
	3000	0.399424	0.000458	7.7E-05	-4.11342
	6000	0.399343	0.000539	9.06E-05	-4.04305
	10000	0.399213	0.000669	0.000112	-3.94919
4#	1	0.399021	0	0	
	10	0.39901	1.05E-05	1.77E-06	-5.75262
	100	0.398924	9.69E-05	1.63E-05	-4.78816
	200	0.398804	0.000217	3.65E-05	-4.43785
	1000	0.398759	0.000262	4.41E-05	-4.35592
	3000	0.398699	0.000322	5.42E-05	-4.26629
	6000	0.398627	0.000394	6.62E-05	-4.17941
	10000	0.398518	0.000503	8.45E-05	-4.07332
6#	1	0.407594	0	0	
	10	0.407578	1.58E-05	2.65E-06	-5.57653
	100	0.407522	7.21E-05	1.21E-05	-4.91647
	200	0.407484	0.00011	1.84E-05	-4.73439
	1000	0.40746	0.000134	2.25E-05	-4.64711
	3000	0.40739	0.000204	3.42E-05	-4.46578
	6000	0.407326	0.000267	4.49E-05	-4.3473
	10000	0.407225	0.000369	6.2E-05	-4.20766

Table B.10 T5A-CRM Base Course at 40 °F

Specimen	Cycle	Stroke	Deformation	Strain	Log (strain)
2a#	1	0.414801	0	0	
	10	0.414707	9.39E-05	1.58E-05	-4.80184
	100	0.414471	0.000331	5.56E-05	-4.25529
	200	0.414411	0.000391	6.57E-05	-4.18274
	1000	0.41417	0.000631	0.000106	-3.97447
	3000	0.41405	0.000751	0.000126	-3.89875
	6000	0.413964	0.000838	0.000141	-3.85147
	10000	0.413907	0.000894	0.00015	-3.8232
3a#	1	0.412112	0	0	
	10	0.412048	6.39E-05	1.07E-05	-4.96933
	100	0.411945	0.000167	2.81E-05	-4.55142
	200	0.411762	0.000349	5.87E-05	-4.23129
	1000	0.411485	0.000627	0.000105	-3.97706
	3000	0.411289	0.000823	0.000138	-3.85933
	6000	0.411263	0.000849	0.000143	-3.84567
	10000	0.411255	0.000856	0.000144	-3.84184
4a#	1	0.411714	0	0	
	10	0.411522	0.000192	3.22E-05	-4.49221
	100	0.411045	0.000669	0.000112	-3.94936
	200	0.41073	0.000984	0.000165	-3.78147
	1000	0.410407	0.001307	0.00022	-3.6582
	3000	0.41026	0.001454	0.000244	-3.61207
	6000	0.41023	0.001484	0.000249	-3.60318
	10000	0.410106	0.001608	0.00027	-3.56833

Table B.11 T5A-CRM Base Course at 77 °F

Specimen	Cycle	Stroke	Deformation	Strain	Log (strain)
2#	1	0.455801	0	0	
	10	0.455799	1.88E-06	3.14E-07	-6.50263
	100	0.45512	0.000682	0.000114	-3.94272
	200	0.45486	0.000941	0.000157	-3.80279
	1000	0.454857	0.000945	0.000158	-3.80106
	10000	0.454714	0.001087	0.000182	-3.73995
3#	1	0.460298	0	0	
	10	0.458928	0.00137	0.00023	-3.63896
	100	0.458496	0.001802	0.000302	-3.51995
	200	0.457959	0.002339	0.000392	-3.40667
	1000	0.457309	0.002989	0.000501	-3.30021
	10000	0.456911	0.003387	0.000568	-3.2459
4#	1	0.447094	0	0	
	10	0.447089	4.7E-06	7.86E-07	-6.10447
	100	0.446961	0.000132	2.22E-05	-4.65422
	200	0.44689	0.000204	3.41E-05	-4.46698
	1000	0.446871	0.000223	3.73E-05	-4.42869
	10000	0.446781	0.000313	5.24E-05	-4.28099

Table B.12 T5A-CRM Base Course at 104 °F

Specimen	Cycle	Stroke	Deformation	Strain	Log (strain)
1#	1	0.447091	0	0	
	10	0.447074	1.69E-05	2.83E-06	-5.54788
	100	0.446984	0.000107	1.79E-05	-4.74624
	200	0.44697	0.000121	2.02E-05	-4.69375
	1000	0.446954	0.000137	2.3E-05	-4.63879
	3000	0.446933	0.000158	2.64E-05	-4.57784
	6000	0.44686	0.000231	3.87E-05	-4.41221
	10000	0.44683	0.000261	4.37E-05	-4.3591
5#	1	0.441356	0	0	
	10	0.441301	5.56E-05	9.34E-06	-5.02951
	100	0.441299	5.75E-05	9.66E-06	-5.01508
	200	0.441256	0.000101	1.69E-05	-4.77164
	1000	0.441147	0.00021	3.52E-05	-4.45314
	3000	0.44106	0.000296	4.97E-05	-4.30325
	6000	0.440974	0.000382	6.43E-05	-4.19203
	10000	0.440933	0.000424	7.12E-05	-4.14747
6#	1	0.445787	0	0	
	10	0.445786	1.5E-06	2.53E-07	-6.59772
	100	0.44562	0.000167	2.8E-05	-4.55239
	200	0.44547	0.000317	5.33E-05	-4.27343
	1000	0.445256	0.000531	8.93E-05	-4.04933
	3000	0.445049	0.000738	0.000124	-3.90663
	6000	0.444929	0.000858	0.000144	-3.84108
	10000	0.444779	0.001008	0.000169	-3.77099

APPENDIX C

PLOTS OF PERMANENT STRAIN VS. LOADING CYCLES FOR TEST SPECIMENS

133
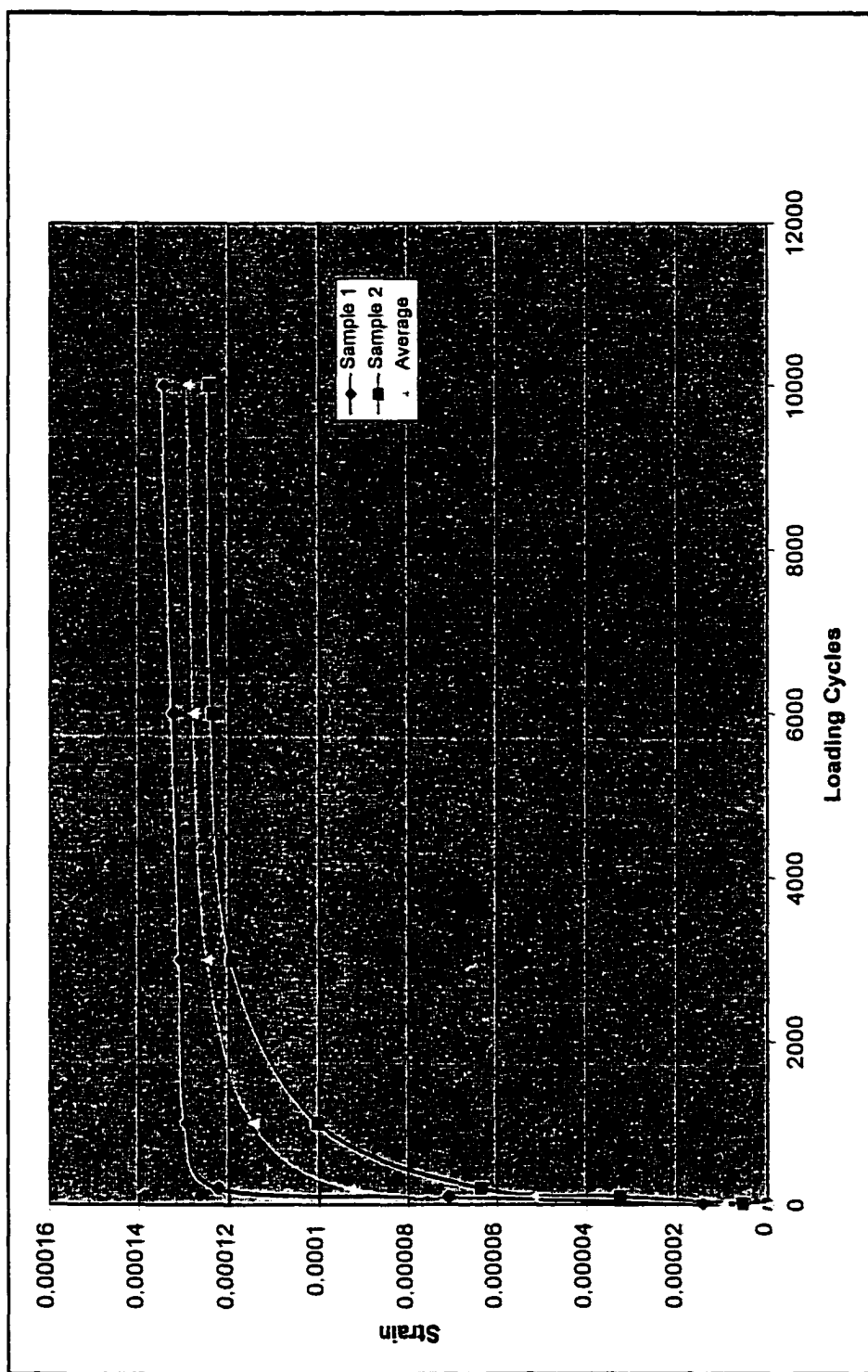
Figure C.1 Strains of Conventional Wearing Course Samples at 40°F
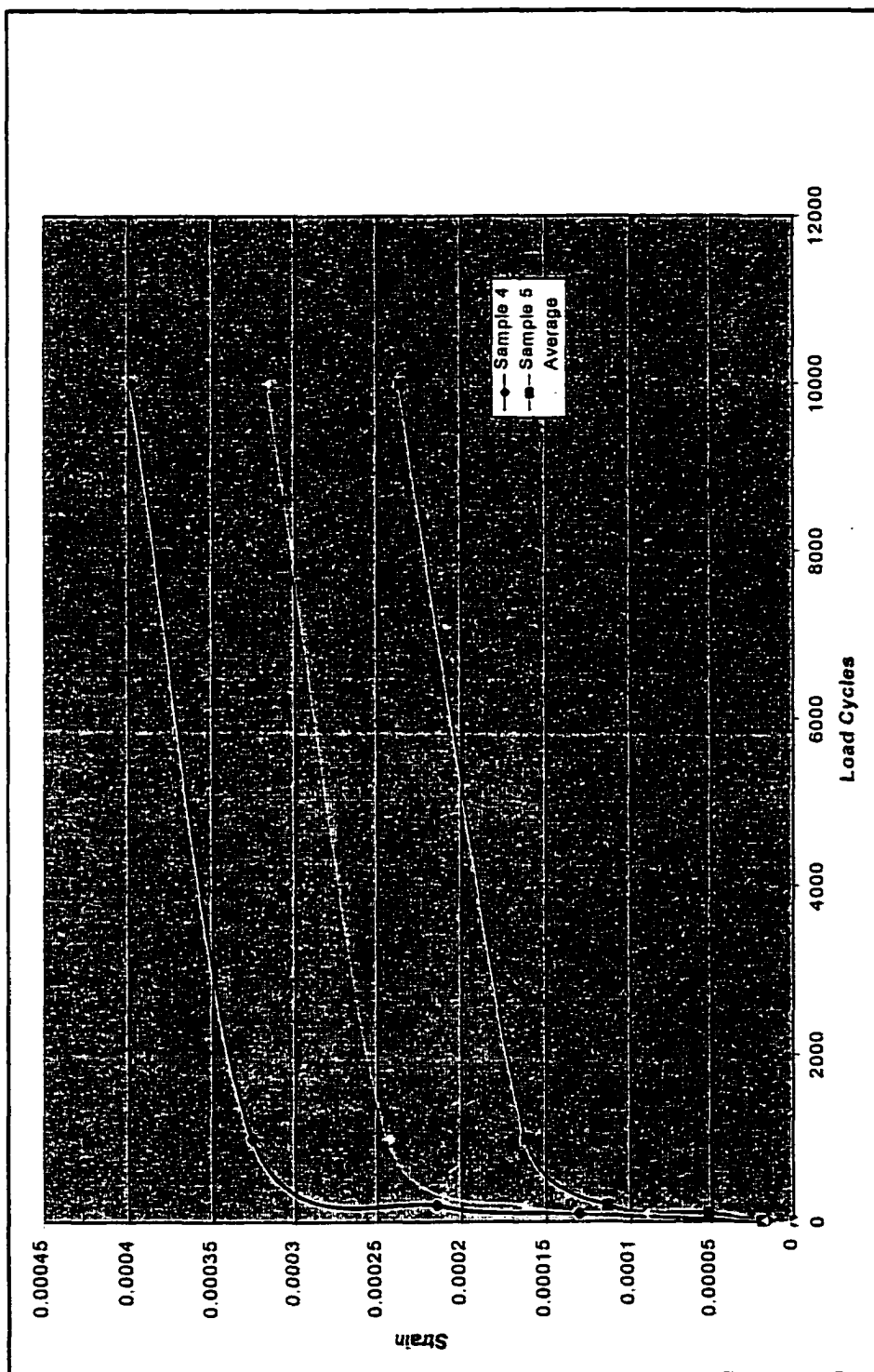
Figure C.2 Strains of Conventional Wearing Course Samples at 77°F
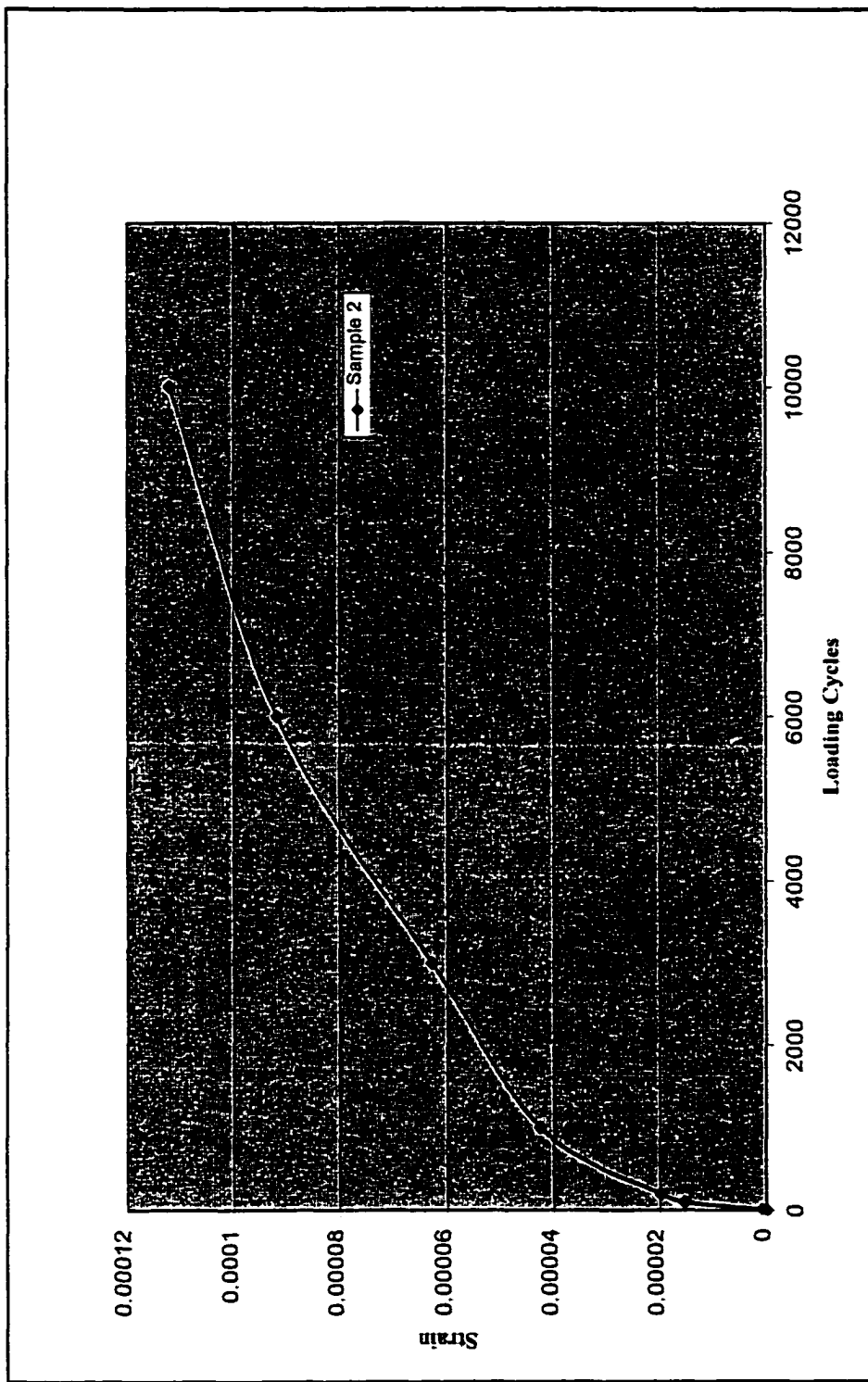
Figure C.3 Strains of Conventional Wearing Course Samples at 104°F
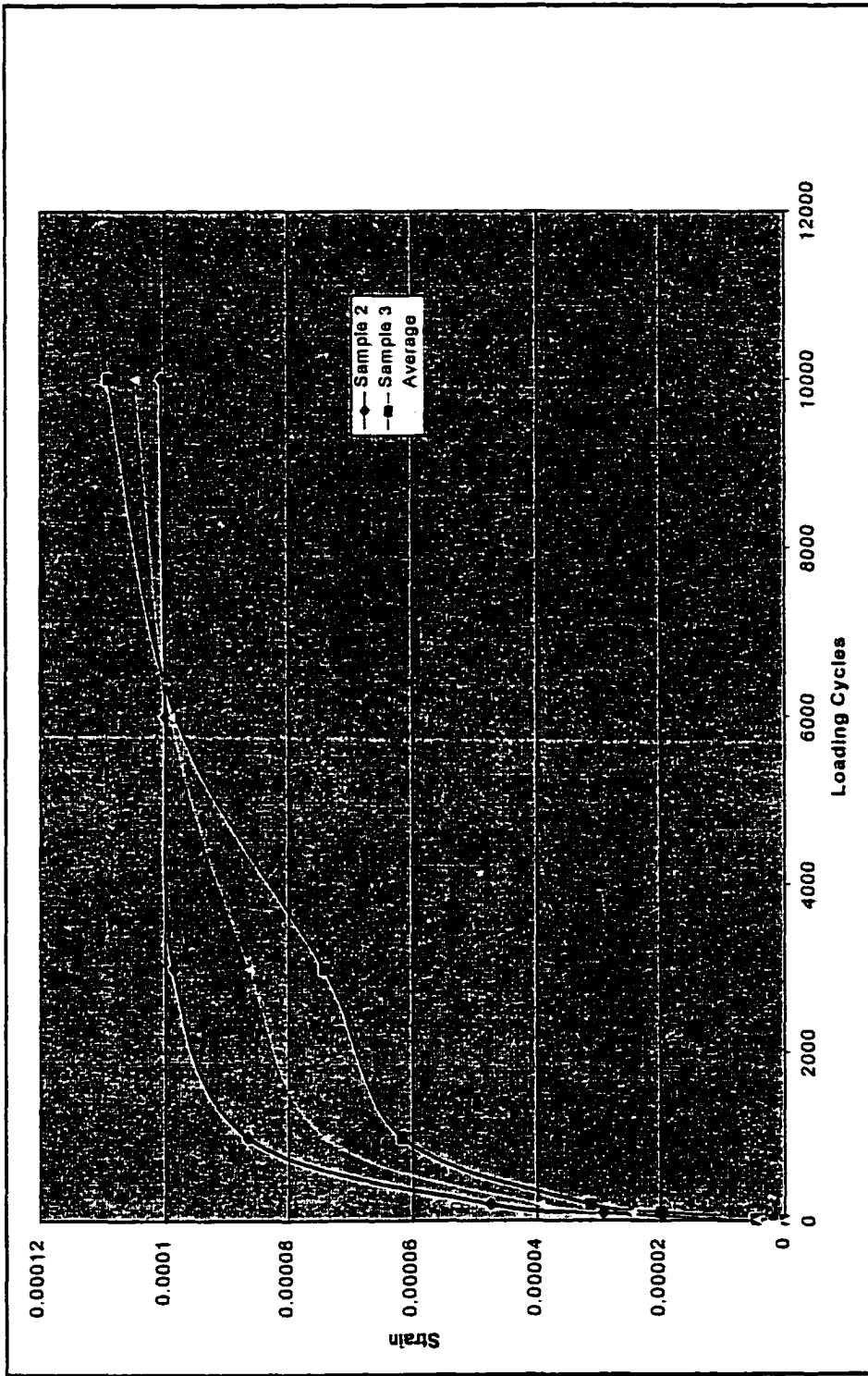
Figure C.4 Strains of Crumb Rubber Wearing Course Samples at 40°F
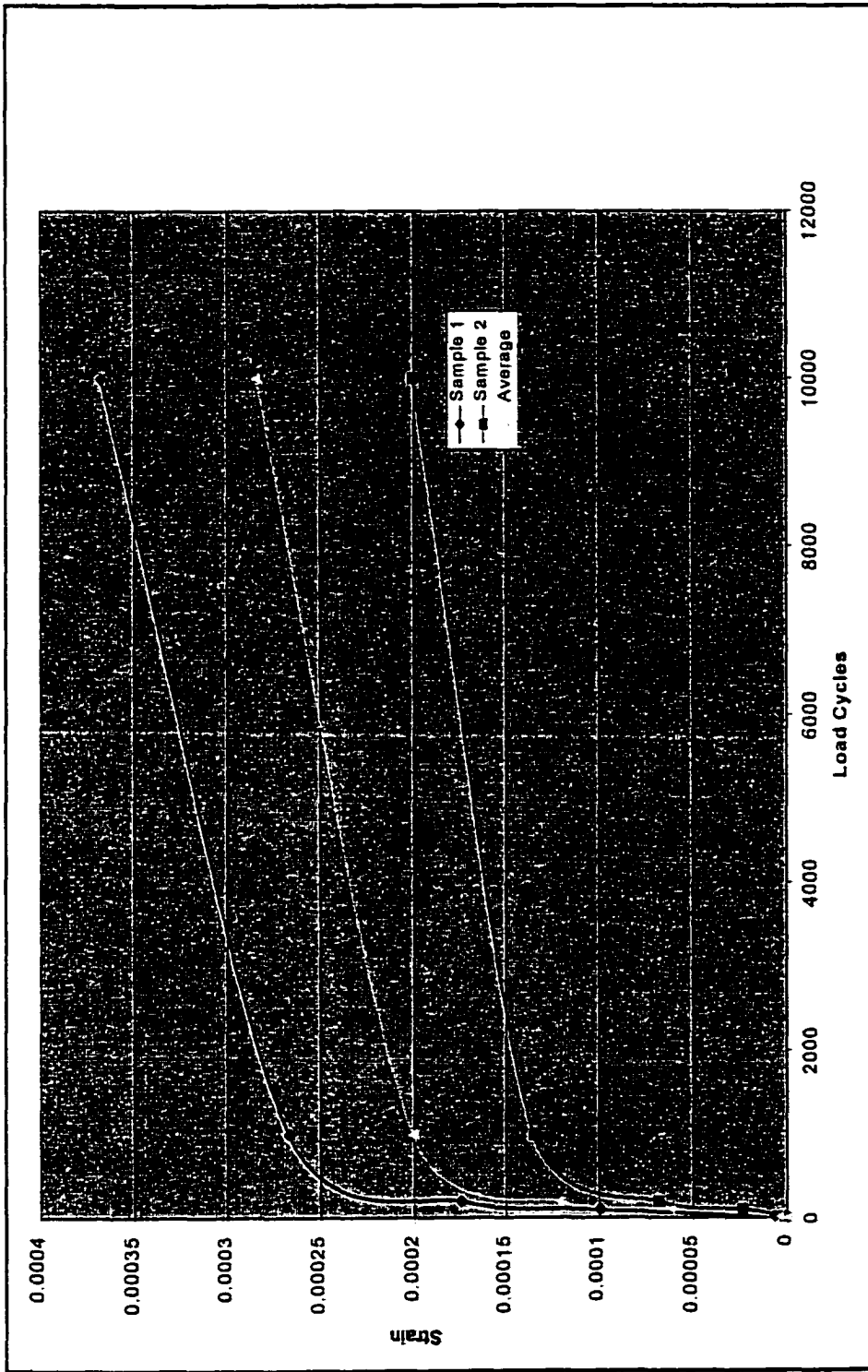
Figure C.5 Strains of Crumb Rubber Wearing Course Samples at 77°F
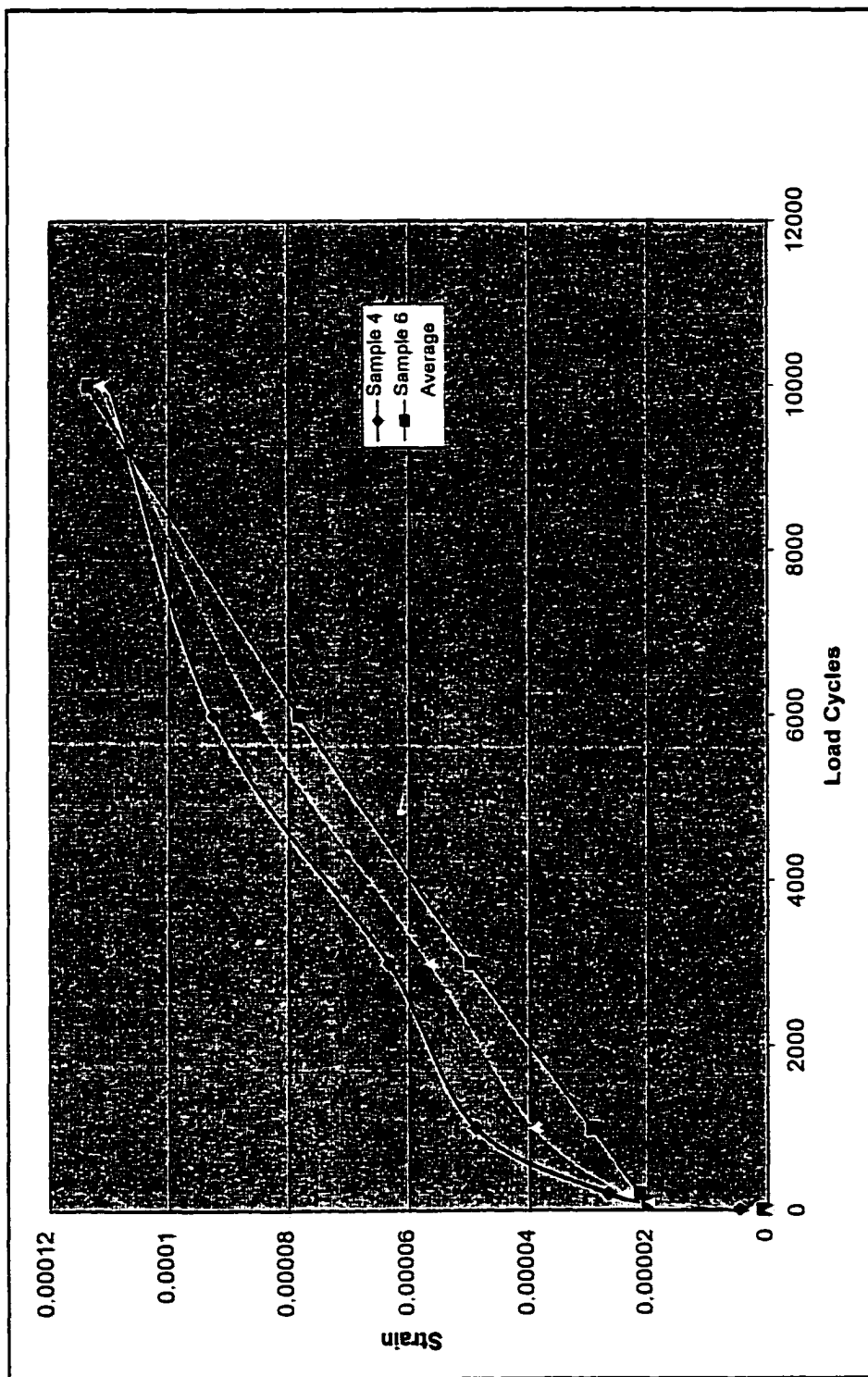
Figure C.6 Strains of Crumb Rubber Wearing Course Samples at 104°F
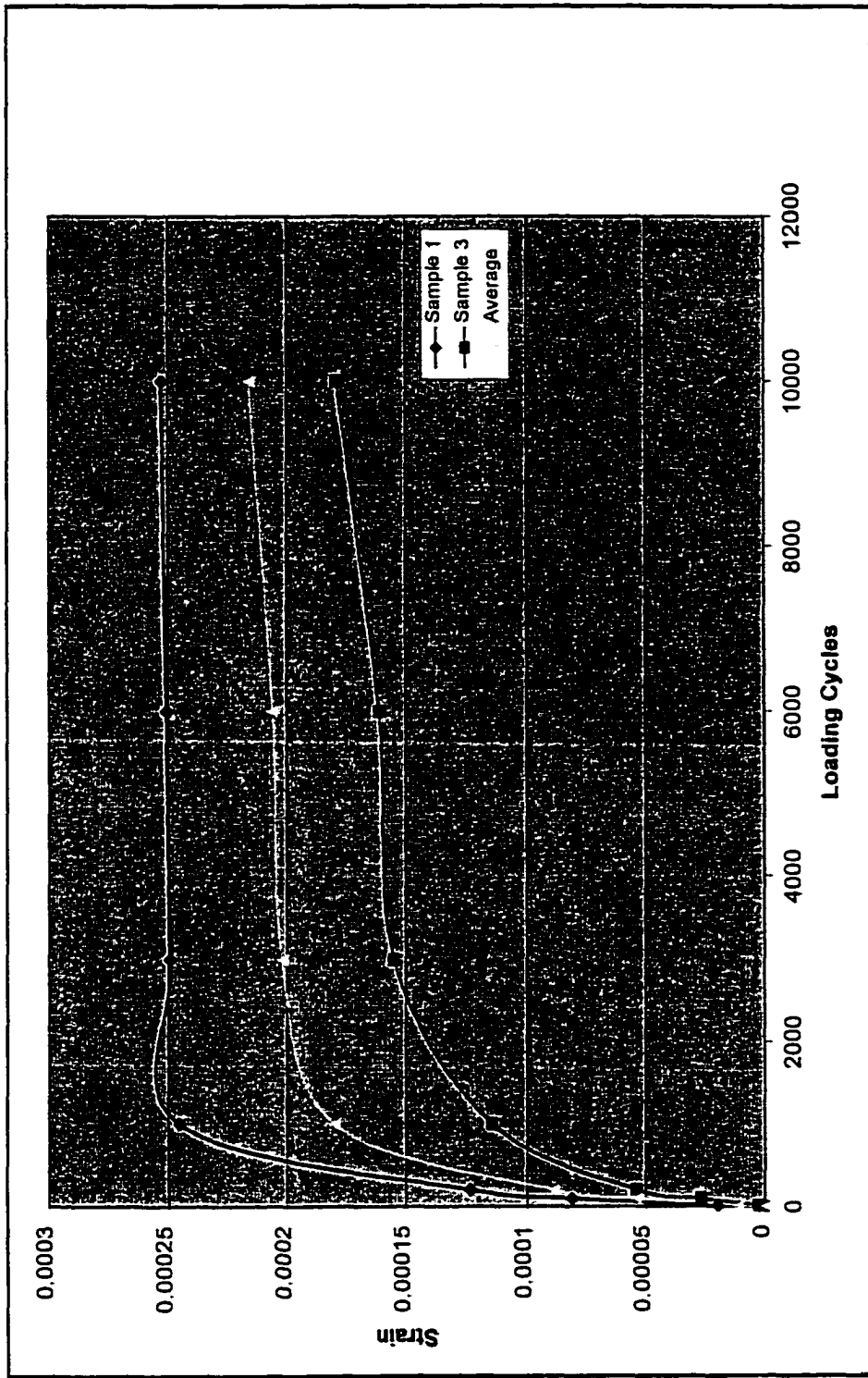
Figure C.7 Strains of Conventional Base Samples at 40°F
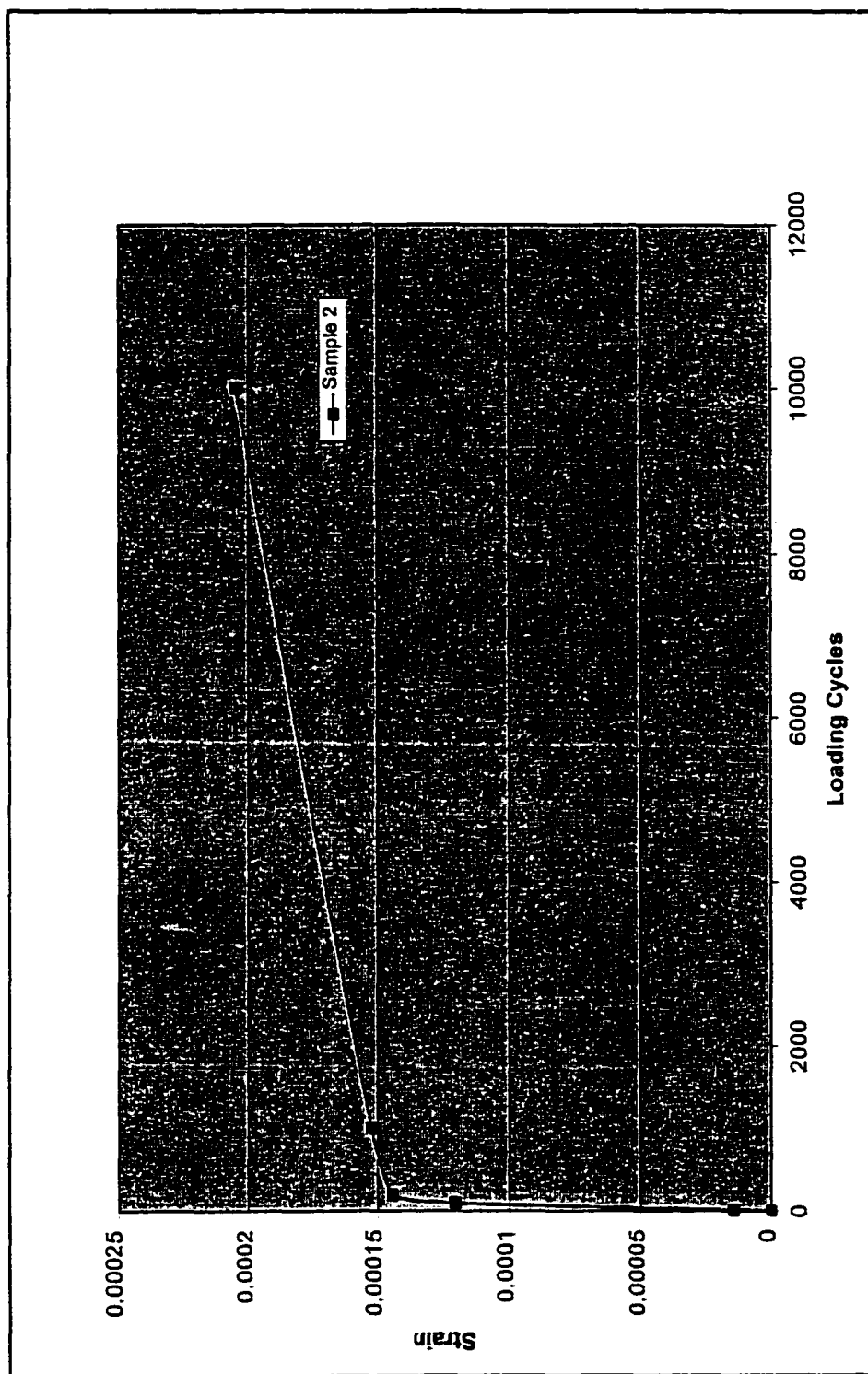
Figure C.8 Strains of Conventional Base Samples at 77°F
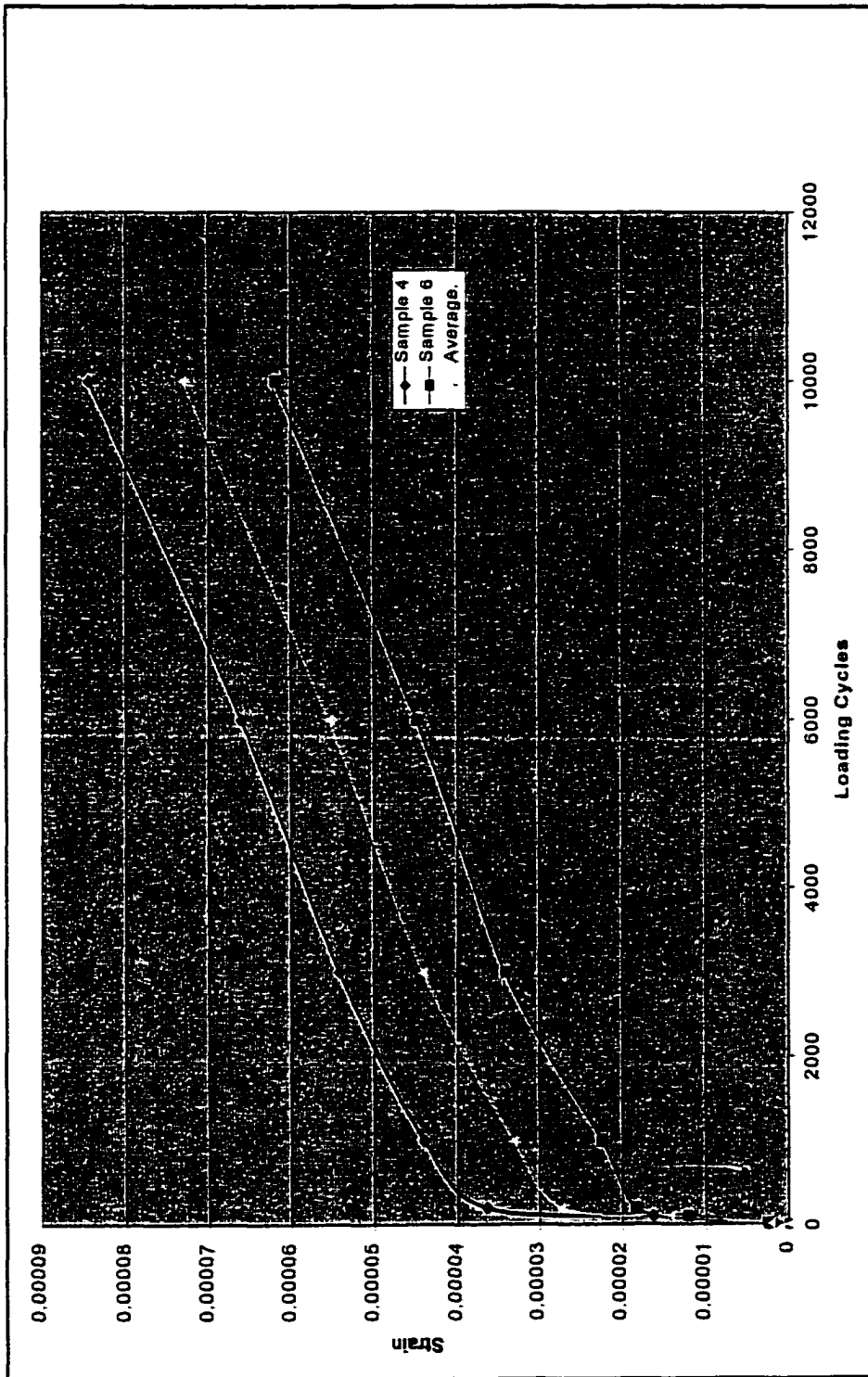
Figure C.9 Strains of Conventional Base Samples at 104°F
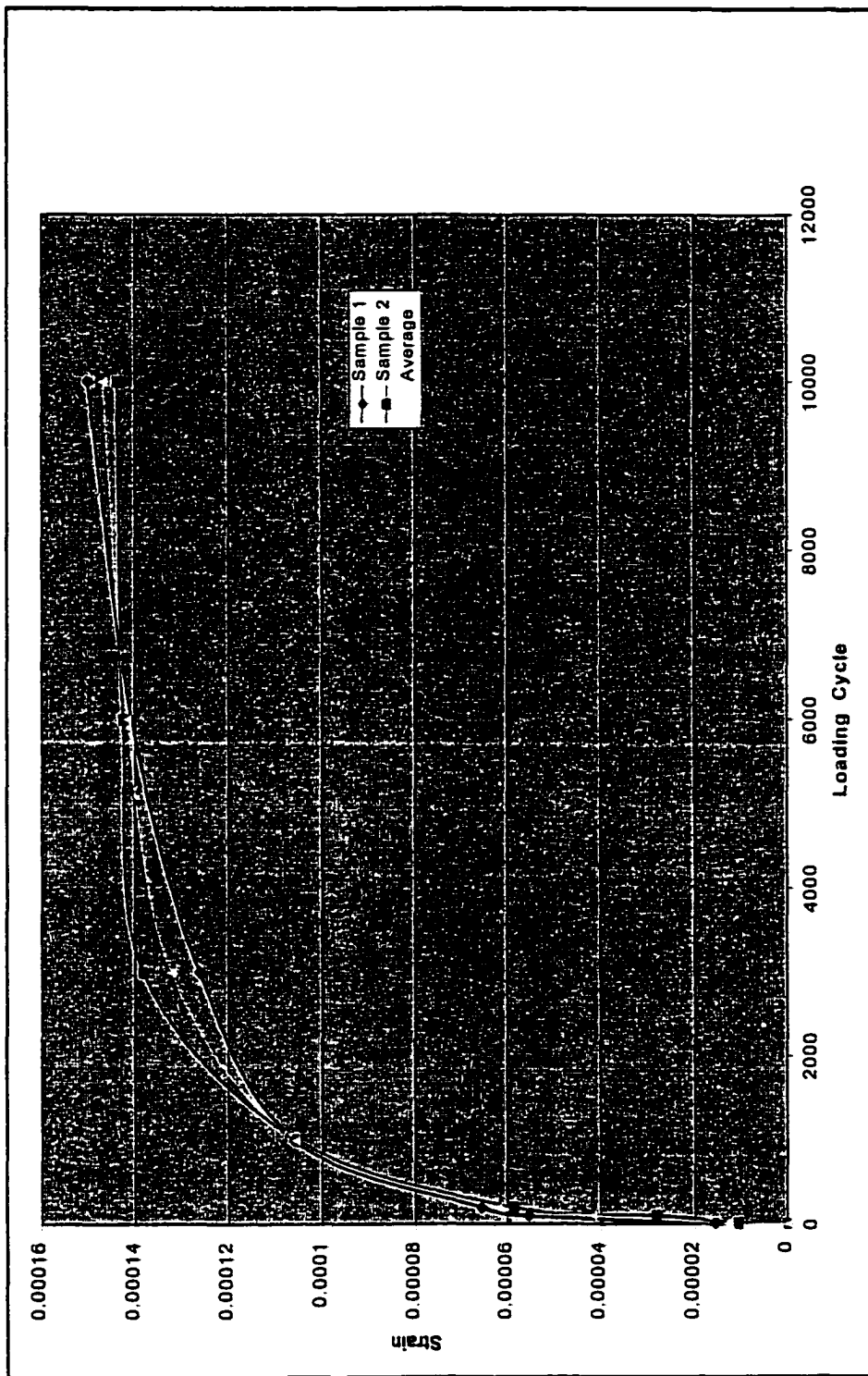
Figure C.10 Strains of Crumb Rubber Base Samples at 40°F
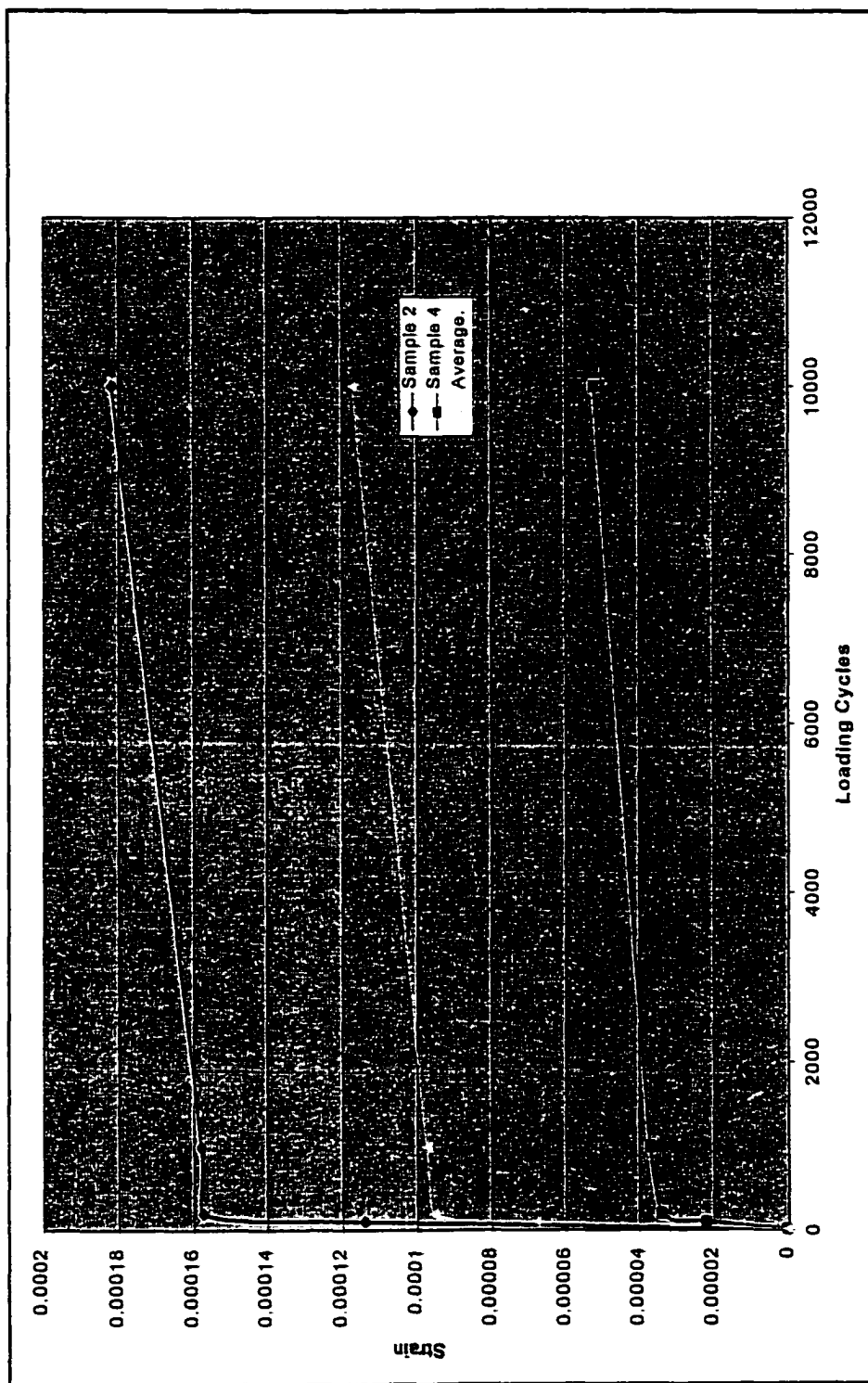
Figure C.11 Strains of Crumb Rubber Base Samples at 77°F
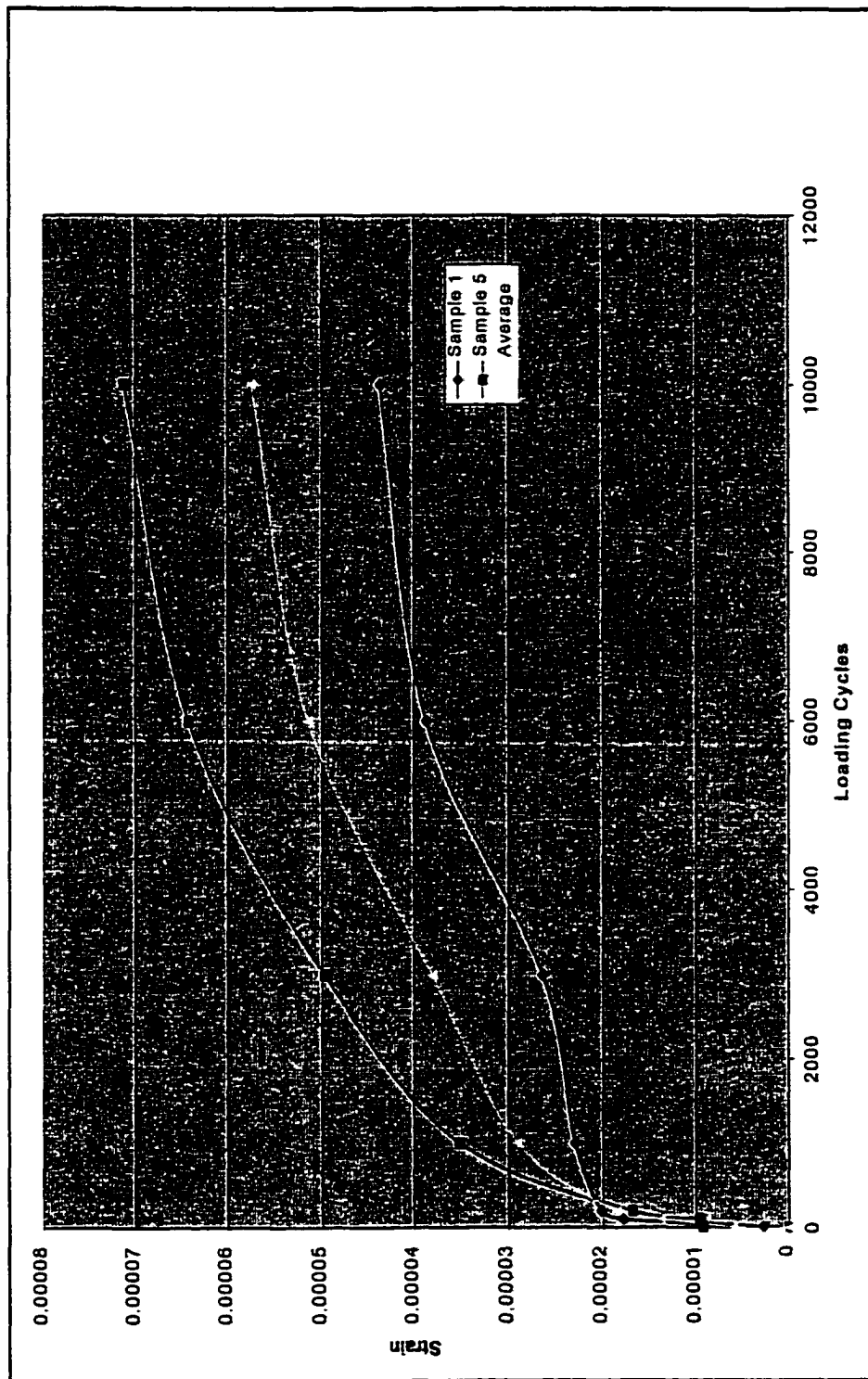
Figure C.12 Strains of Crumb Rubber Base Samples at 104°F

146
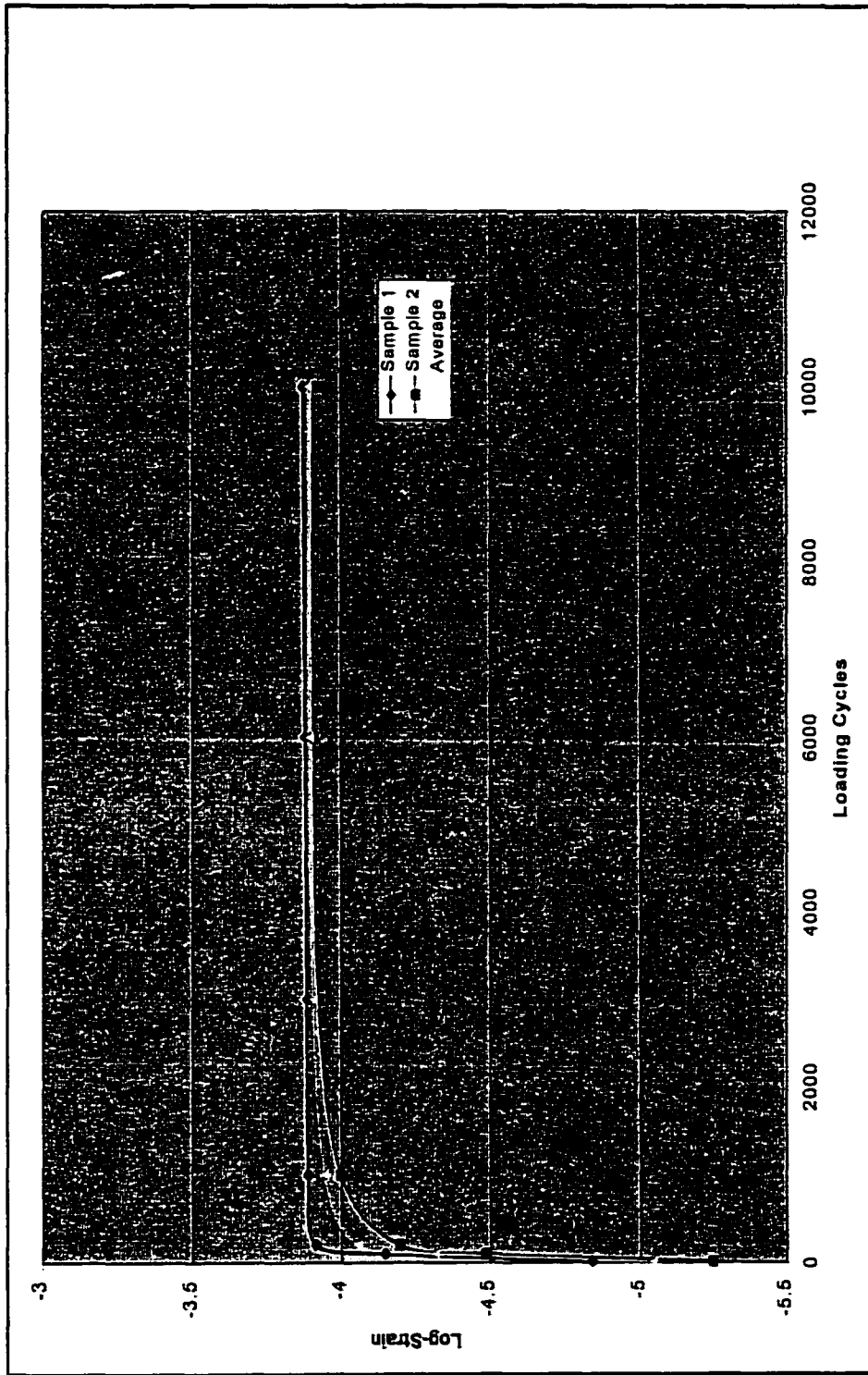
Figure C.13 Plot of log Strains vs. Cycles of Conventional Wearing Course Samples at 40°F
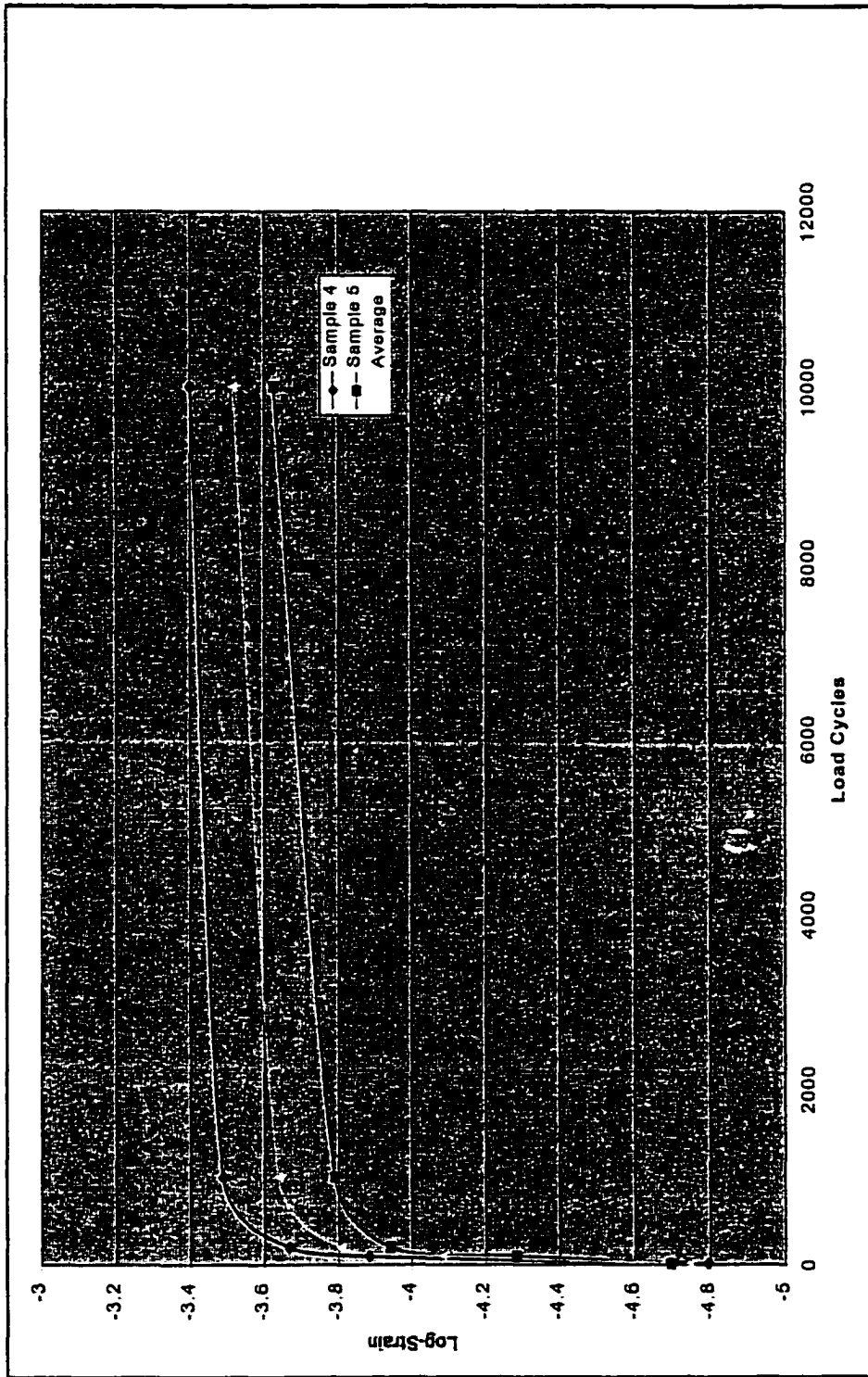
Figure C.14 Plot of log Strains vs. Cycles of Conventional Wearing Course Samples at 77°F
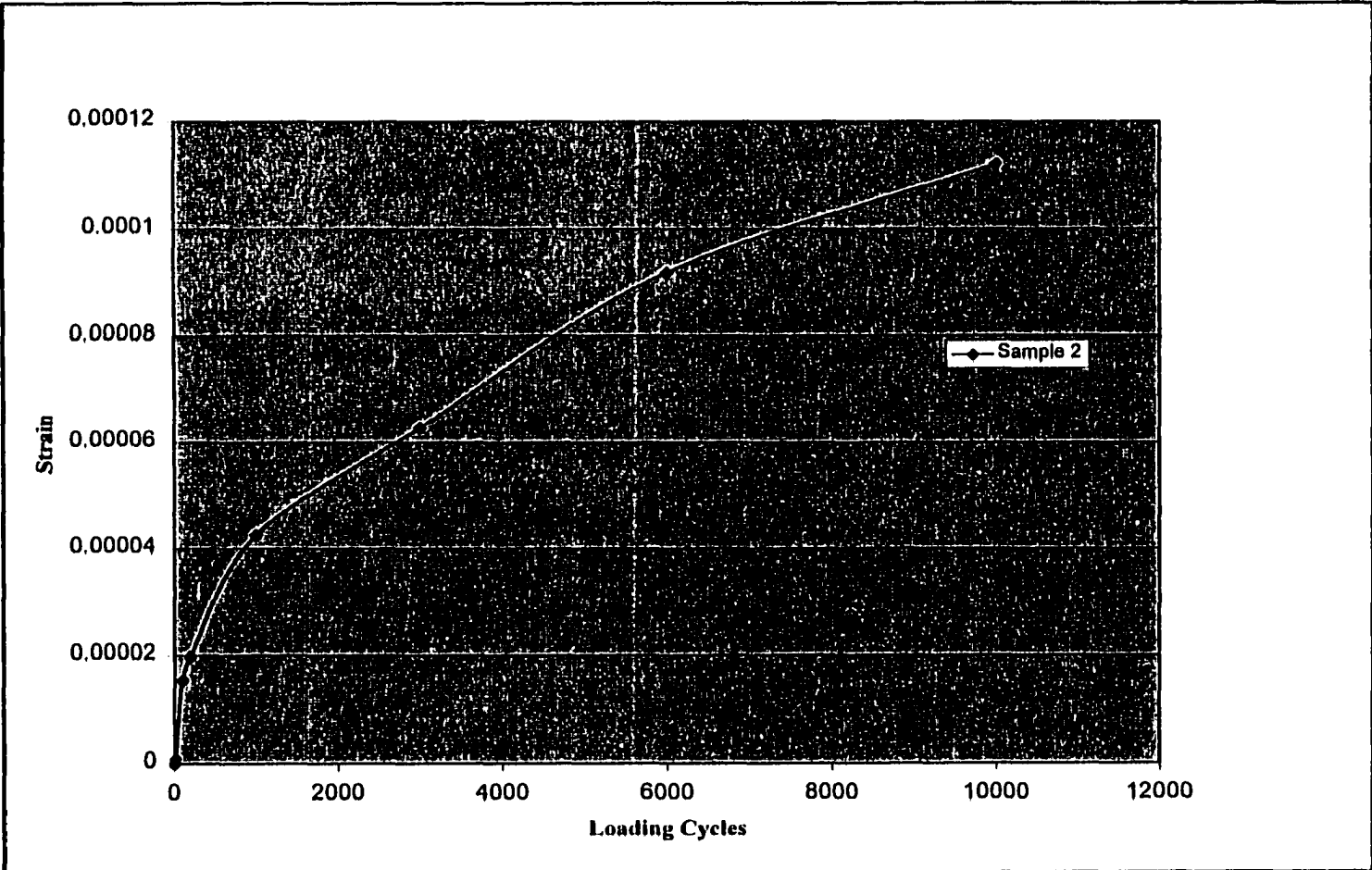
Figure C.15 Plot of log Strains vs. Cycles of Conventional Wearing Course Samples at 104°F
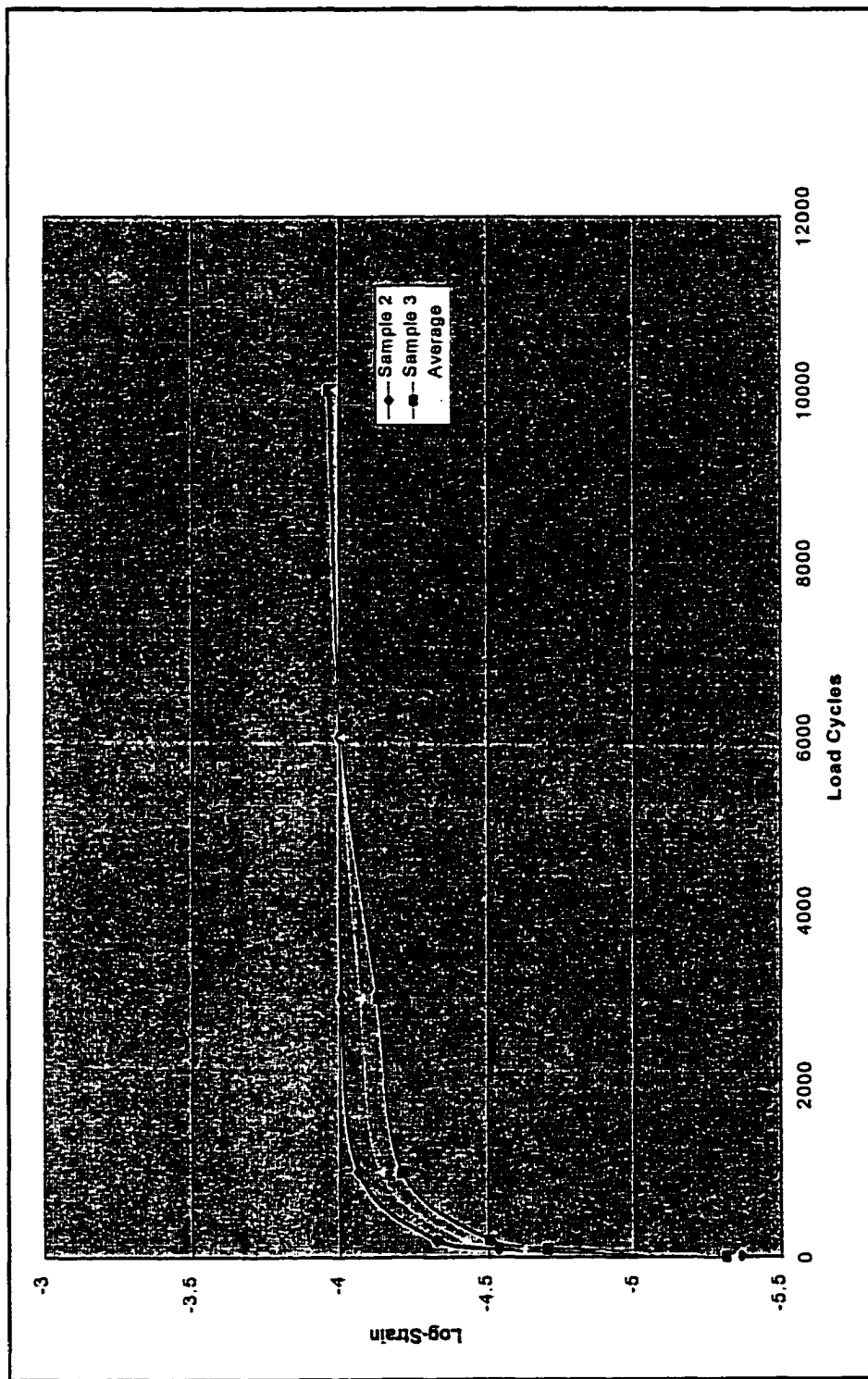
Figure C.16 Plot of log Strains vs. Cycles of Crumb Rubber Wearing Course Samples at 40°F
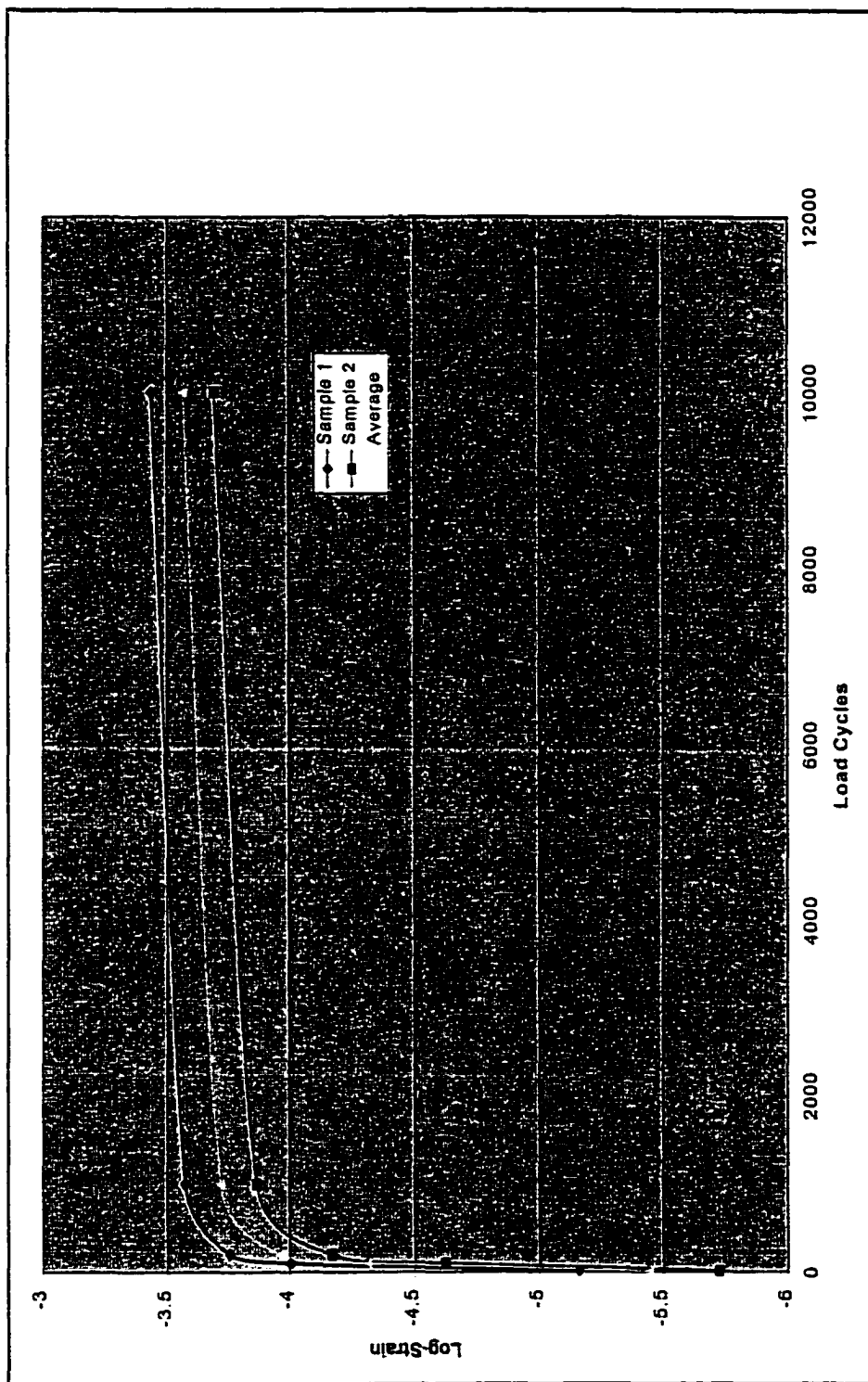
Figure C.17 Log Plot of Strains vs. Cycles of Crumb Rubber Wearing Course Samples at 77°F
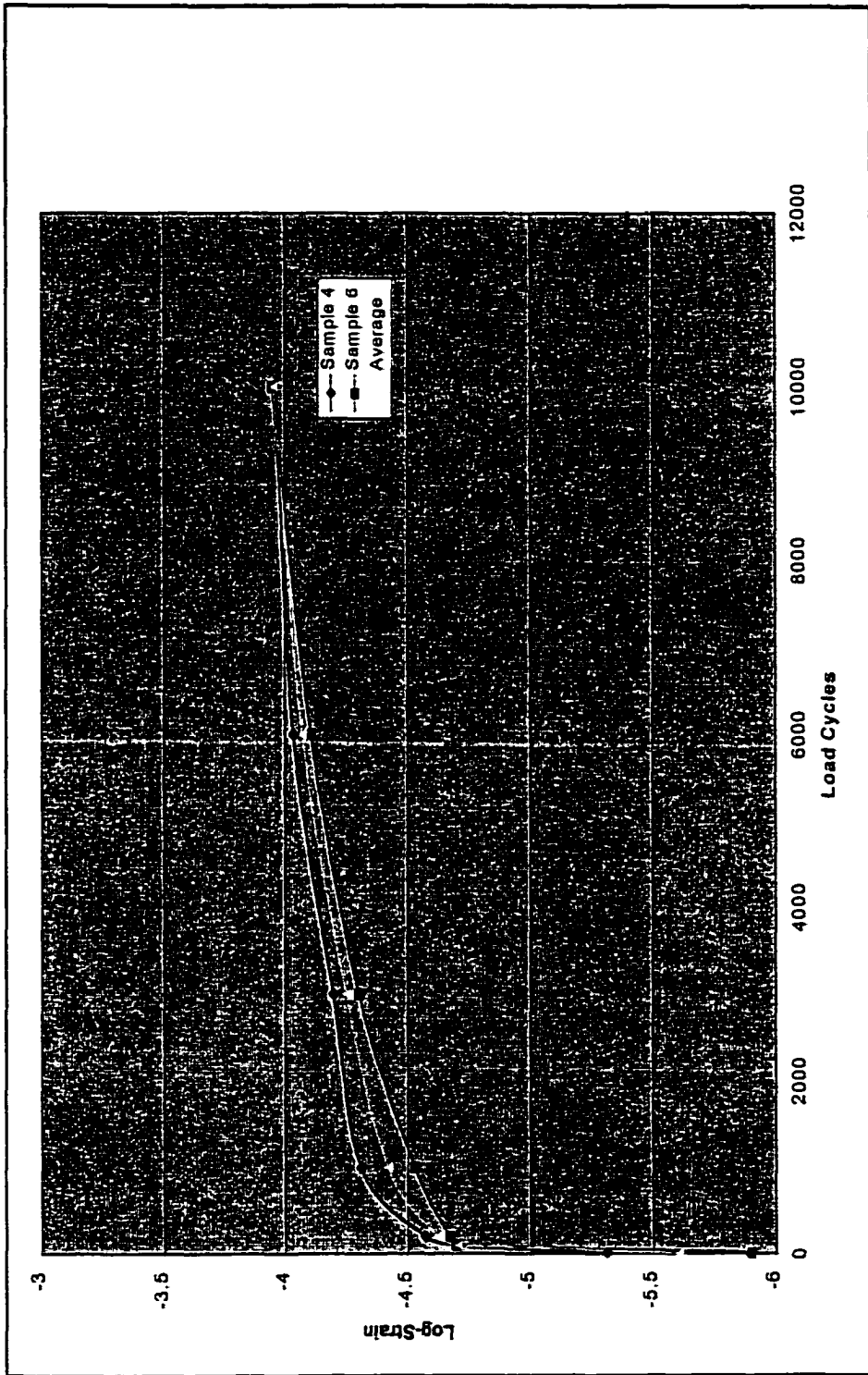
Figure C.18 Plot of log Strains vs. Cycles of Crumb Rubber Wearing Course Samples at 104°F
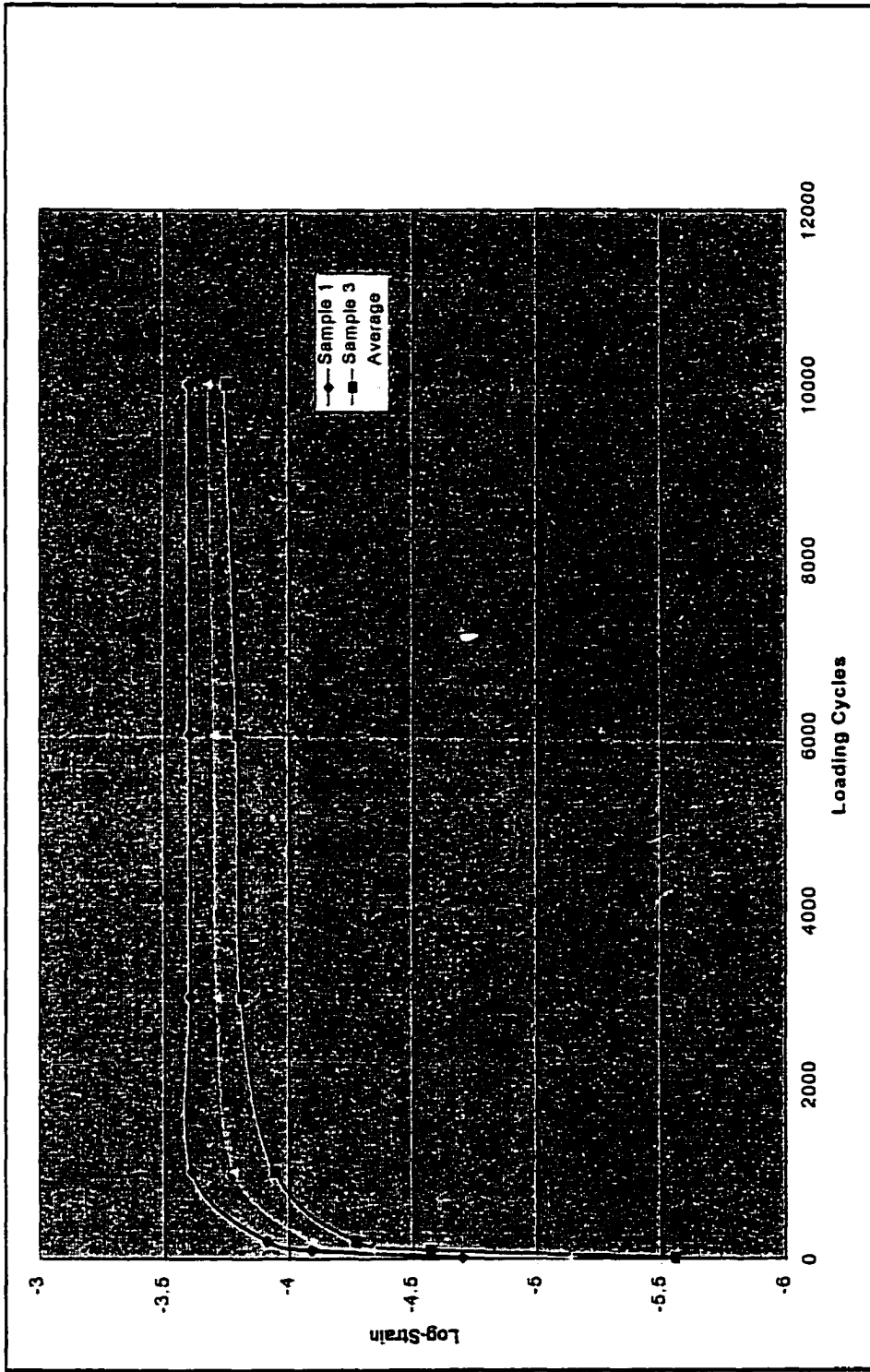
Figure C.19 Plot of log Strains vs. Cycles of Conventional Black Base Course Samples at 40°F
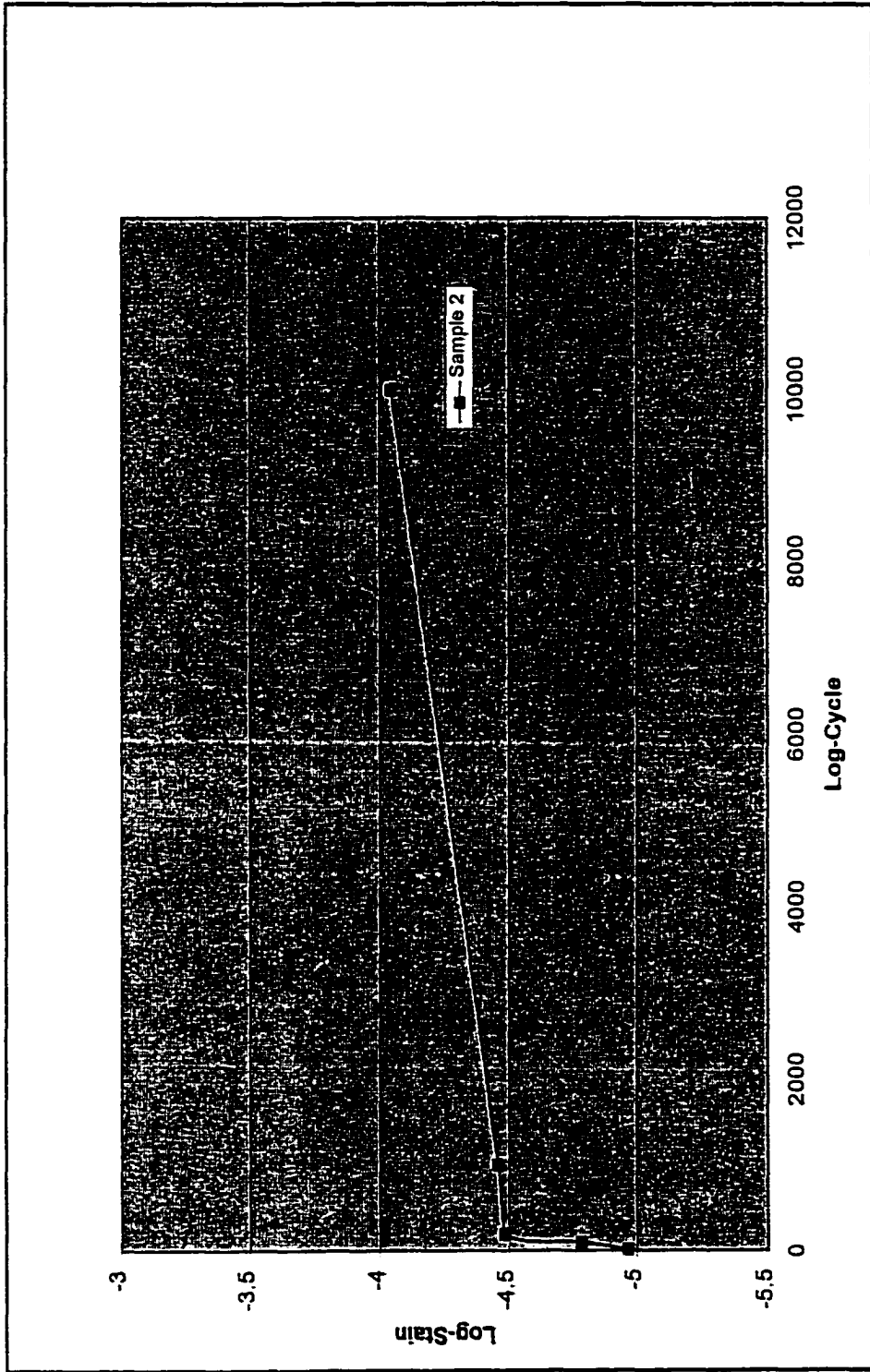
Figure C.20 Plot of log Strains vs. Cycles of Conventional Black Base Course Samples at 77°F
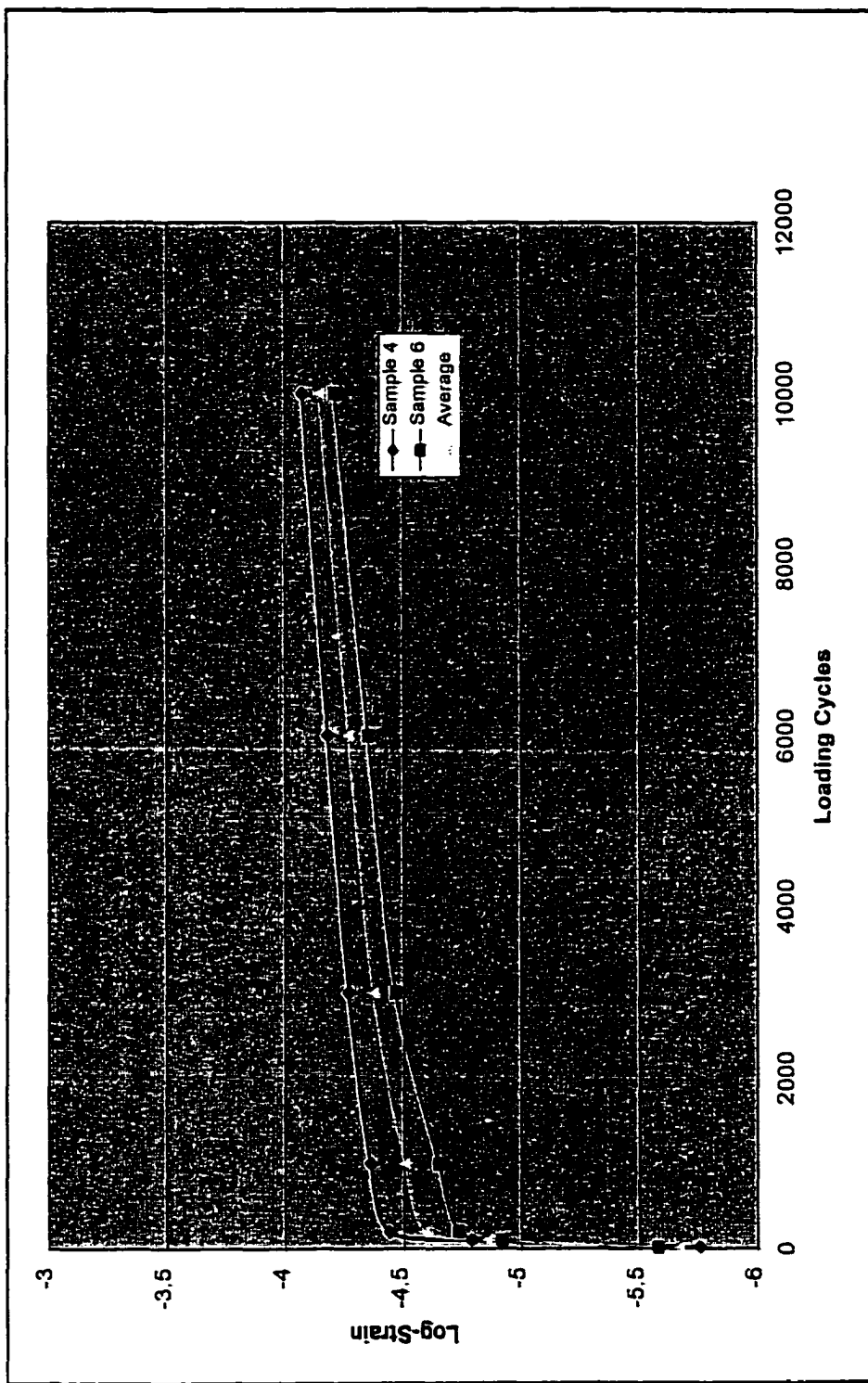
Figure C.21 Plot of log Strains vs. Cycles of Conventional Black Base Course Samples at 104°F
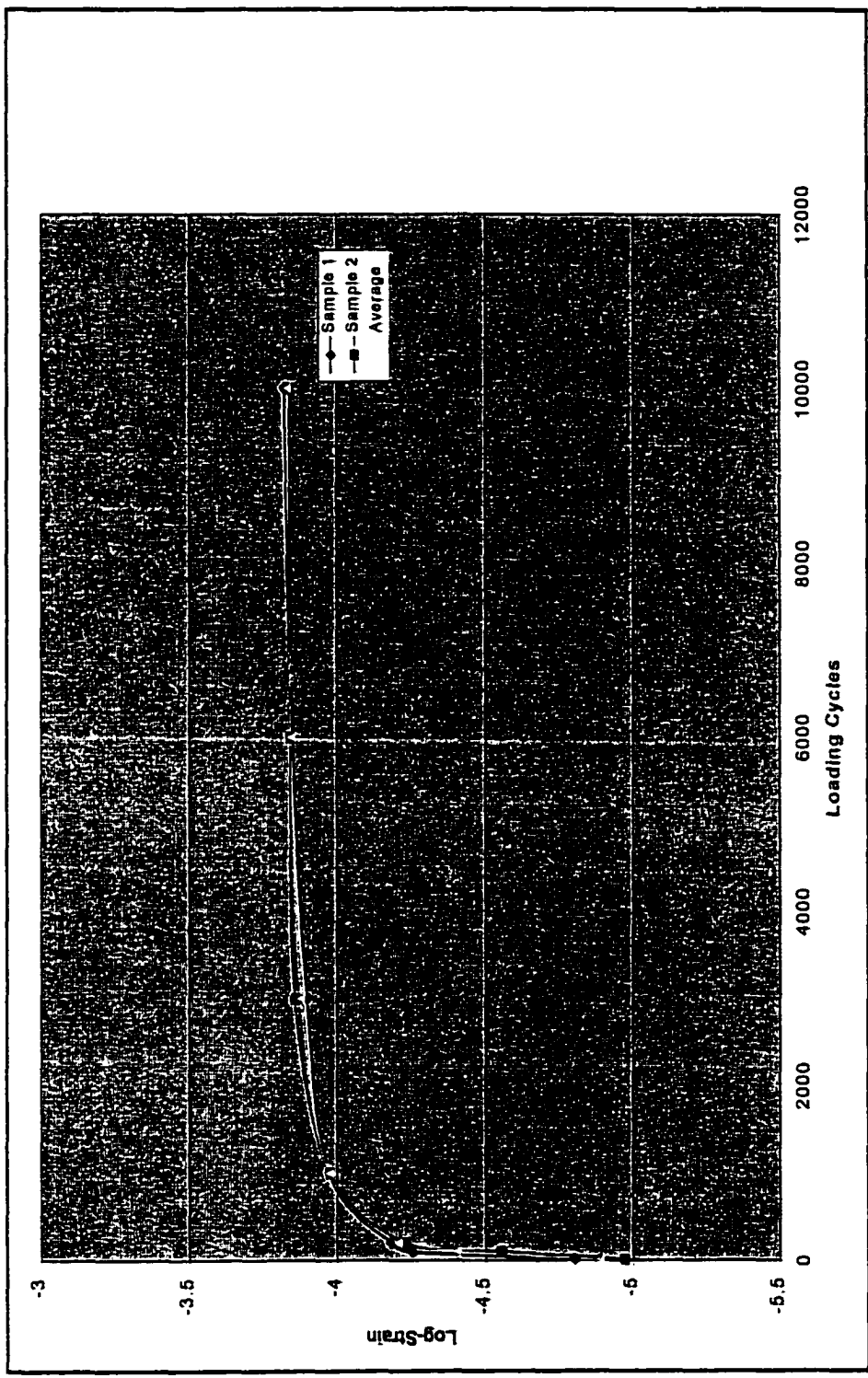
Figure C.22 Plot of log Strains vs. Cycles of Crumb Rubber Base Course Samples at 40°F
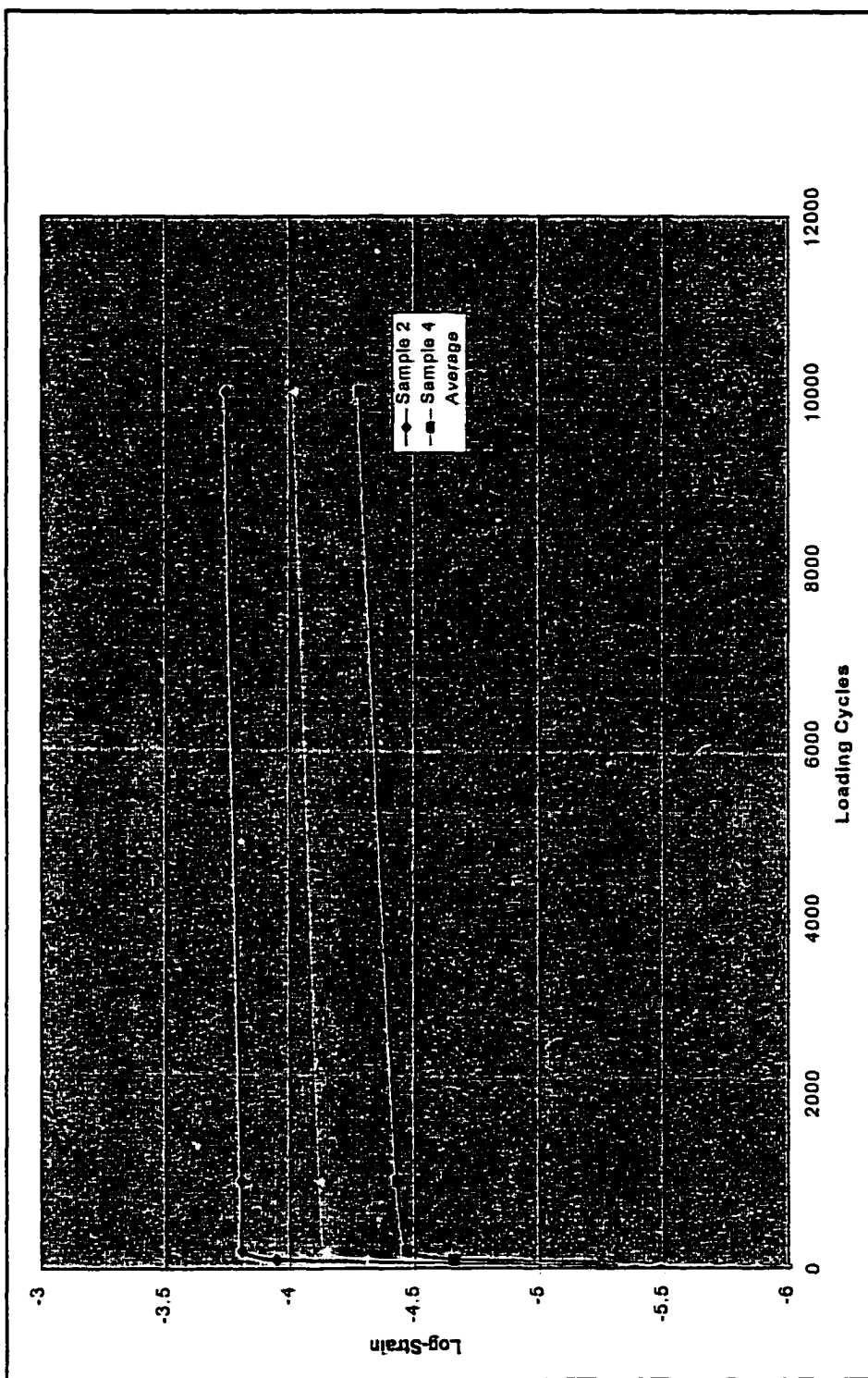
Figure C.23 Plot of log Strains vs. Cycles of Crumb Rubber Base Course Samples at 77°F
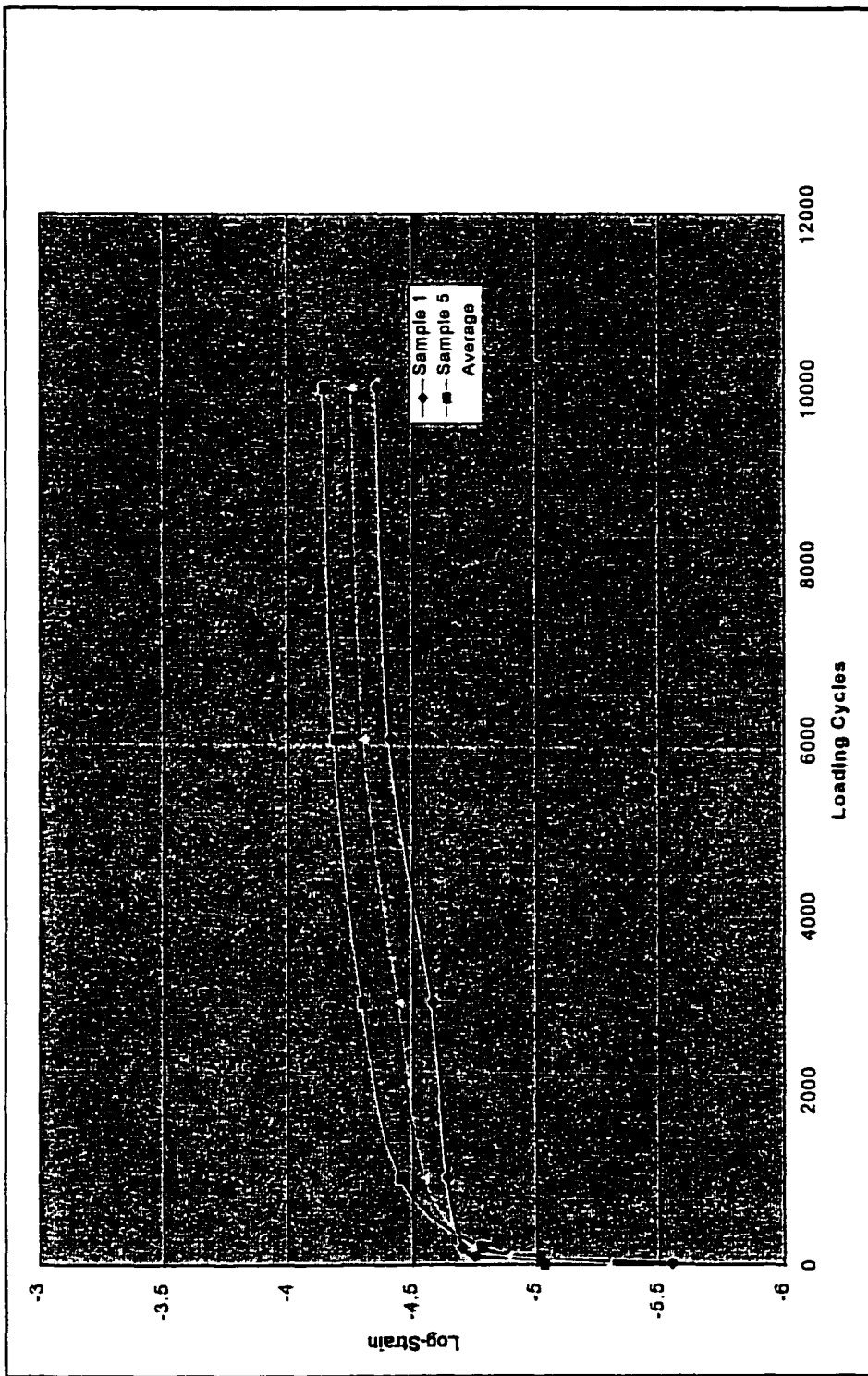
Figure C.24 Plot of log Strains vs. Cycles of Crumb Rubber Base Course Samples at 104°F

APPENDIX D

PLOTS OF REGRESSION RESULTS OF TEST MATERIALS

158
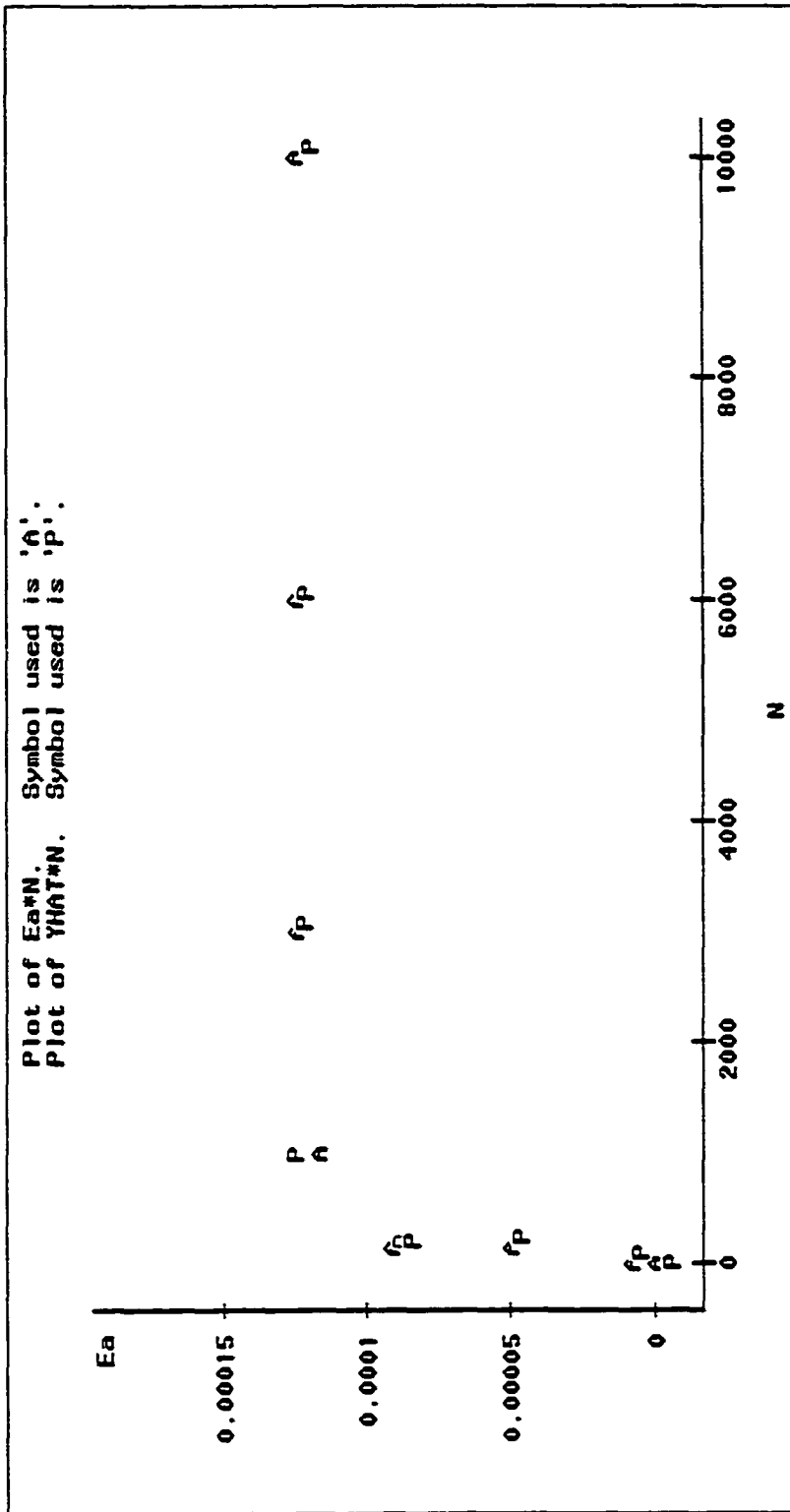
Figure D.1 Regression Result of T8F Wearing Course at 40°F
(A--actual data, P--prediction result)

```
        Plot of Ea*N.    Symbol used is 'A'.
        Plot of YHAT*N.  Symbol used is 'P'.
```


Figure D.2 Regression Result of T8F Wearing Course at 77°F
(A--actual data, P--prediction result)
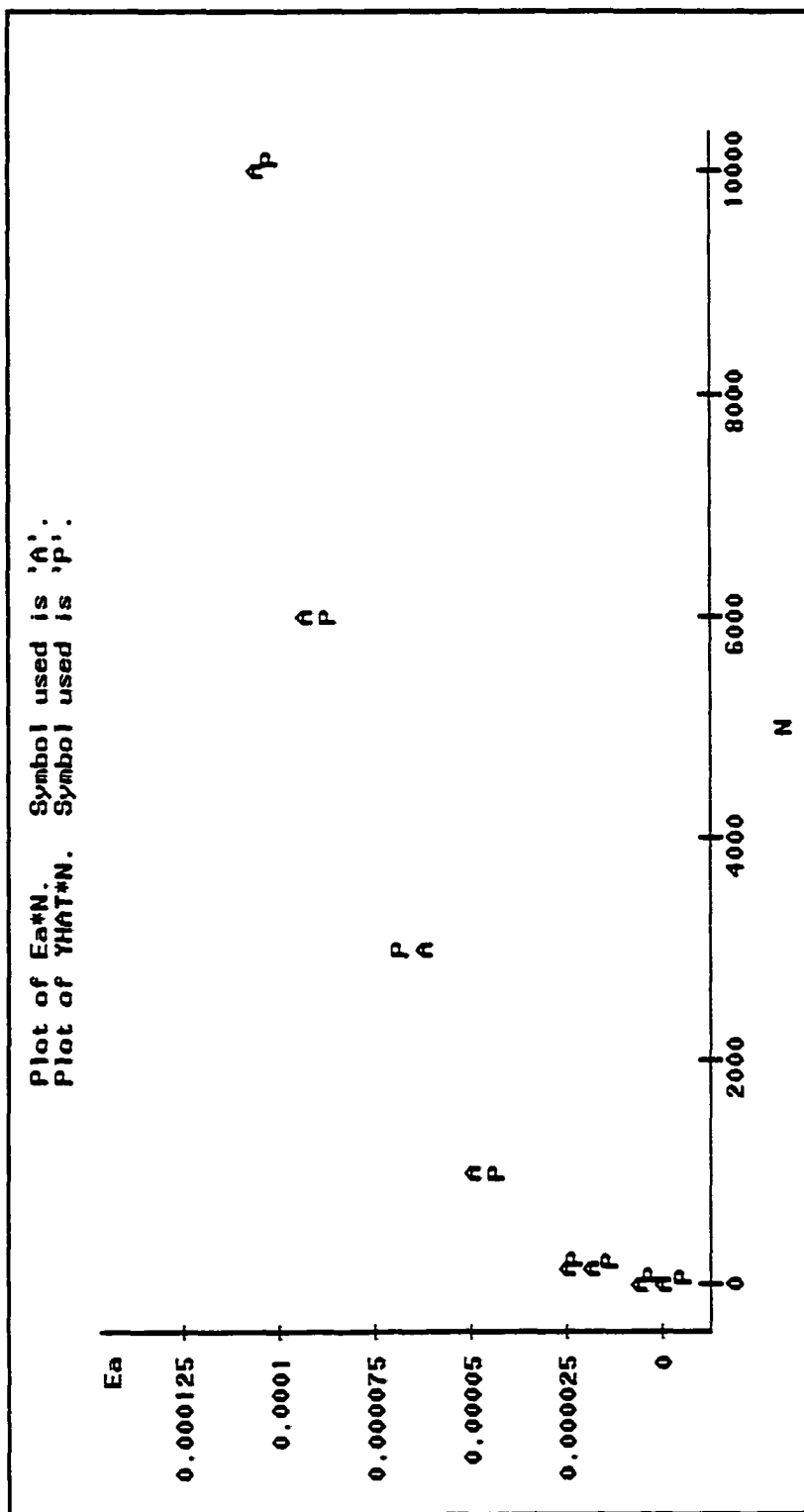
Figure D.3 Regression Result of T8F Wearing Course at 104°F
(A--actual data, P--prediction result)
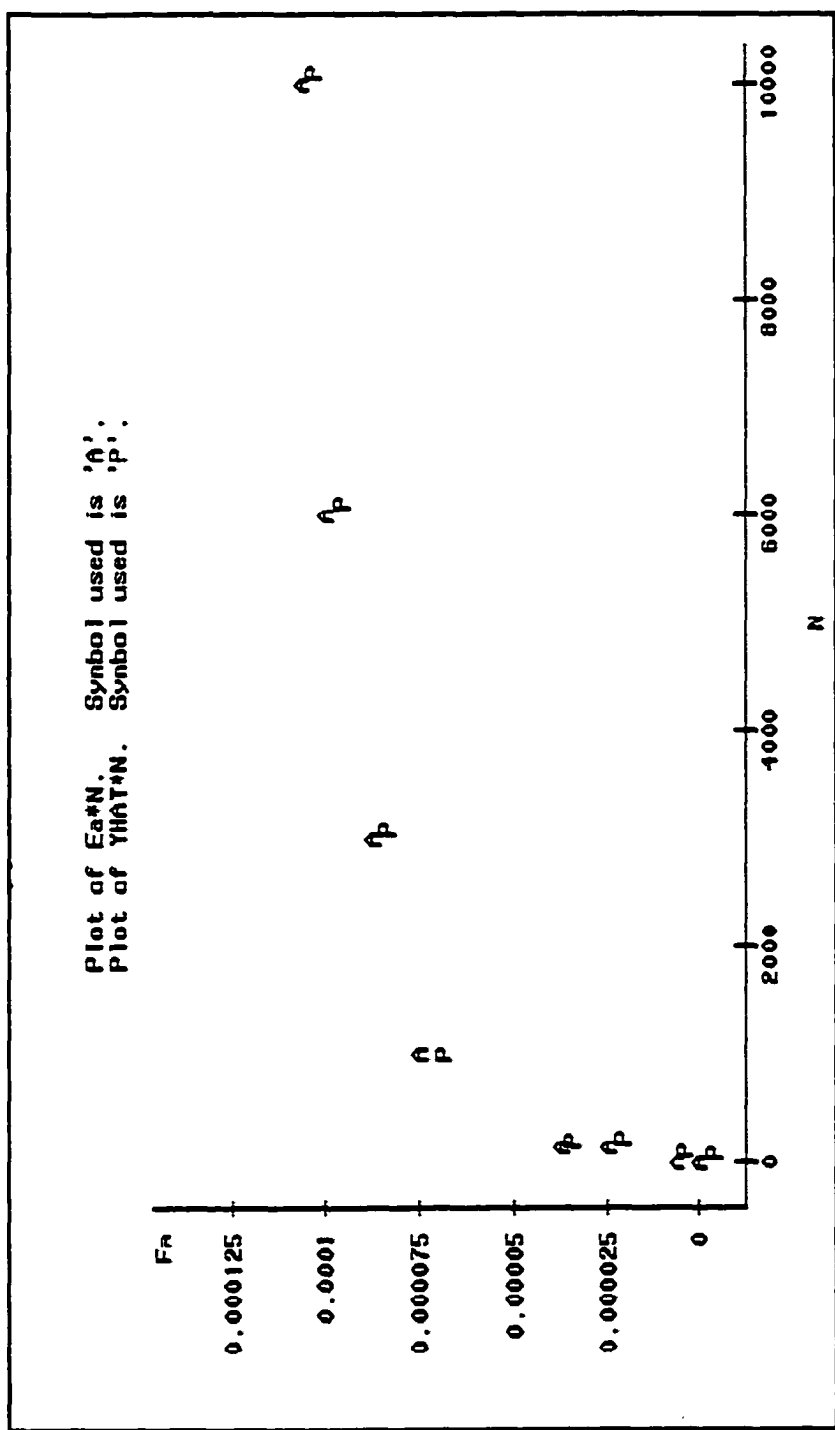
**Figure D.4 Regression Result of T8F-CRM Wearing Course at 40°F
(A--actual data, P--prediction result)**

Plot of Ea*N.   Symbol used is 'A'.
Plot of YHAT*N. Symbol used is 'P'.

Ea

0.0003

0.0002

0.0001

0.0000

0   2000   4000   6000   8000   10000

N
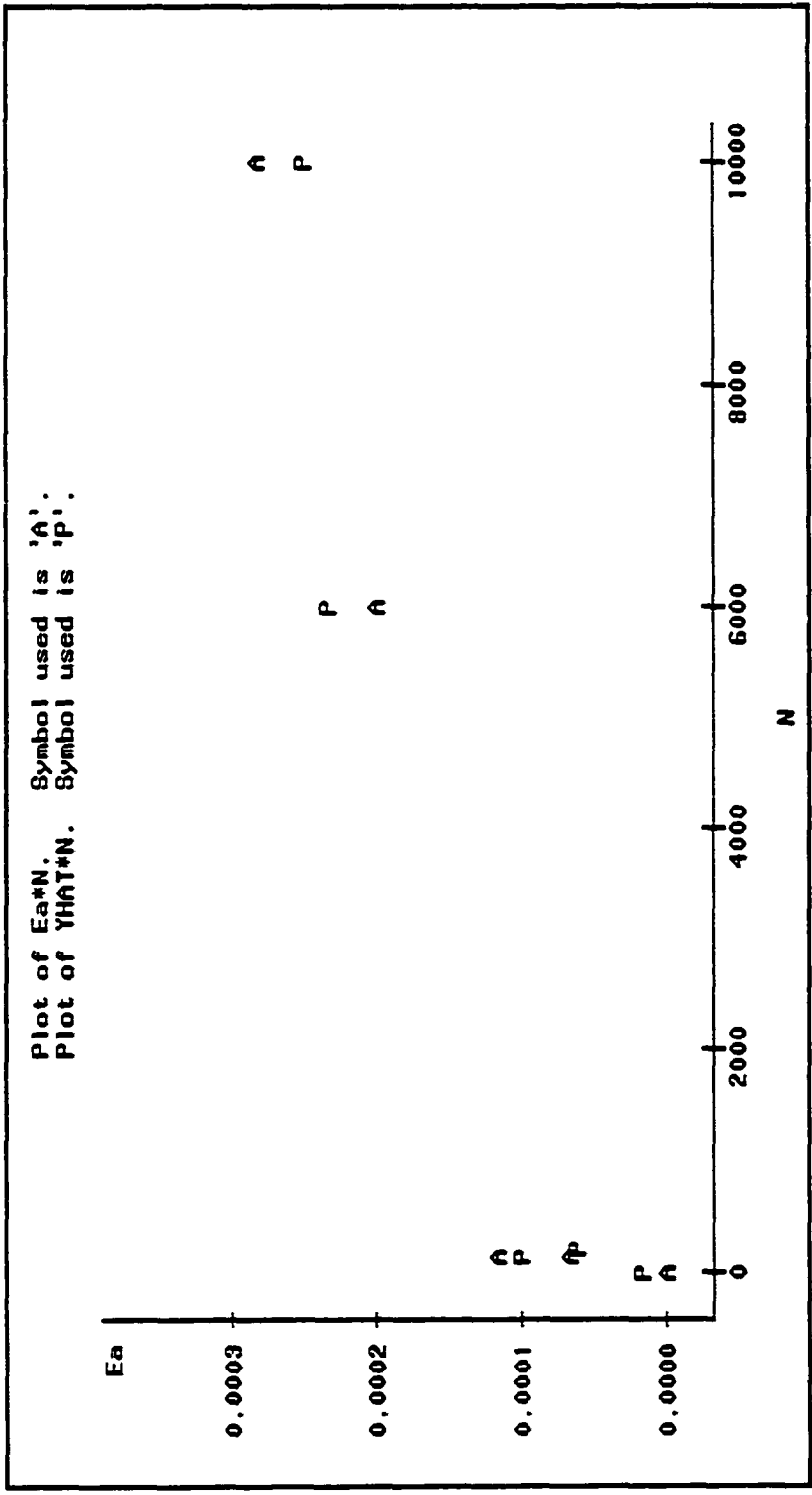
Figure D.5 Regression Result of T8F-CRM Wearing Course at 77°F
(A--actual data, P--prediction result)
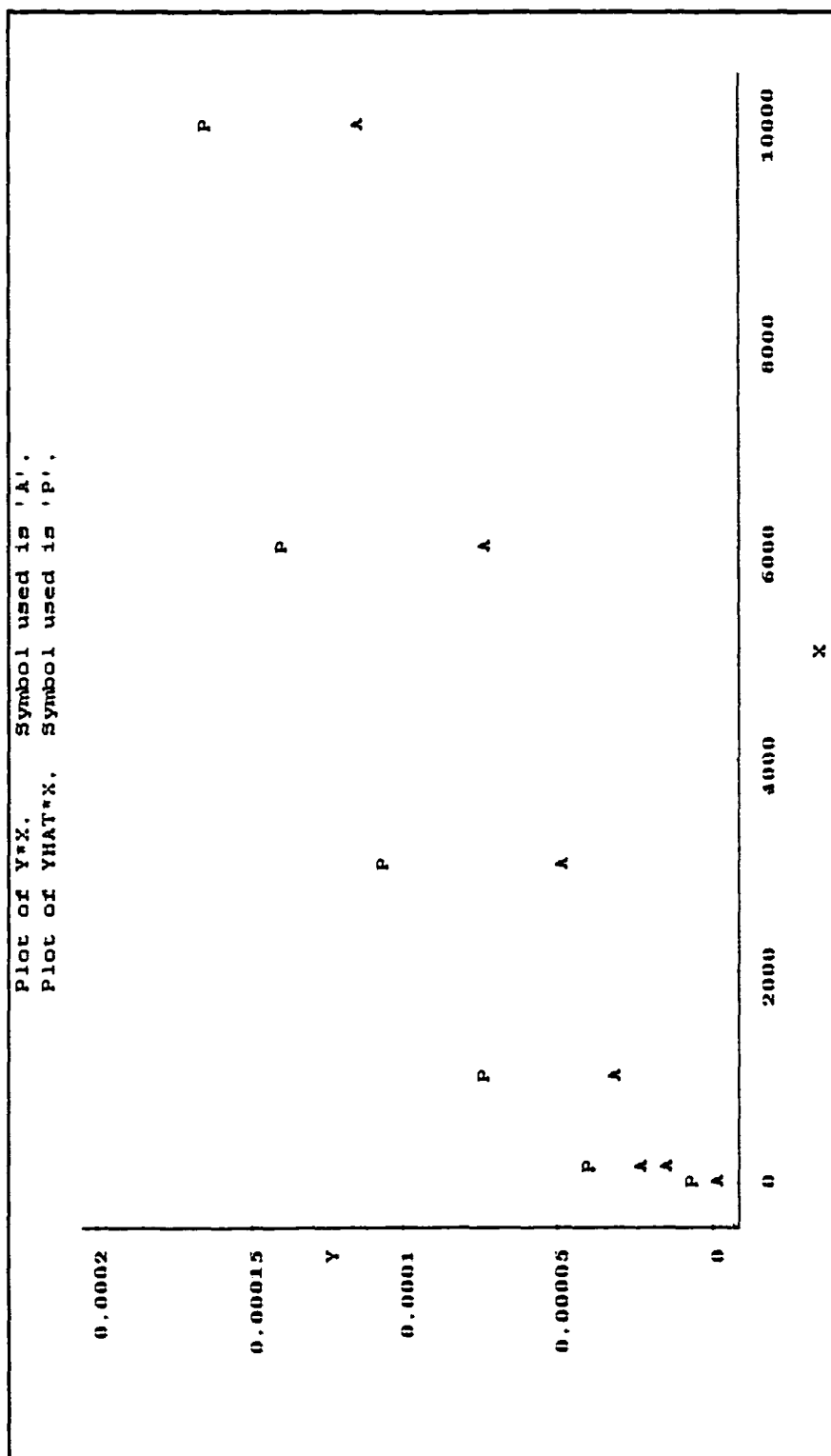
Figure D.6 Regression Result of T8F-CRM Wearing Course at 104°F
(A--actual data, P--prediction result)
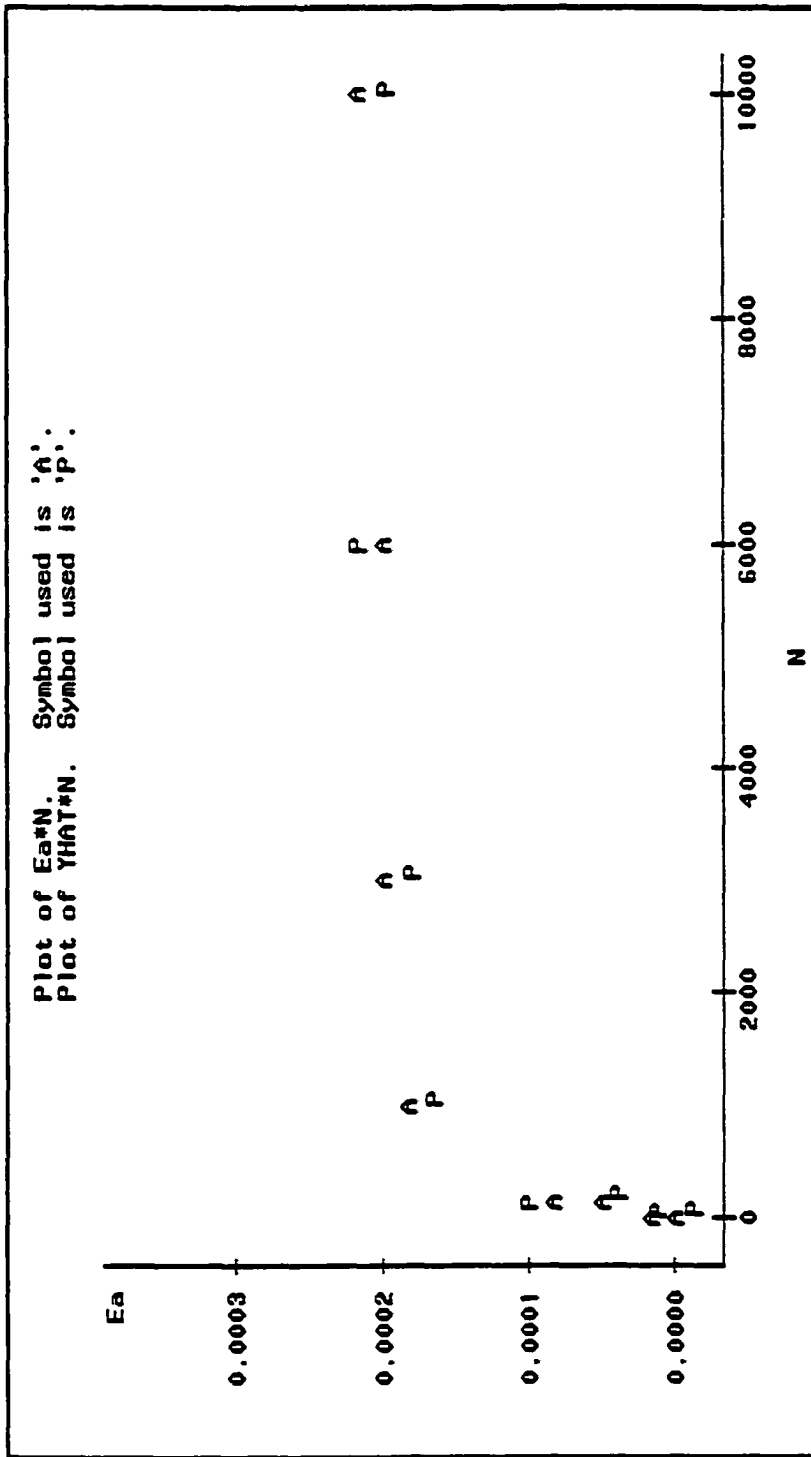
Figure D.7 Regression Result of T5A Black Base Course at 40°F
(A--actual data, P--prediction result)

Plot of Ea*N.   Symbol used is 'A'.
Plot of YHAT*N.   Symbol used is 'P'.
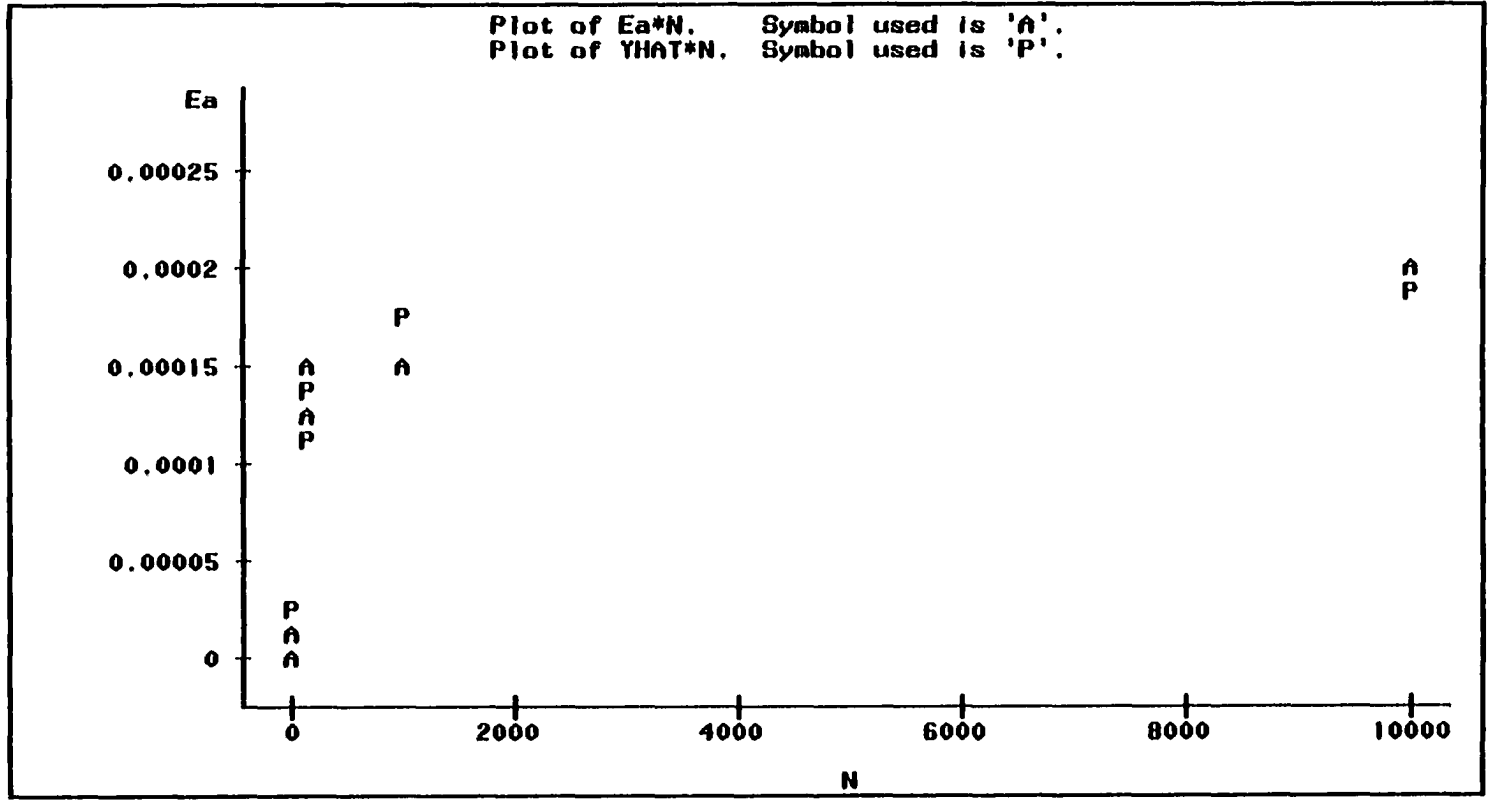
Figure D.8 Regression Result of T5A Black Base Course at 77 °F
(A--actual data, P--prediction result)

Plot of Ea*N.   Symbol used is 'A'.
Plot of YHAT*N. Symbol used is 'P'.
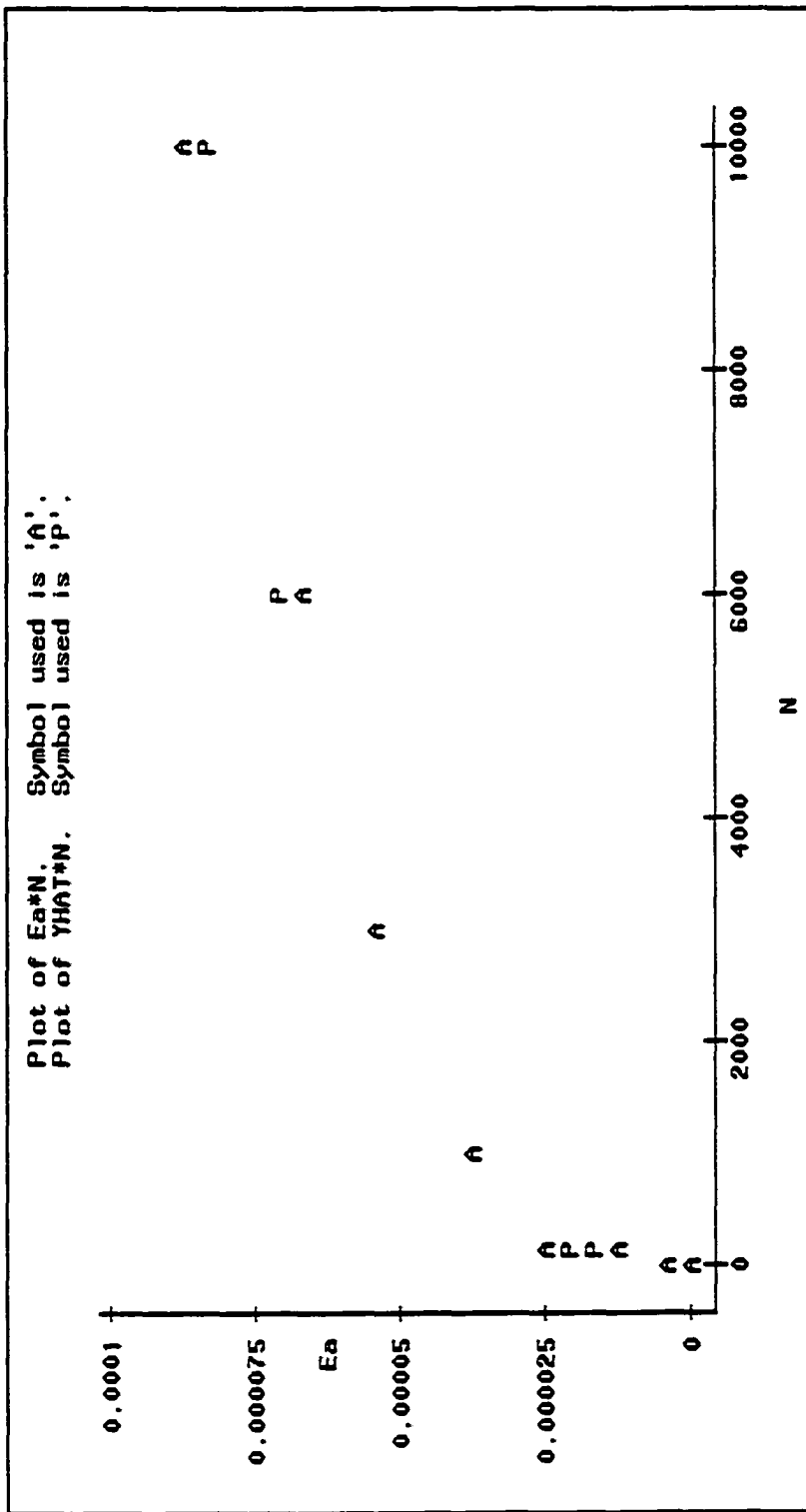
Figure D.9 Regression Result of T5A Black Base Course at 77 °F
(A--actual data, P--prediction result)
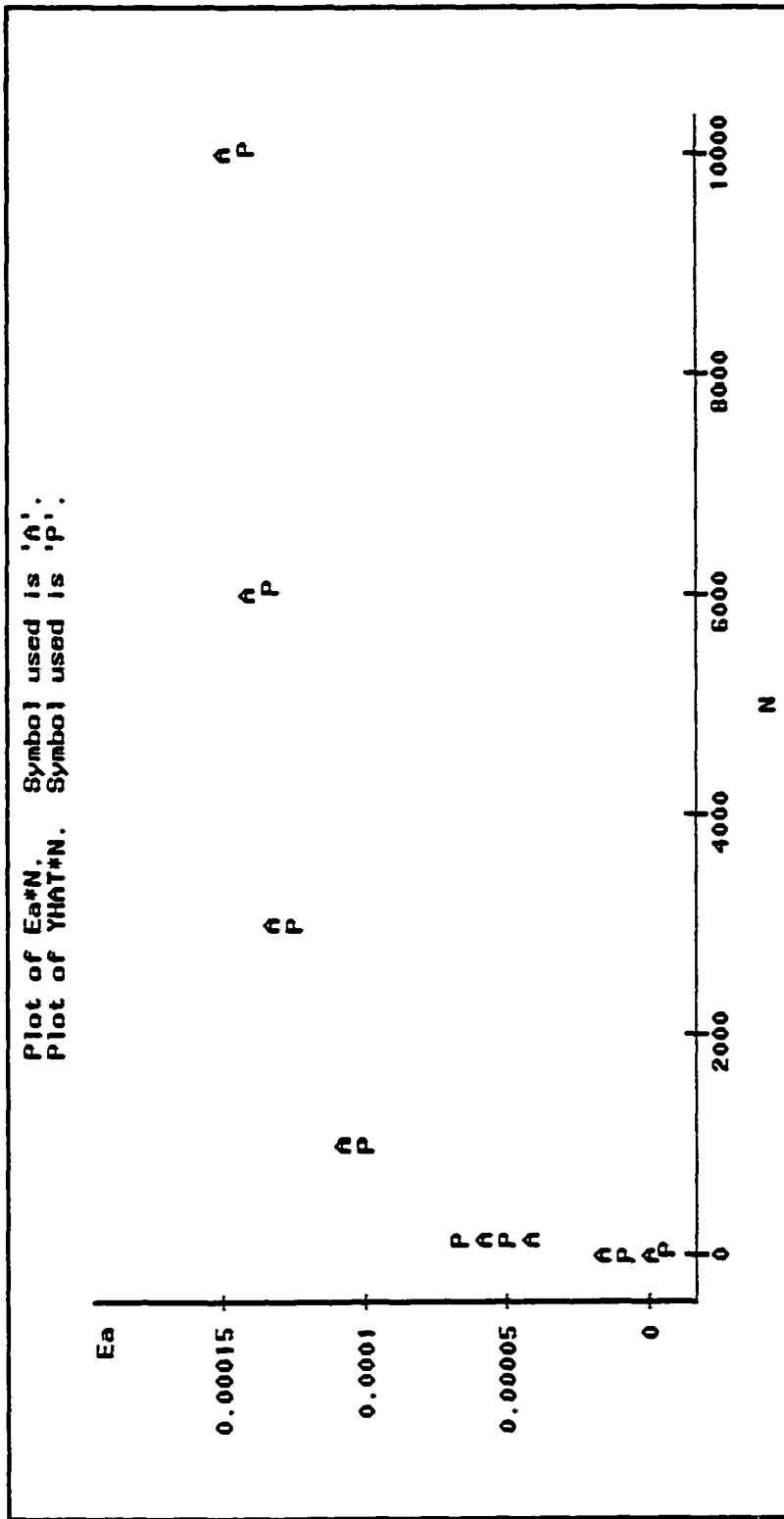
Figure D.10 Regression Result of T5A-CRM Base Course at 40 °F
(A—actual data, P—prediction result)
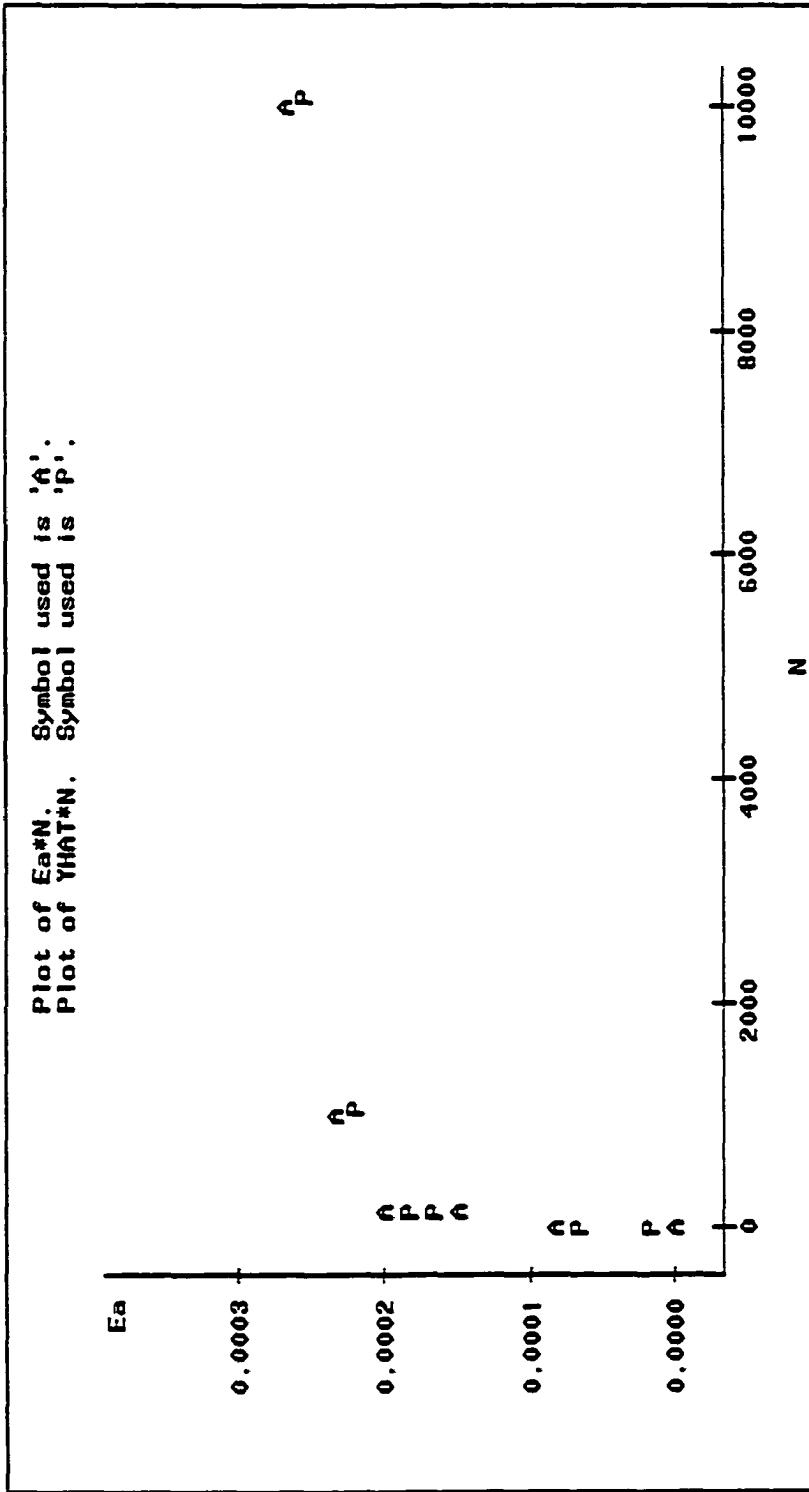
Figure D.11 Regression Result of T5A-CRM Base Course at 77 °F (A--actual data, P--prediction result)
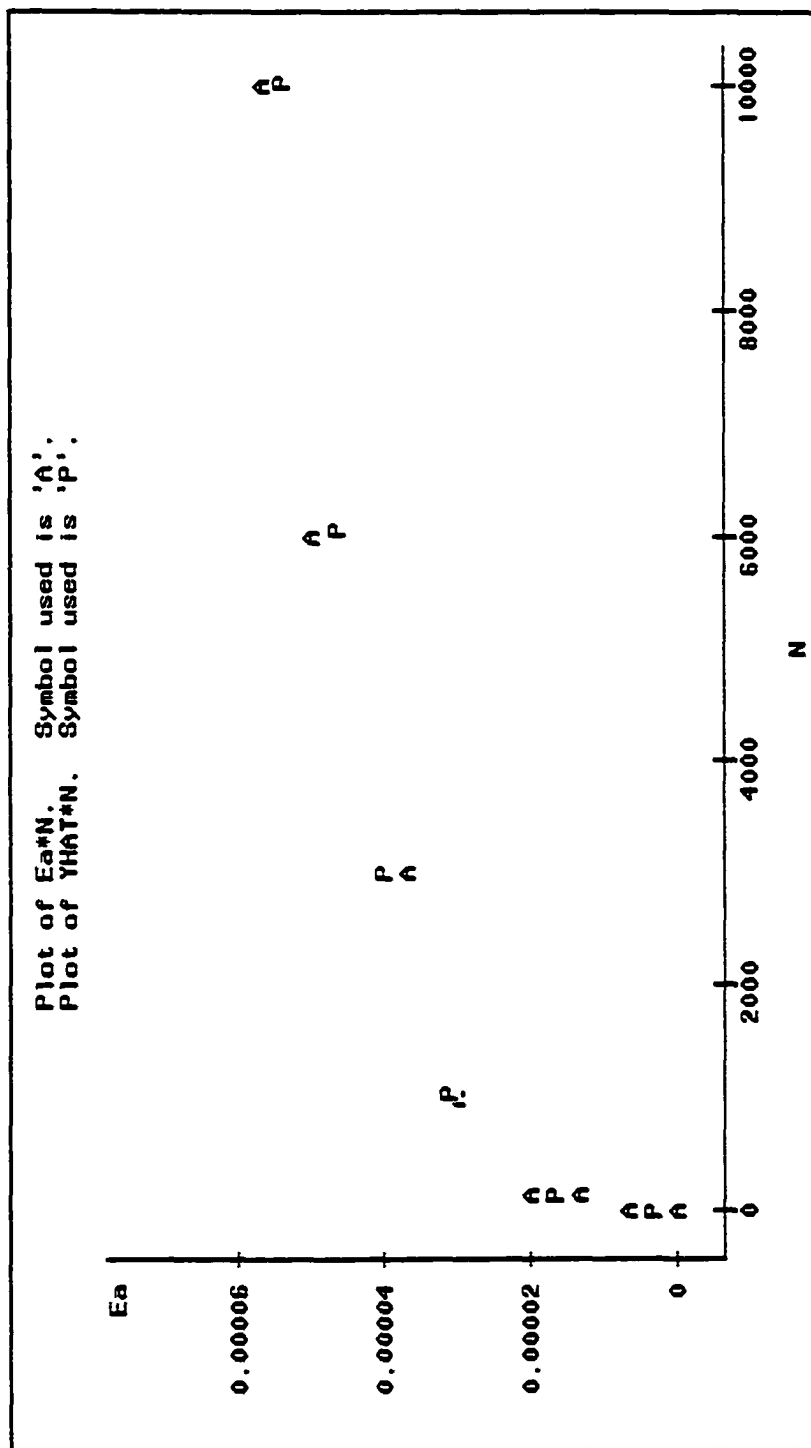
Figure D.12 Regression Result of T5A-CRM Base Course at 104 °F
(A--actual data, P--prediction result)

APPENDIX E

THE PERMANENT DEFORMATION PARAMETERS OF TEST
MATERIALS VERSUS TEMPERATURE RELATIONSHIPS

171
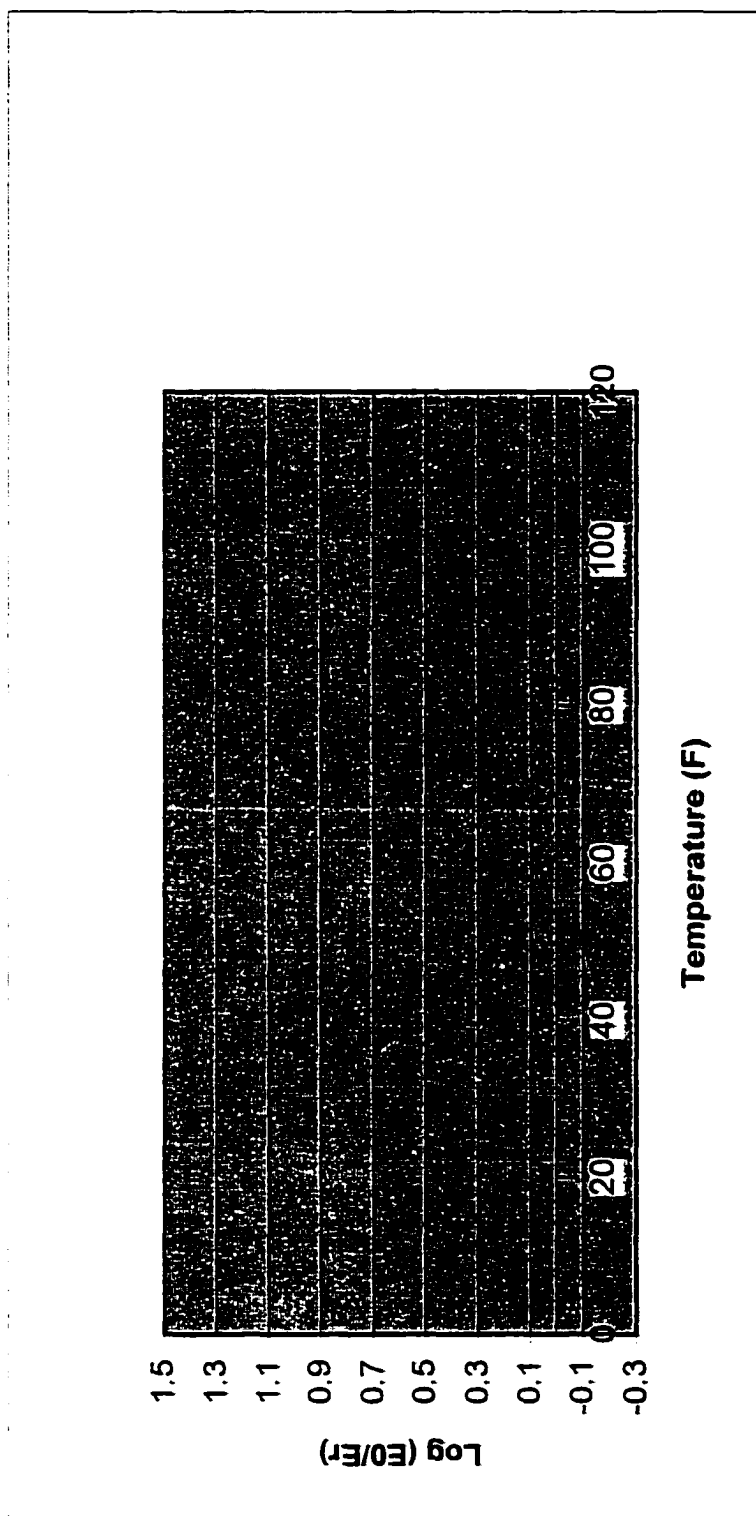
Figure E.1 Plot of log (initial strain/ resilient strain) vs. Temperature for Conventional T8 Wearing Course
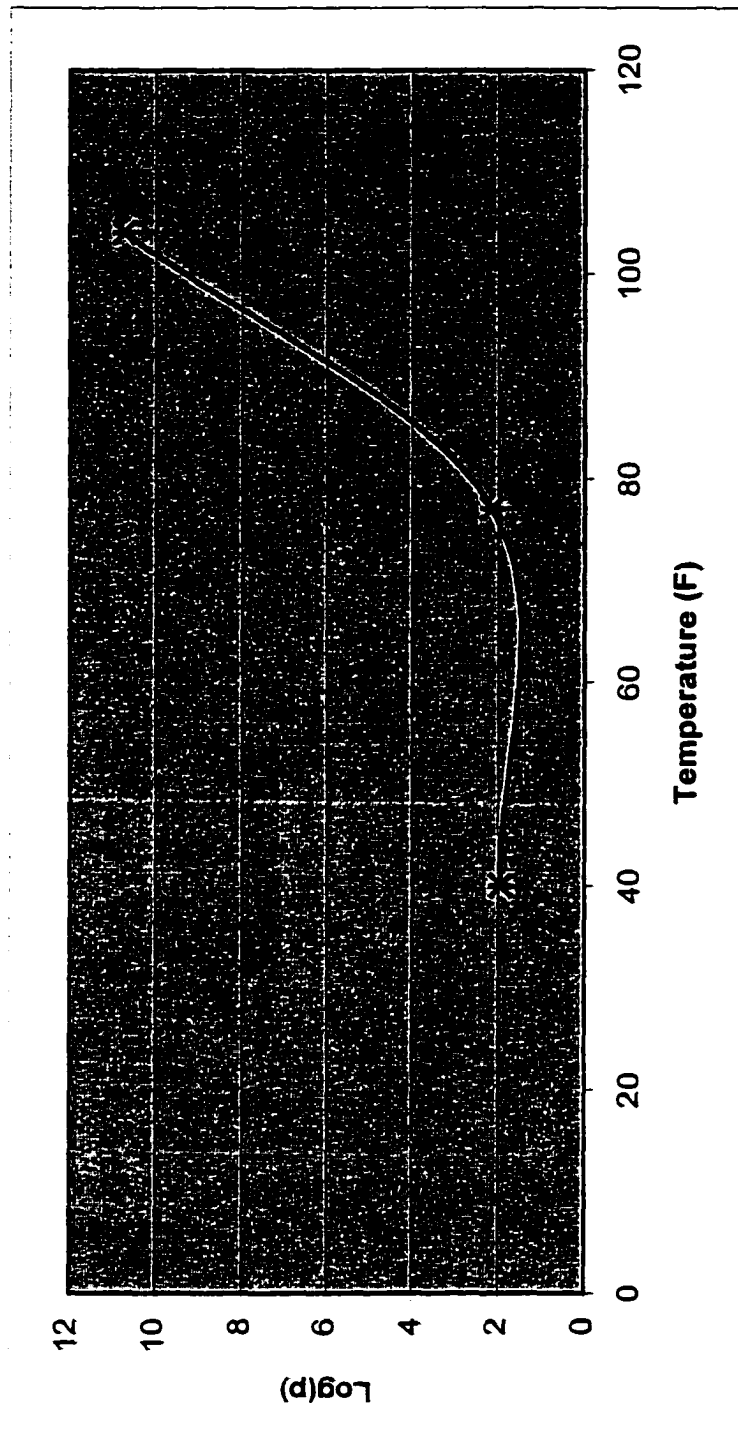
Figure E.2 Plot of log (Rho) vs. Temperature for Conventional T8 Wearing Course
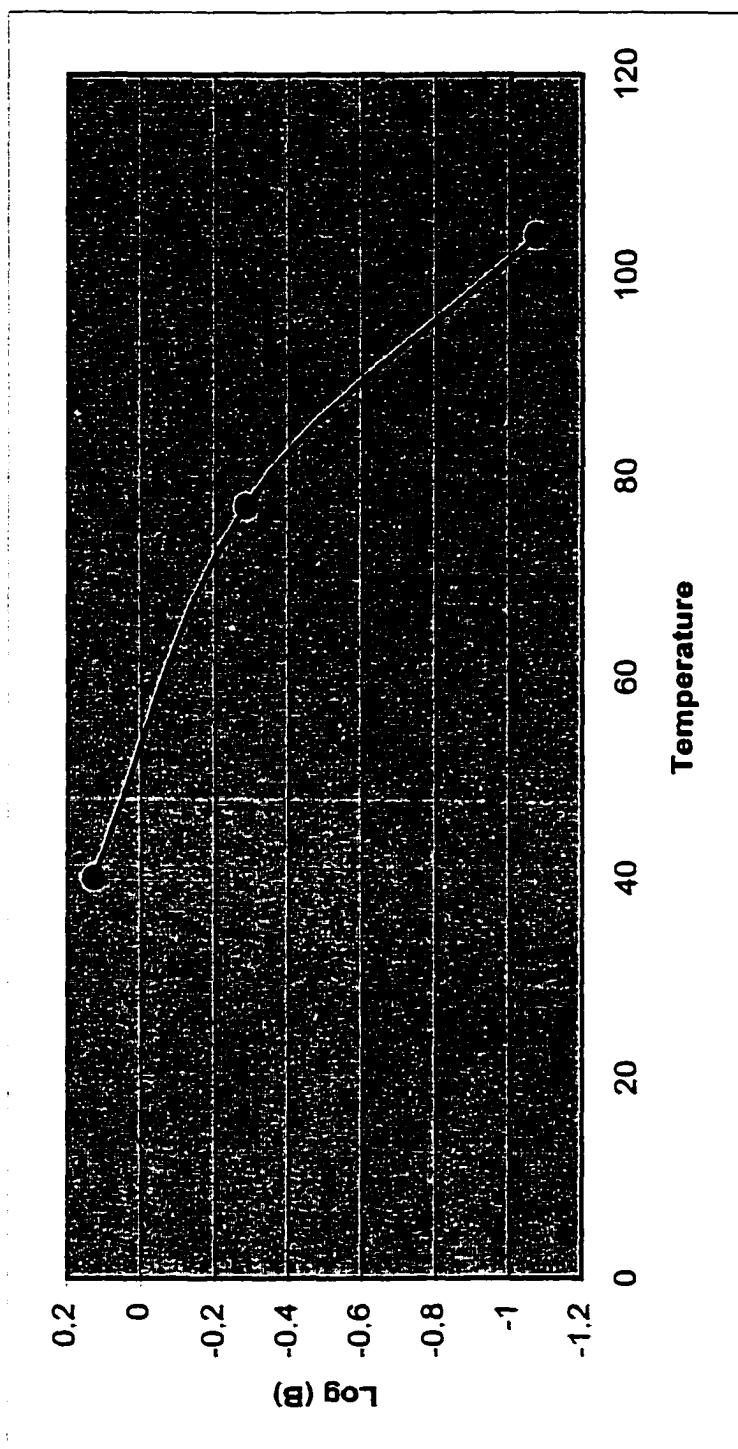
Figure E.3 Plot of log (Beta) vs. Temperature for Conventional T8 Wearing Course
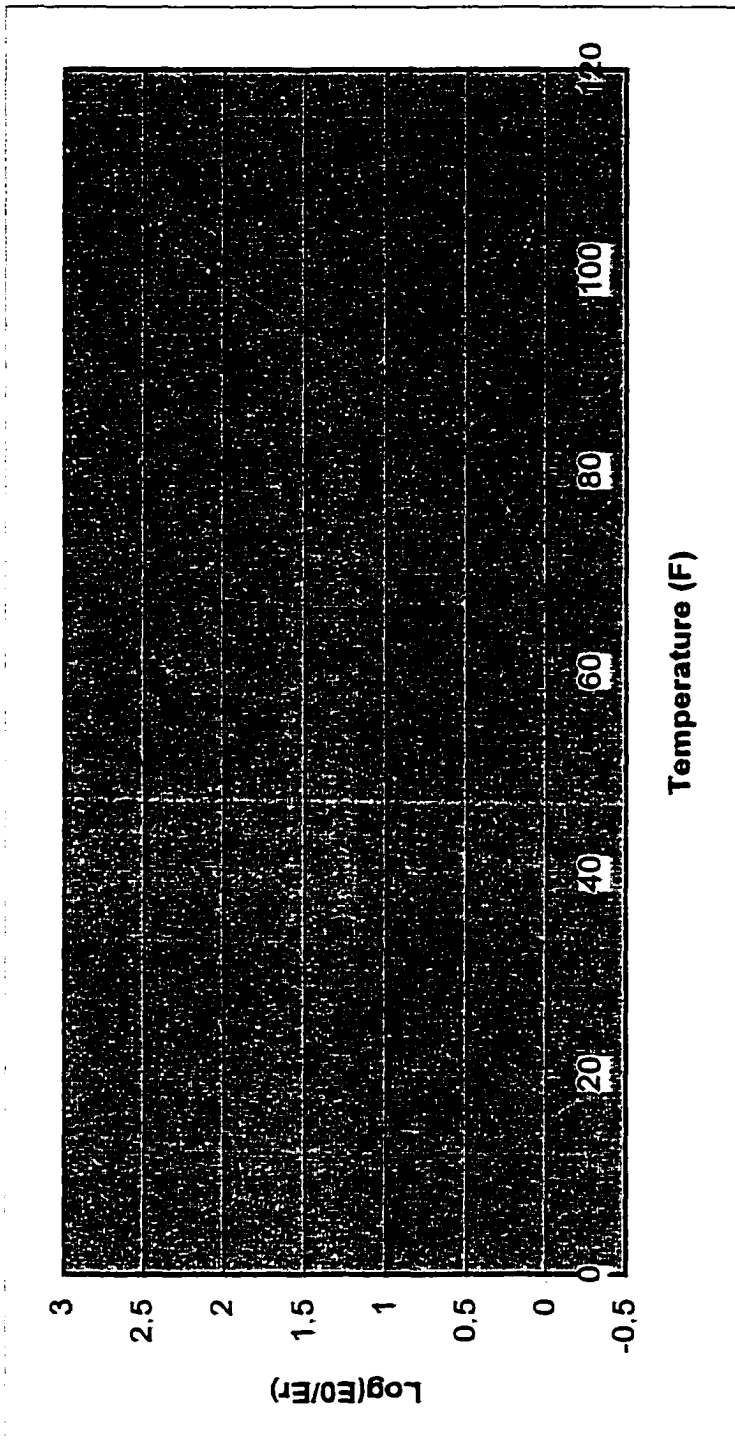
Figure E.4 Plot of log (initial strain/ resilient strain) vs. Temperature for AR-HMA Wearing Course
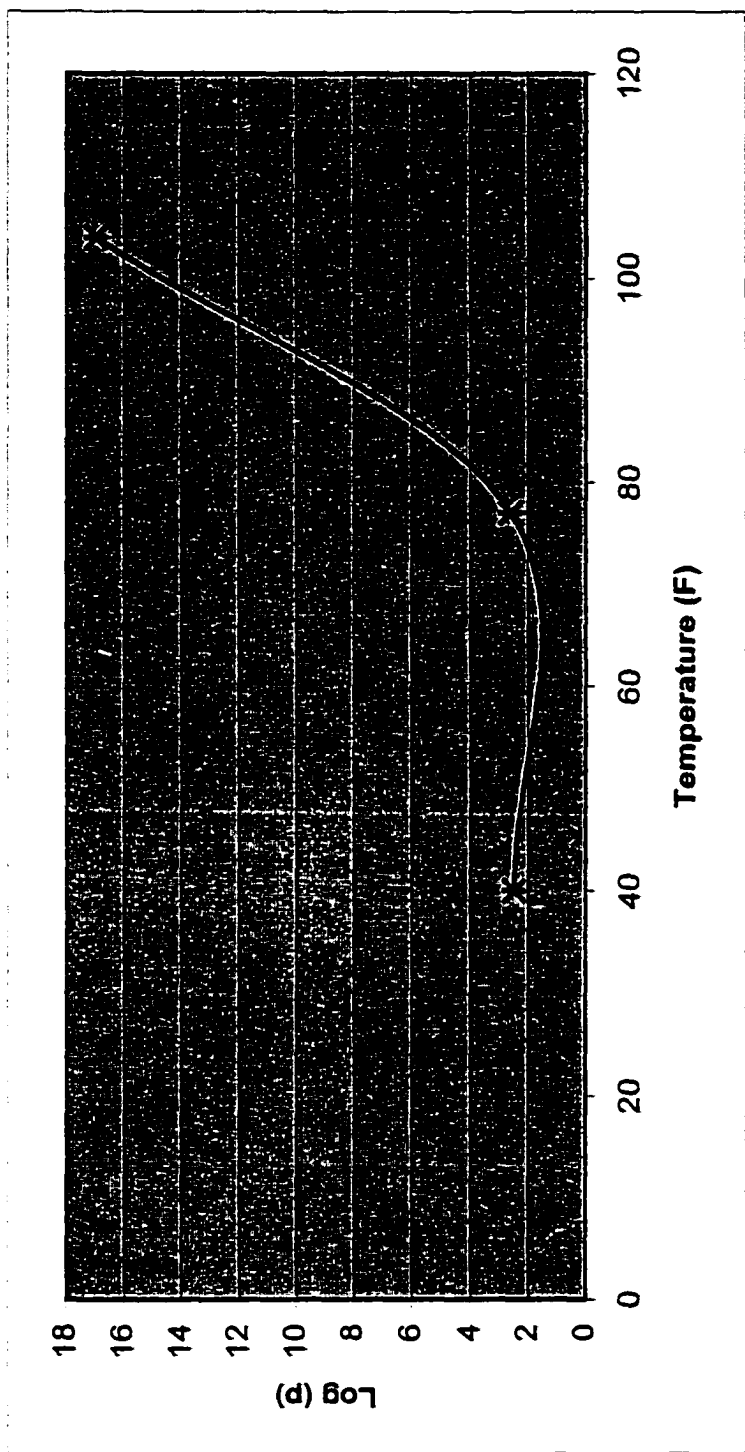
Figure E.5 Plot of log (Rho) vs. Temperature for AR-HMA T8 Wearing Course
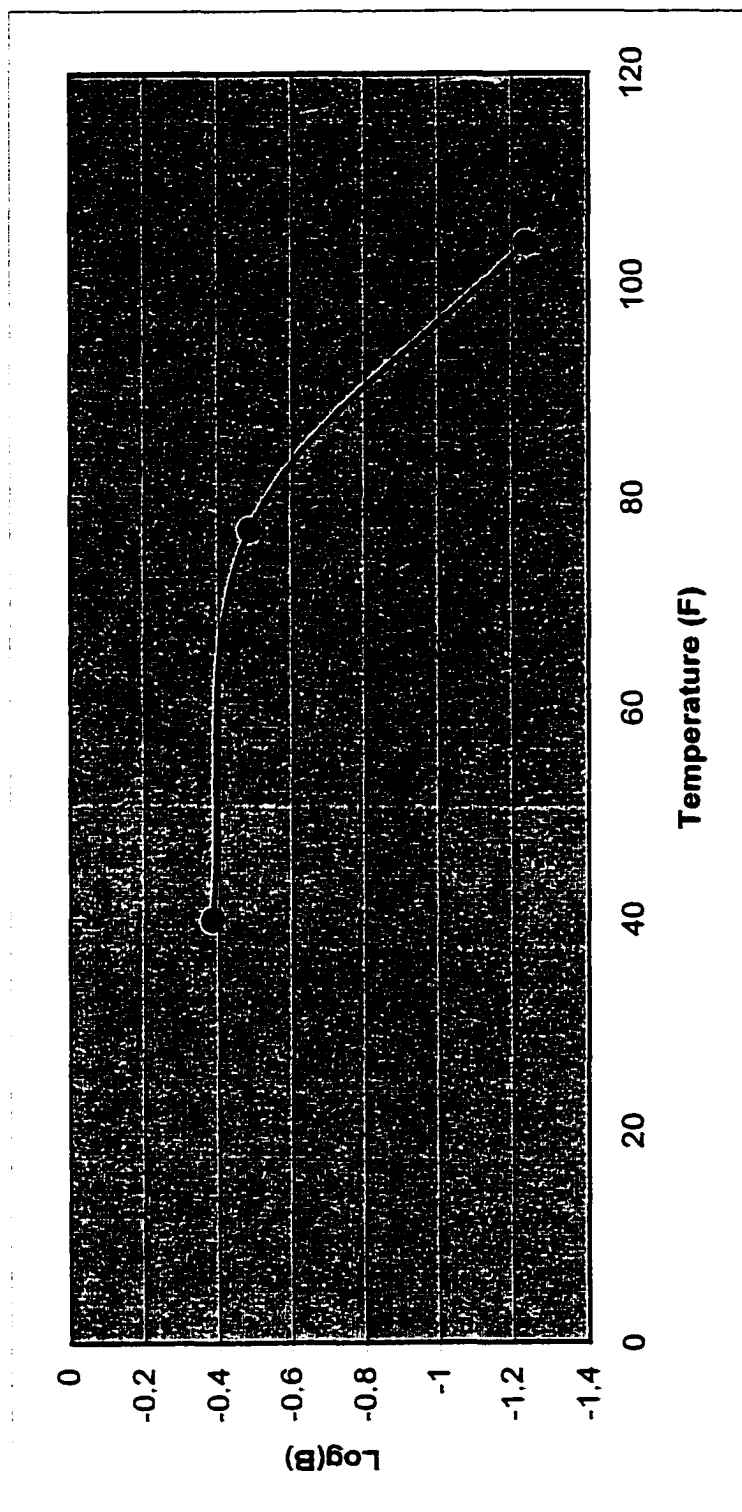
Figure E.6 Plot of log (Beta) vs. Temperature for AR-HMA T8 Wearing Course
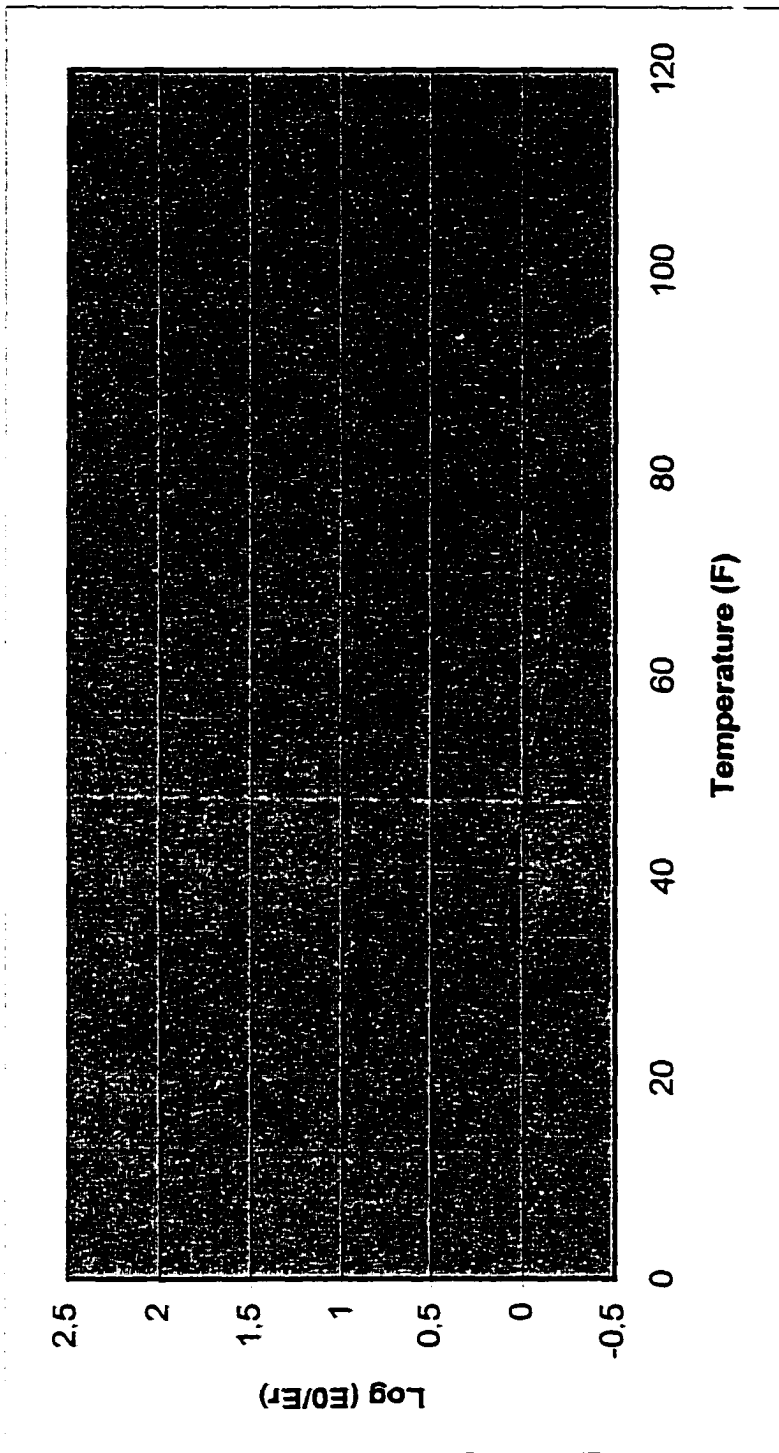
Figure E.7 Plot of log (initial strain/ resilient strain) vs. Temperature for Conventional T5A Base Course
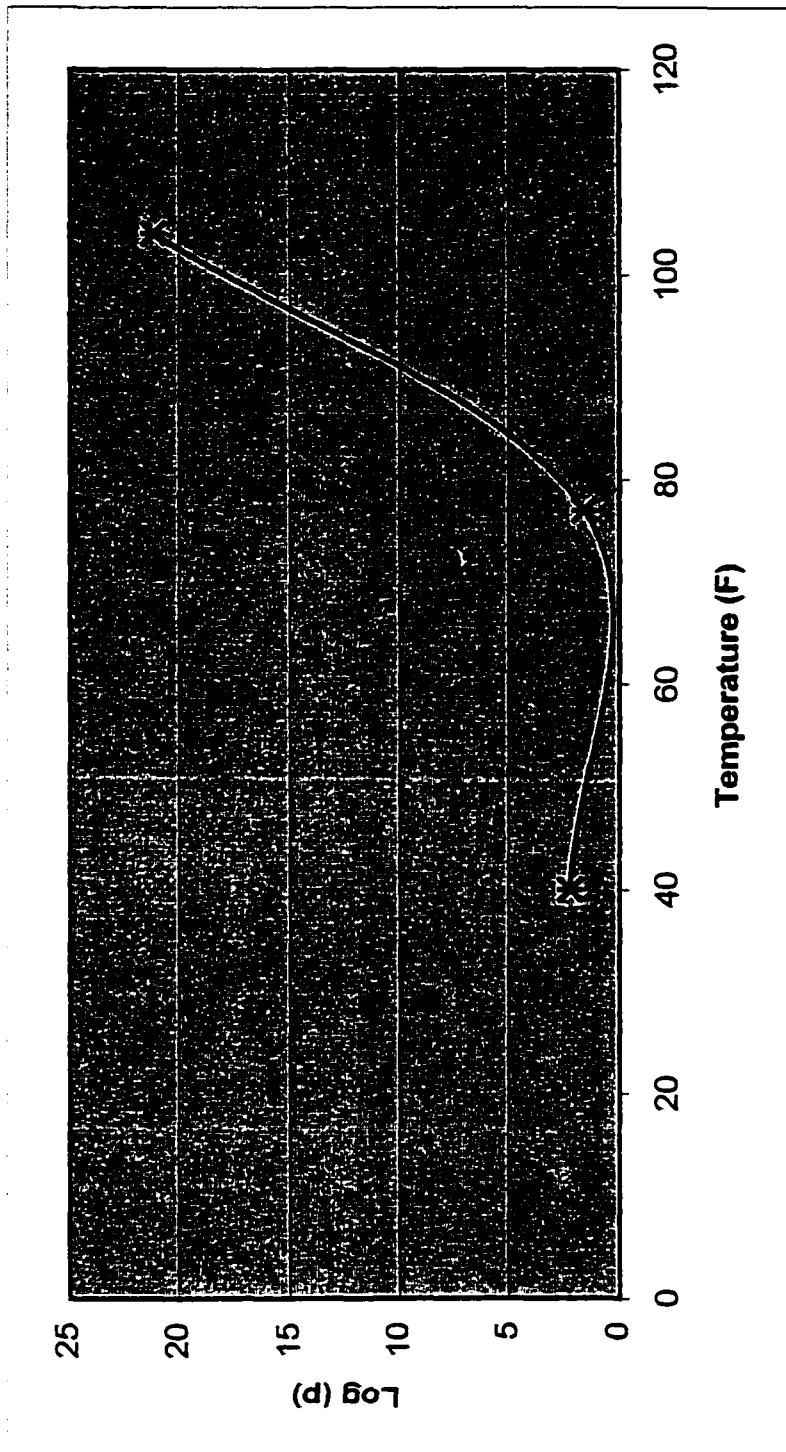
**Figure E.8 Plot of log (Rho) vs. Temperature for Conventional T5A Black Base Course**
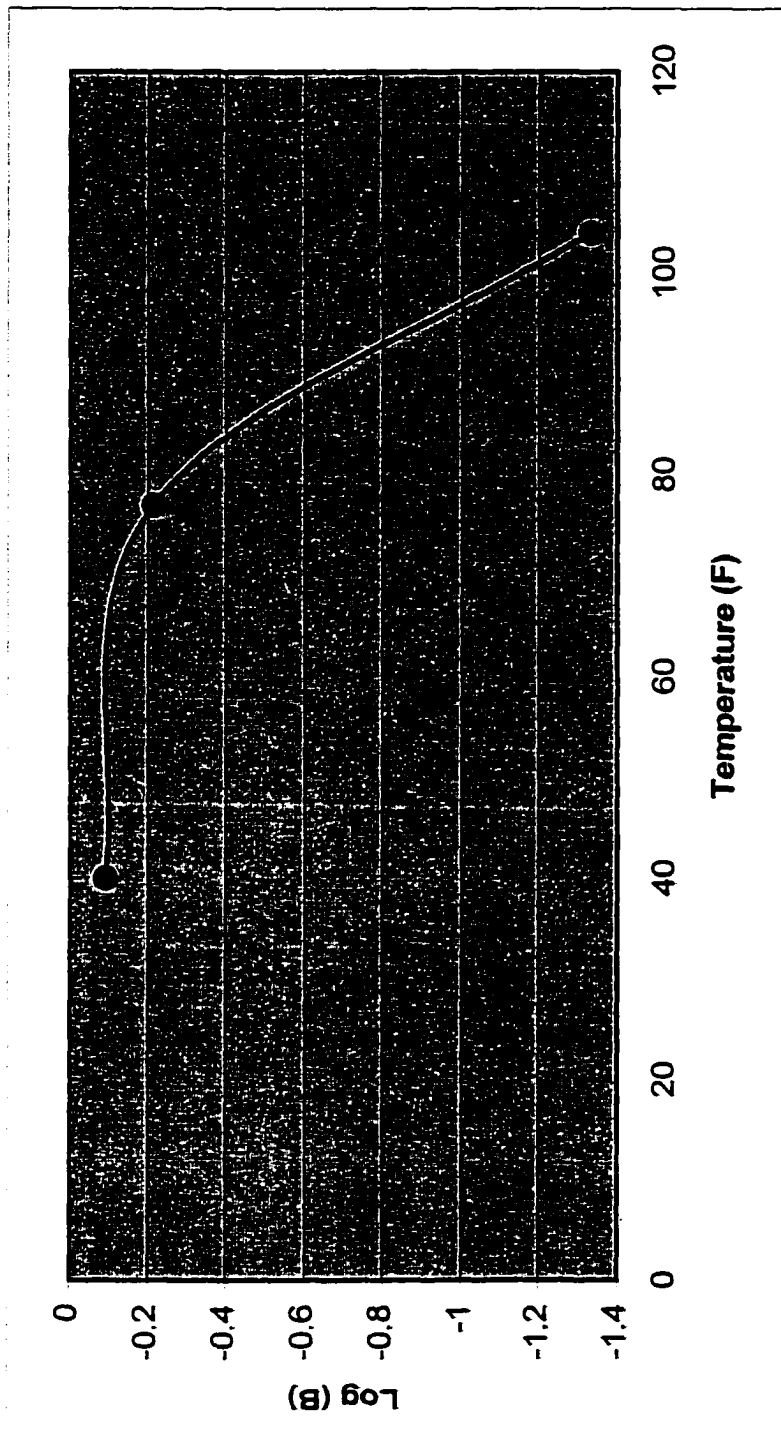
Figure E.9 Plot of log (Beta) vs. Temperature for Conventional T5A Black Base Course
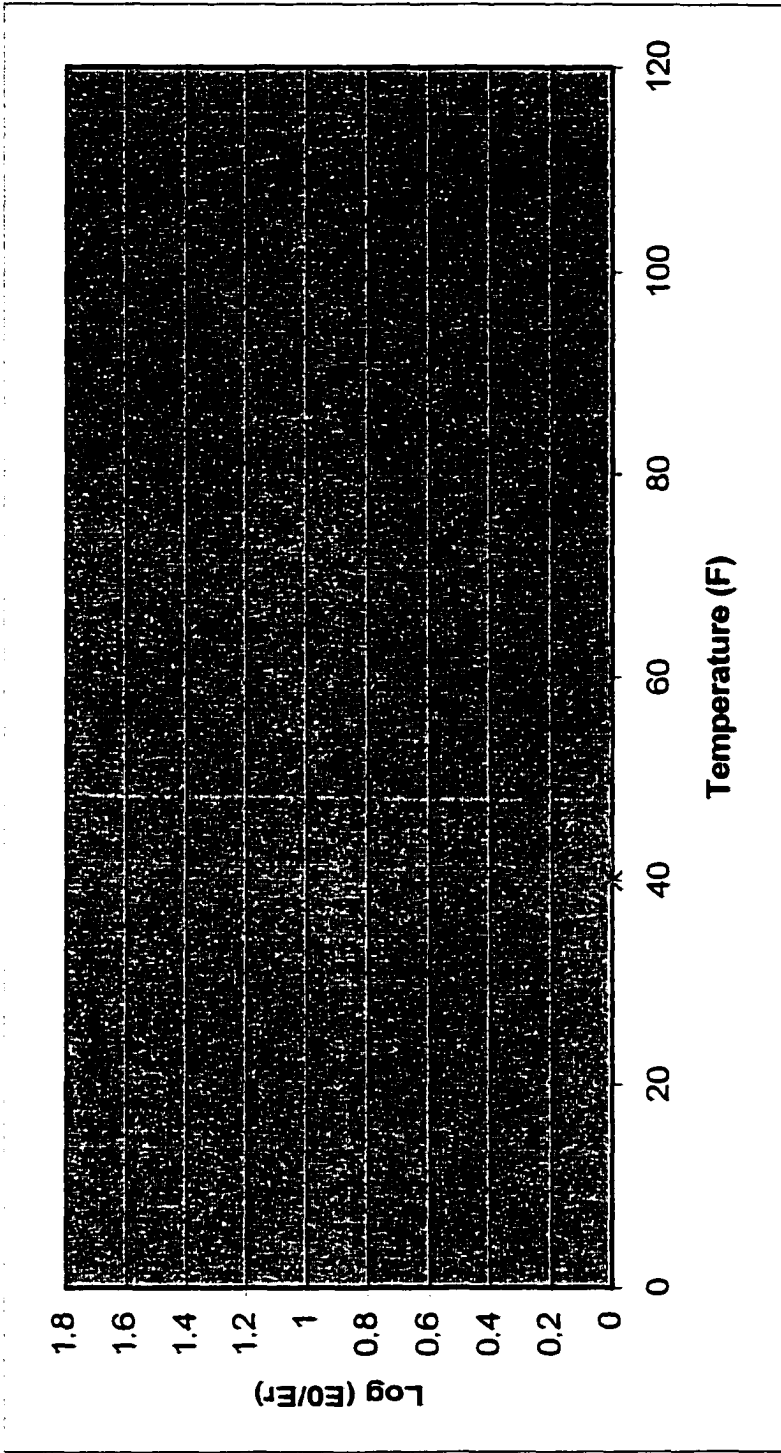
**Figure E.10 Plot of log (initial strain/ resilient strain) vs. Temperature for AR-HMA T5A Base Course**
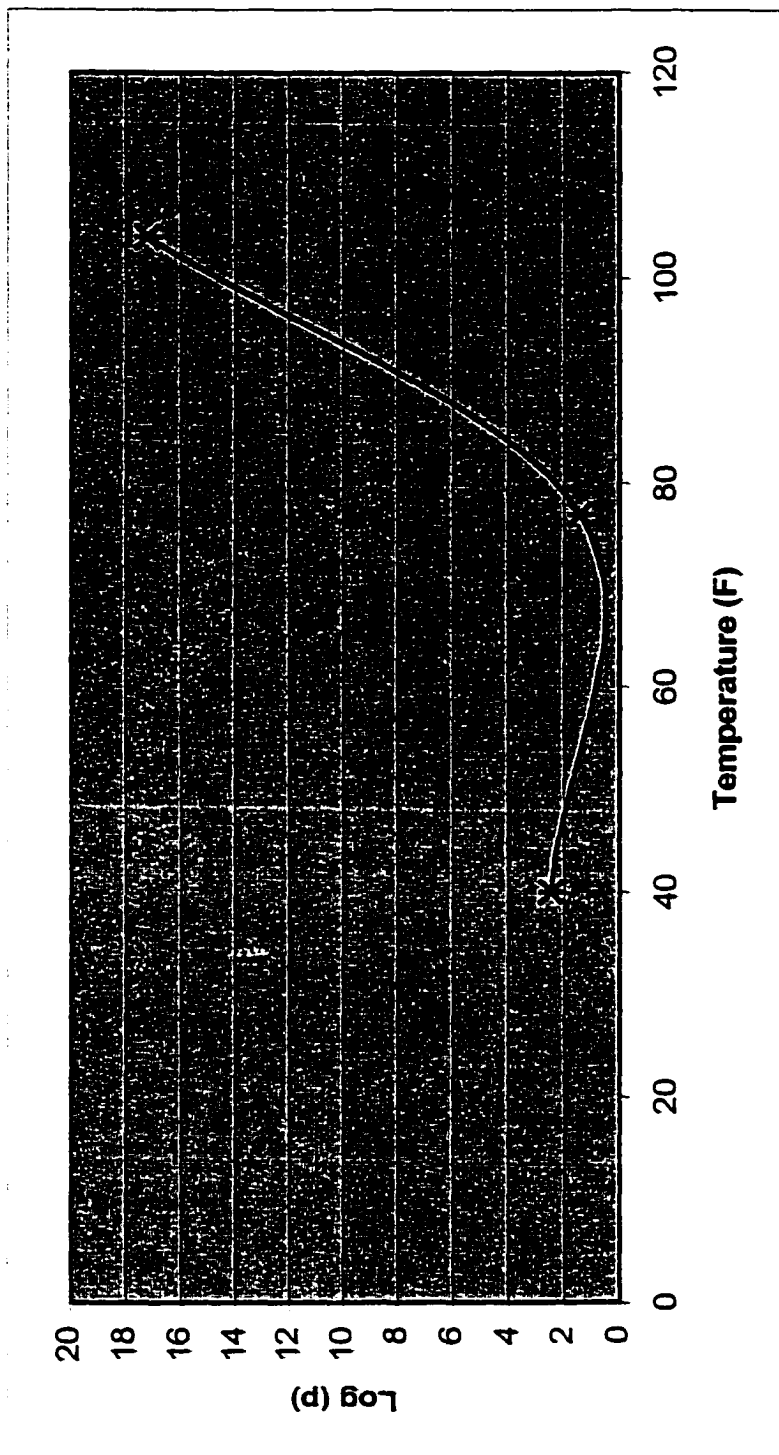
Figure E.11 Plot of log (Rho) vs. Temperature for AR-HMA T5A Base Course
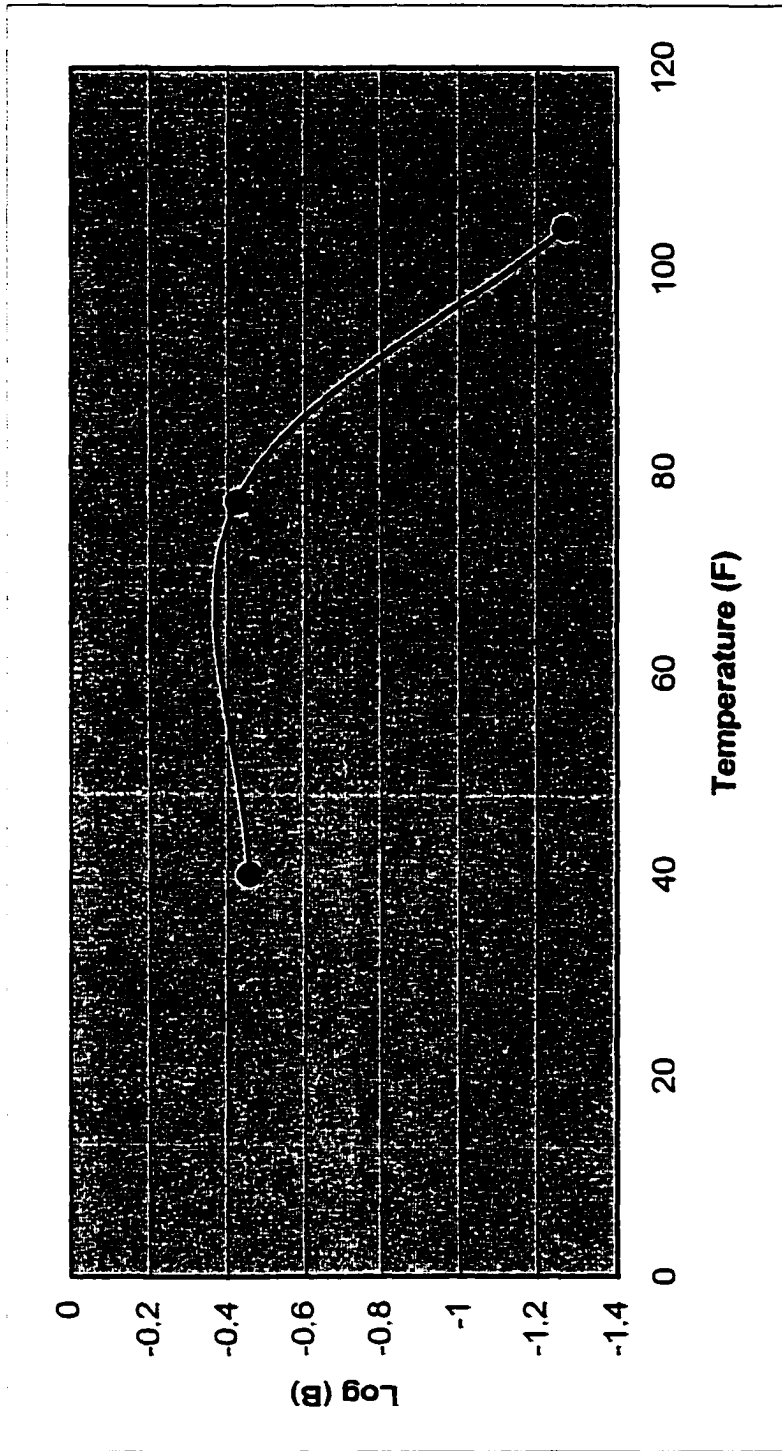
Figure E.12 Plot of log (Beta) vs. Temperature for AR-HMA T5A Base Course

REFERENCES

[1] PUBLIC LAW, "Intermodal Surface Transportation Efficiency Act of 1991", Public Law 102-204, Dec.18, 1991.

[2] Mohammad, L. N., Huang, B., Roberts, F.L., and Rasoulian, M. "Accelerated Loading Performance and Laboratory Characterization of Crumb Rubber Asphalt Pavements", Road Materials and Pavement Design, Volume 1-No. 4/2000, pp 467-493.

[3] Heitzman, M., "State of the Practice- Design and Construction of Asphalt Paving Materials with Crumb Rubber Modifier." Research Report No. FHWA-SA-92-022, Federal Highway Administration, Washington D.C., May 1992.

[4] King, W.M., and Abadie, C. "Comparative Performance of Conventional and Rubberized Hot Mix under Accelerated Loading, Construction Report". FHWA/LA-99/331. LTRC, Baton Rouge, LA, March 2000.

[5] Way, G. B., "Prevention of Reflective Cracking Minnetonka-East", Report Number 1979GWI, Arizona Department of Transportation, Phoenix, AZ, August 1979.

[6] Page, G., "Florida's Initial Experience Utilizing Ground Tire Rubber in Asphalt Concrete Mixes," Research Report FL/Dot/MO89-366, Florida Department of Transportation, Materials Office, Tallahassee, FL, September 1989.

[7] Troy, K., Sebaaly, P., and Epps, J., "Evaluation Systems for Crumb Rubber Modified Binders and Mixtures", Transportation Research Board, TRR Record No. 1530, pp 3-10, Washington D.C., 1996.

[8] Hoyt, D., Lytton, R., and Roberts, F.L. "Criteria for Asphalt-Rubber Concrete in Civil Airport Pavements: Evaluation of Asphalt-Rubber Concrete", Texas Transportation Institute, Texas A&M University, College Station, 1986.

[9] Metcalf, J. B., "Application of Full-Scale Accelerated Pavement Testing", NCHRP Synthesis 235, Transportation Research Board. Washington, D.C., 1996.

[10] Kadar, P., "Findings and Results of Three Years Accelerated Testing of Typical Heavy Duty Pavements-An Overview". Proceedings –4th ARRB Conference, 1984. pp 139-148.

[11] Voung, B.T., Sharp, K.G., Baran, E.J., Vertessey, N.J., Johnson-Clarke, J.R., and Reeves, I.N. Performance of Unbound and Stabilized Materials under Accelerated

Loading: Summary Report of Beerburrum II ALF trial. Research Report No. ARR286, Australian Road Research Board, Melbourne, Victoria, Australia, June 1996 (APRG16/).

[12] Kadar, P., and Walter P.D., "The Performance of Slag Roadbases under Accelerated Trafficking – Results and Findings of the Prospect ALF Trial", Research Report No. ARR No. 170, Australian Road Research Board, Melbourne, Victoria, Australia, November 1989.

[13] Statton, J.E., and Kadar, P., "The Performance of Pavement Rehabiliations Under Accelerated Loading – The Callinton ALF Trial", Proceedings 15th. ARRB Conference Part 2. Australia. 1992.

[14] Jameson, G.W., Sharp, K.G., and Leo, R., "Cement Treated Crushed Rock Pavement Fatigue under Accelerated Loading: The Mulgrave (Victoria) ALF Trial. 1989-1991", Research Report No. ARR No. 229. Australian Road Research Board, Melbourne, Victoria, Australia, July 1992.

[15] Jameson, G.W., J.R., Sharp, K.G., and Walter, P.D., "The Performance of Pavement with Geotextile Reinforced Seals: The Brewarrina, N.S.W. ALF Trial", Research Report No. ARR No. 241. Australian Road Research Board, Melbourne, Victoria, Australia, February 1993.

[16] Jameson, G.W., Dash, D.M., Tharan, Y., and Vertessy, N.J., " Performance of deep-lift in situ pavement recycling under accelerated loading the Cooma ALF Trial 1994", ARRB Research Report ARR 265, Australian Road Research Board, Melbourne. Victoria, Australia, June 1995.

[17] RTA, Guide to In-Situ Deep-Lift Recycling of Granular Pavements 1994.

[18] Austroads Pavement Research Group. Performance of cement-stabilised flyash under accelerated loading: the Erraring ALFTrial, AUSTROADS Pavement Research Group Report No. 15, 1995.

[19] Sharp, K.G. Proposal for an accelerated loading facility trial on insitu stabilisation treatments and axle load equivalency. AUSTROADS Pavement Research Group Report No. 95/06 November 1995.

[20] Mitchell, T., "Test Roads: Designing the Pavements of the Future", Public Roads. Fall 1996.

[21] Bonaquist, R., "Summary and Pavement Performance Test Using the Accelerated Loading Facility, 1986-1990", Transportation Research Record 1354. Transportation Research Board. Washington, D.C. 1992.

[22] Western Association of State Highway and Transportation Officials. Asphalt Pavement Rutting, Western States. Research Report No. FHWA/TS-84-211. FHWA, U.S. Department of Transportation, Washington, D.C., 1984.

[23] LTRC, Minutes of the ALF project meeting on Jan. 20, 2000, Accelerated Loading Faculty, Port Allen, LA. 2000.

[24] Churilla, C. J.," Ultra-Thin Whitetopping", Public Roads, September/October 1998, Vol 62, No.2, Federal Highway Administration.

[25] Cumbaa, S.L., et al. "Construction and Comparision of Louisiana's Conventional and Alternative Base Courses under Accelerated Loading", FHWA. Research Study, 1993 - 1996.

[26] Metcalf, J.B., Romanoschie, S., and Li., Y., "Construction and Comparison of Louisiana's Conventional and Alternative Bases under Accelerated Loading", Interim Report 1, Phase 1. Louisiana Transportation Research Center. Louisiana Department of Transportation and Development, Baton Rouge, LA, 1998.

[27] Metcalf, J.B., Romanoschie, S., and Li., Y., "The Louisiana Accelerated Loading Facility", Report 2, Experiment 1, Phase 3. Louisiana Transportation Research Center. Louisiana Development of Transportation and Development, Baton Rouge, LA, 1998.

[28] Djakfar, L., "Implementation of ALF Results to Designing Flexible Pavements in Louisiana", A Dissertation for the Degree Doctor of Engineering, Louisiana Tech University, Ruston, LA, April 1999.

[29] Wathugala, W., Huang, B., and Pal, S., "Numerical Simulation of Geosynthetic-Reinforced Flexible Pavement", Transportation Research Record 1534, Transportation Research Board. Washington, D.C. 1996.

[30] Kenis, W. J., "Predictive Design Procedures, VESYS User Manual - An Interim Design Method for Flexible Pavements Using VESYS Structural Subsystem", FHWA-RD-77-154, Federal Highway Administration, Washington, D.C., January 1978.

[31] Zaghloul, S., and White, T., "Use of a Three-Dimensional, Dynamic Finite Element Program for Analysis of Flexible Pavement", Transportation Research Board. Transportation Research Record 1388, Washington, D.C., 1993, pp. 60-69.

[32] Construction Engineering Laboratory and Facilities Group, "ILLIPAVE-A Finite Element Program for the Analysis of Pavements", Department of Civil Engineering, University of Illinois at Urbana-Champaign, Urbana-Champaign, IL, May 1982.

[33] Fernando, E.G., Tseng, K.H., Lytton, R.L., "Flexible Pavement Analysis Structural System (FLEXPASS Release 2.0), User's Guide", Texas Transportation Institute, Texas A&M University, College Station, TX, October, 1989.

[34] Lytton, R.L., and Tseng, K.H., "Fatigue Damage Properties of Asphaltic Concrete Pavements", Transportation Research Board, Transportation Research Record 1286, Washington, D.C. 1990.

[35] Tseng, K.H., "A Finite Element Method for the Performance Analysis of Flexible Pavement", Ph.D. Dissertation. Texas A&M University, College Station, TX,1988.

[36] Gabrielson, J.R., "Evaluation of Hot Mix Asphalt (HMA) Static Creep and Repeated Load Tests", Ph.D. Dissertation. Auburn University, Auburn, Alabama. 1992.

[37] Smith, R. E., Darter, M. I., and Herrin, S. T., "Highway Distress Identification Manual", Interim Report, Federal Highway Administration, U.S. Dept. of Transportation, Washington, D.C., March 1979.

[38] Huang, B., "Fundamental Characterization and Numerical Analysis of Large Stone Asphalt Mixture", Ph.D. Dissertation, Louisiana State University, Baton Rouge, LA, 2000.

[39] Monismith, C. L., "Flexibility Characteristics of Asphalt Pavement Mixtures" Proceedings, Association of Asphalt Paving Technologists, Vol 27, 1958.

[40] Roberts, F. L., Tielking, J. T., Middleton, D.,.Lytton, R. L, and Tseng, K., "Effects of Tire Pressures on Flexible Pavements", TTI research Report No. 372-1F, Texas Transportation Institute, Texas A&M University, College Station, Texas, December, 1985.

[41] Little, D. N., Al-Balbissi, A. H., Gregory, C., and Richey, B., "Design and Characterization of Paving Mixtures Based on Plasticized Sulfur Binders-Engineering Characterization", TTI Draft Final Report RF 4247, Texas Transportation Institute, Texas A&M University, College Station, Texas, July 1984.

[42] The AASHO Road Test: Report 5, Pavement Research. Highway Research Board, Special Report 61 E, 1962.

[43] Rada, G., and Witczak, M. W., "Comprehensive Evaluation of Laboratory Resilient Moduli Results for Granular Material", Transportation Research Record 810. Transportation Research Board. Washington, D.C. 1981. pp 23 - 32.

[44] HKS, "ABAQUS User's Manual, Version 5.8", Hibbit, Karlsson & Sorensen, Inc., Pawtucket, RI, 1998.

[45] Kadar, P., "The First Accelerated Loading Facility (ALF) Pavement Trial at Somerby-NSW-Test Results", Research Report No. AIR 415-3, Australian Road Research Board, Melbourne, Victoria, Australia. September 1985.

[46] Kadar, P., Baran, E., and Gordon, R.G. "The Performance of CTB Pavements under Accelerated Loading-The Beerburrum, Queensland ALF trial 1987/1988", ARRB Research Report ARR 158, Australian Road Research Board, Melbourne, Victoria. Australia, 1989.

VITA

The author, Hanlin Qin, was born and raised in a very scenic city, Guilin, in China. She entered Huazhong University of Science and Technology in China and earned a Bachelor of Engineering degree in Structural Engineering in 1988. In the same year, she entered the graduate school of Tianjin University, and majored in Civil Engineering. She received a Master of Engineering degree in Tianjin University in 1991. After her Master's degree, she entered the Civil Engineering Department of Guangxi University, China, in 1991 as an assistant professor for two years. After that, she moved to Hong Kong and joined a consulting company that specializes in metropolitan commercial, industrial, and residential building design in the Chinese First Special Economic Zone, Shenzhen, which lies about 30 miles north of Hong Kong. For the next five years, she worked as a project engineer and participated in the design of over 50 building structures, most of which high-rise buildings. The structural types included masonry, frame-shear wall structure, tube-in-tube structure, prestressed concrete structure, and structural steel.

In 1998, she was admitted to Louisiana Tech University to pursue the Doctor's degree of Engineering. During her graduate study, she worked on this subject project, the Comparative Performance of Conventional and Rubberized Hot Mix under Accelerated Loading, funded by the Louisiana Transportation Research Center.

189